ORNL

Dr-940

THERMONUCLEAR DIVISION ANNUAL PROGRESS REPORT

Period Ending December 31, 1973

OAK RIDGE NATIONAL LABORATORY

OPERATED BY UNION CARBIDE CORPORATION • FOR THE U.S. ATOMIC ENERGY COMMISSION

ORNL-4982
UC-20 – Controlled Thermonuclear Processes

Contract No. W-7405-eng-26

THERMONUCLEAR DIVISION
ANNUAL PROGRESS REPORT
For Period Ending December 31, 1973

NOTICE

This report was prepared as an account of work sponsored by the United States Government. Neither the United States nor the United States Atomic Energy Commission, nor any of their employees, nor any of their contractors, subcontractors, or their employees, makes any warranty, express or implied, or assumes any legal liability or responsibility for the accuracy, completeness or usefulness of any information, apparatus, product or process disclosed, or represents that its use would not infringe privately owned rights.

SEPTEMBER 1974

OAK RIDGE NATIONAL LABORATORY
Oak Ridge, Tennessee 37830
operated by
UNION CARBIDE CORPORATION
for the
U.S. ATOMIC ENERGY COMMISSION

Reports previously issued in this series are as follow:

ORNL-2693	Period Ending January 30, 1959
ORNL-2802	Period Ending July 31, 1959
ORNL-2926	Period Ending January 31, 1960
ORNL-3011	Period Ending July 31, 1960
ORNL-3104	Period Ending January 31, 1961
ORNL-3239	Period Ending October 31, 1961
ORNL-3315	Period Ending April 30, 1962
ORNL-3392	Period Ending October 31, 1962
ORNL-3472	Period Ending April 30, 1963
ORNL-3564	Period Ending October 31, 1963
ORNL-3652	Period Ending April 30, 1964
ORNL-3760	Period Ending October 31, 1964
ORNL-3836	Period Ending April 30, 1965
ORNL-3908	Period Ending October 31, 1965
ORNL-3989	Period Ending April 30, 1966
ORNL-4063	Period Ending October 31, 1966
ORNL-4150	Period Ending April 30, 1967
ORNL-4238	Period Ending October 31, 1967
ORNL-4401	Period Ending December 31, 1968
ORNL-4545	Period Ending December 31, 1969
ORNL-4688	Period Ending December 31, 1970
ORNL-4793	Period Ending December 31, 1971
ORNL-4896	Period Ending December 31, 1972

Contents

Abstracts

1. THE ORMAK PROGRAM

1.1 ORMAK Operations

The work on ORMAK can be divided into three major phases:

1. Preinjection installation studies of Ohmically heated plasmas. The data obtained from these experiments reinforced our conclusion that the predicated advantages of low aspect ratio were indeed obtained.
2. Injection modification. The device was modified to allow for the use of up to four neutral beam injection systems (two were installed at the time of modification). In addition, the electrical insulation was upgraded, and the ceramic insulators in the liquid nitrogen system were replaced with an improved design.
3. Injection heating experiments. Experiments were started (and are still in process) with supplemental heating using the 250 kW of installed neutral beam injection power.

Ion and electron temperature measurements on plasmas with an injected neutral beam indicate plasma heating which is in agreement with theory for the case of a beam injected parallel to the plasma current. Heating has not been observed, however, for an antiparallel beam. Experiments are under way which should help explain this phenomenon.

1.2 ORMAK Planning and Engineering Group

Two injection heating systems were constructed and installed successfully on ORMAK at midyear. Design continues on improvements for the second two systems. A detailed plan for increasing the toroidal magnetic field into the High Field ORMAK experiment was proposed for and submitted to the AEC-DCTR, and the review process was started by the end of the year. At midyear a conceptual design study was initiated for a feasibility burning experiment (F/BX), and an interim report (reference design version 1) was produced after the end of the year.

Responsibility for major modifications to the ORMAK device and for development of plans for future devices was formalized during the year into the charter of the ORMAK Planning and Engineering Group within the ORMAK Section. The three major activities pursued in this period were preparation for and installation of injection hardware, preparation of detailed plans for a high-field modification to ORMAK, and the initiation of a conceptual design study for a feasibility burner device.

2. PLASMA THEORY AND COMPUTATION

This annual progress report, consisting of very brief descriptions of work undertaken during 1973, is intended only to indicate areas of active interest and not to give a technically adequate summary of results. In many instances, reference is made to more comprehensive descriptions of the research, and in all cases the principal investigator is identified to enable the interested reader to seek additional information. The report is divided into five sections relating respectively to the tokamak program (2.1), the ELMO Bumpy Torus program (2.2), the magnetic mirror program (terminated in June 1973) (2.3), the activities of the Data Handling Group (2.4), and the recently initiated plasma engineering program (2.5).

3. HIGH-BETA PLASMAS

ELMO Bumpy Torus (EBT) construction was completed and operation commenced on September 13, 1973, with four mirror sectors energized. Toroidal feed of particles to the high-beta annuli was observed to uniformly control the energy level of the mirror-confined annuli; data for this are shown. Data from preliminary observations on the resulting toroidal plasma in EBT are also given.

BLANK PAGE

4. ENERGETIC PARTICLE INJECTION

The primary effort of the Energetic Particle Injection Group has been fabrication and reliable operation of the ORMAK beam lines. Two neutral-injection heating units were installed on ORMAK. Each unit is capable of delivering up to 100 kW of neutral-injected power. Both cold gas streaming and impurity input due to beam operation are within acceptable limits.

Improvements in grid design have significantly improved the beam power efficiency. Plasma studies have led to the development of a plasma source which will be a prototype for an ion source employing a 10-cm-diam extraction grid, an increase of a factor of 2 over the present ORMAK source.

5. ATOMIC CROSS SECTIONS, PLASMA DIAGNOSTICS, AND THE CONTROLLED FUSION ATOMIC DATA CENTER

As part of our study of D production, we have measured the total and differential scattering cross sections for D^- formation when D^+, D_2^+, and D_3^+ pass through cesium vapor. The scattering of D^- formed by double electron capture was less than 1% for 90% containment of the D^-. Scattering from incident D_2^+ and D_3^+ was much larger and showed structure indicative of electron capture into repulsive levels of D_2 and D_3. Measurements have been completed of the cross sections for D^- production from H_2^+, H_3^+, and HD_2^+ incident on H_2 gas in the energy range 100 to 600 keV. Cross sections decreased monotonically with energy, and the negative ion equilibrium fraction was the same as that expected for an equivalent-velocity proton passing through H_2. To aid in the interpretation of the heavy-ion probe as a plasma diagnostic technique, we have measured the electron capture and loss cross sections of thallium and potassium ion beams passing through H_2.

In diagnostic developments, the resolution of the ORMAK perpendicular neutral particle spectrometer has been decreased, resulting in increased counting rates and better statistics. A parallel spectrometer has been constructed and calibrated. Preliminary results obtained from a typical ORMAK plasma indicate that (1) the parallel temperature is equal to the perpendicular temperature, (2) the energy spectrum of injected neutrals shows a broad spectrum peaking between 8 and 14 keV, (3) scanning across the horizontal plane of ORMAK indicated a flat density profile for the Maxwellian plasma. During the year, improvements have been made on the pyroelectric bolometer which is to be used to measure energy flow from the ORMAK plasma.

6. MAGNETICS AND SUPERCONDUCTIVITY

The efforts of the Magnetics and Superconductivity Group have been in support of both the present plasma physics programs in the division and the planning of future programs. For the present programs a variety of analytical studies of magnet designs, including thermal performance and field calculations, have been completed. A resistance-optimized 50-kG coil for ORMAK with circular bore and rectangular external shape has been fabricated from machined copper plate and is ready for vacuum potting with epoxy. Proof testing of this coil is planned for the coming year. The coils for the ELMO Bumpy Torus have been completed and placed in service after extensive performance and safety tests showed that operation at 30% above design current would be permissible. Field errors are very low (1.5×10^{-4} times the unperturbed axial field) as required for the experimental program.

Investigation of platinum underlayers for gold-coated stainless steel to reduce migration of substrate constituents was completed, and this double-layer technique was used to coat a new liner for ORMAK. Numerous diagnostic components were also coated for ORMAK. A program to systematically investigate refractory metal coating for future plasma physics experiments has been started. The first materials of concern are vanadium and niobium.

The 166-kG, 7.5-cm-bore Nb_3Sn superconducting magnet was damaged by internal arcing during quench discharges and has been rewound on a newly designed spool to prevent similar damage in the future. A 150-kG Nb_3Sn magnet has been designed for the Physics Division and materials ordered for construction early next year. The major thrust of the superconductivity program has been toward large coils required for future toroidal confinement devices. Conceptual and feasibility designs are being prepared for the feasibility/burning experimental device proposals.

7. CRYOGENIC DIELECTRIC MEASUREMENTS

A literature search has established the limitations of existing data on the dielectric strength of cryogenic liquids and gases. A program to extend the data with statistically evaluated measurements has started, with initial results confirming and extending the existing data in the literature. These early measurements are confined to intermediate ac voltages up to 130 kV, but extensions to 80 kV ac and subsequently to 600 kV dc, 700 kV ac, and 1500 kV impulse are planned.

The conductor materials programs in the Metals and Ceramics Division proceeded to initial characterization but are on standby due to lack of funds for FY 1974.

One paper was presented at the Annual NAS NRC Dielectrics and Insulation Conference.

8. FUSION REACTOR TECHNOLOGY

During the past year the fusion reactor technology studies have included the following areas of investigation: (1) magnetohydrodynamic effects in fusion reactor blankets, (2) materials compatibility studies, (3) neutronics, (4) radiation damage studies, (5) surface studies, (6) system studies, and (7) tritium handling and recovery.

1. The ORMAK Program

D. D. Bates[1] G. R. Dyer S. O. Lewis[2] R. V. Neidigh
L. A. Berry P. H. Edmonds D. C. Lousteau[2] T. F. Ravburn
J. F. Clarke William Halchin[2] J. F. Lyon W. J. Redmond
R. J. Colchin G. R. Haste L. A. Massengill R. G. Reinhardt
G. A. Culton R. E. Hill[2] J. R. McNally, Jr. Michael Roberts
J. S. Culver[2] G. G. Kelley V. J. Meece J. D. Rylander[2]
S. M. DeCamp N. H. Lazar Masanori Murakami W. R. Wing
J. L. Dunlap

1.1 OHMICALLY HEATED EXPERIMENTS

1.1.1 Ion Temperatures in ORMAK from Doppler Broadening[3]

J. R. McNally, Jr. R. V. Neidigh

Rapid scanning spectrometric techniques have permitted the determination of ion temperatures in ORMAK (Oak Ridge tokamak) as a function of time during the discharge pulse for ORMAK plasma currents up to 180 kA. Emission spectra of hydrogen atoms are Doppler broadened in the line wings, characteristic of the initial proton motions prior to charge exchange, and give ion "temperatures" generally less than $kT_i \sim 300$ eV. Impurity spectra of C III and O V, as well as the spectra of He II in helium discharges, lead to somewhat hotter ion temperatures ranging up to a maximum of $kT_i \sim 700$ eV.

1.1.2 Ion Energy Confinement in the Oak Ridge Tokamak[4]

L. A. Berry J. F. Clarke
J. T. Hogan

The ORMAK (Oak Ridge tokamak) experiment gives the first extensive measurement of ion transport in a collisionless plasma. We find a transition from neutral domination to a thermal-conduction limit as the ratio of central electron density to central neutral density varies by an order of magnitude. The results agree with neoclassical predictions of ion thermal transport throughout the whole range.

1.1.3 Thomson Scattering Measurements in ORMAK[5]

M. Murakami W. R. Wing
P. H. Edmonds

Measurements have been made of electron temperatures in the Oak Ridge tokamak, ORMAK, using Thomson-scattered light from a Q-switched ruby laser. The measurements described here were made during the spring of 1973. The measured electron temperature ranges from 0.20 keV to 1.2 keV for average electron densities of 1×10^{13} to 3×10^{13} cm^{-3}. The radial electron temperature profiles observed in stable discharges are broad (flat over about half the limiter radius), while a tendency toward sharpened profiles appears when the discharges become unstable at low safety factor. In these measurements, β_p (plasma kinetic pressure/poloidal magnetic field pressure) is observed to vary as $\bar{n}_e I$, and the resistivity enhancement or anomaly factor (experimental resistivity/Spitzer resistivity) as $1/\bar{n}_e$ at constant current. An empirical expression for the energy confinement time is discussed.

---

1 Instrumentation and Controls Division.
2 General Engineering Division.
3 Abstract of paper in *Nucl. Fusion* 13, 919 (1973).
4 Abstract of paper in *Phys. Rev. Lett.* 32, 36? (1974).
5 Abstract of paper accepted for publication by *Nuclear Fusion*.

BLANK PAGE

1.1.4 The Hot Ion Distribution Function in ORMAK[6]

J. F. Clarke R. V. Neidigh
D. J. Sigmar[7] J. R. McNally, Jr.

If one adds to the neoclassical theory of plasma transport in axisymmetric toroidal confinement systems, the effect of a frictional drag due to charge exchange, then the positive charge acquired by the plasma during initial breakdown should lead to a poloidal rotation in the collisional early stages of the discharge. The theory indicates that the poloidal rotation should be damped by charge-exchange friction with an e-folding time approximately equal to the charge-exchange lifetime. A distortion in the distribution of hot ions, dependent upon Z effective and the ion temperature gradient, is observed as a toroidal plasma flow and becomes the equilibrium condition for ions in the banana regime. We have observed effects in the ORMAK plasma which can be attributed to these processes.

1.1.5 Wall Conditions in ORMAK[8]

R. J. Colchin J. R. McNally, Jr.
L. A. Berry M. Murakami
G. R. Haste R. V. Neidigh
G. G. Kelley J. E. Simpkins
J. F. Lyon W. R. Wing

ORMAK is a diffuse toroidal pinch with typical plasma currents of 100 kA, electron temperatures of 800 eV, and ion temperatures of 300 eV. The walls of the plasma region are made of stainless steel coated with an intermediate layer of platinum 0.05 μ thick and an outer 1- to 2-μ layer of gold. Tests with an ion microprobe mass analyzer have shown that the platinum acts to decrease diffusion of impurities from the stainless steel to the surface. Gold was chosen to inhibit the surface chemical adsorption of gases. Studies with a movable limiter lead us to believe that electron energy is lost at the plasma edge mainly via line radiation and cooling on ions, while ions are lost from the plasma by charge exchange. Thus the walls are bombarded by energetic neutrals, line radiation, and, in addition, bremsstrahlung x rays. The flux of energetic neutrals is measured by a charge-exchange analyzer. Wall bombardment by such neutrals should cause sputtering, and gold has been observed spectroscopically near the limiter, increasing with time during a shot. However, analysis of impurities coated on a window by the discharge indicated very little gold sputtering and redeposition. To measure the sputtering rate, a wall sample was coated with 105 Å of radioactive gold and bombarded with neutrals from ORMAK during a day's run. No measurable sputtering was found within the counting statistics of the measurement, but surface carbon contamination of the sample prevents us from any final conclusions.

1.1.6 Modification of Thomson Scattering Measurements

Following two years of serial redesign and replacement of components in the original Thomson scattering system provided by the University of Rochester, that system has been replaced completely. The original system, together with its problems, is described in ORNL-TM-4354. The system has been replaced by "SCAT-PAK," a single-unit Thomson scattering package carefully designed to provide maximum signal and signal-to-noise ratio.[9] The improvement has been dramatic, a factor of more than 10 increase in available photons and a similar decrease in stray laser light and background plasma light. Simultaneously, the laser access has been redesigned to provide six radial laser measurement points instead of three. Lastly, a computer interface for data acquisition has been implemented.[10] It reads (digitizes and stores) the laser power, as well as all channels of scattered light and plasma background light for each of up to four laser pulses. The interface operates completely in parallel with the oscilloscopes used for monitoring the system performance and in no way perturbs the data signals.

Three examples of data obtained using this system are presented below to illustrate the range of questions that are being attacked with the more detailed and statistically significant data "SCAT-PAK" gives us

---

6. Abstract of paper submitted to *Physical Review Letters*.

7. Consultant, Massachusetts Institute of Technology, Cambridge, Mass.

8. Abstract of paper to be published in the proceedings of the Conference on Surface Effects in Controlled Thermonuclear Fusion Devices and Reactors, in a special issue of the *Journal of Nuclear Materials*.

9. J. S. Culver and M. Murakami, "Mechanical and Optical Coupling of a Thomson Scattering Laser T_e Measurement to the ORMAK Machine," to be published in the Proceedings of the Fifth Symposium on Engineering Problems of Fusion Research, Princeton University, Princeton, N.J., November 5–9, 1973.

10. G. R. Dyer and M. Murakami, "A Low Noise Data Collection System for the Thomson Scattering Apparatus on ORMAK," to be published in the Proceedings of the Fifth Symposium on Engineering Problems of Fusion Research, Princeton University, Princeton, N.J., November 5–9, 1973.

In Fig. 1.1, profiles obtained on the "new" and "old" Thomson scattering systems are compared. Although plasma conditions are different, the reduced scatter in the temperature data is substantially due to the improved equipment. In addition, we can now measure the relative electron density profile because the sensitivity of the system is constant for all spatial points. The discharges from which Fig. 1.1*B* was made, incidentally, have one of the lowest resistance anomalies (referred to the Spitzer resistance) we have measured. Assuming full current penetration, we find $\mathcal{R}/R_{Spitzer} = 2.3$. This is equivalent to a plasma with a uniform effective charge (Z_{eff}) of 3.1.

The initial conditions for the discharges from which the data in Fig. 1.2 were obtained differ only in initial hydrogen gas filling pressure. For convenience we call the narrow, higher density discharge a type A discharge and the broader, lower filling pressure density discharges a type B. The most characteristic signature of a given type of discharge is the magnitude of the helical perturbation in its toroidal current. A type A discharge has a perturbation $(\tilde{B}_p/B_p) \approx 0.2\%$ of the total plasma current while the perturbation of a type B shot is typically only a few hundredths of a percent. The fluctuating fields produced by the rotating helical structure are detected by small magnetic pickup loops. One such loop gives us an estimate of the magnitude of the perturbation, while additional loops which are distributed around minor and major circumferences of the discharge allow us to determine the mode structure of these current fluctuations. The structure in the major direction for the discharges we have examined is always an $n = 1$ mode. The top trace in Fig. 1.3 is a fully developed disturbance (here an $n = 2$ mode but occasionally an $n = 3$) which is characteristic of a type A discharge, and the bottom trace is a weak, higher order mode which is typical of a type B.

Using the profiles at $t = 33$ msec and the measured input power we can construct the following table:

Type	β_p	R/R_{Sp}	Z_{eff}	τ_E (msec)
A	0.35	3.6	4.5	4.3
B	0.29	5.3	8.2	2.8

In this table, τ_E is average plasma energy lifetime and β_p the ratio of plasma pressure to poloidal magnetic field pressure. The trend of larger β_p, lower R/R_{Sp}, and larger τ_E for the type A discharge was found in nearly all of the cases we have studied.

We do not have a satisfactory model for the behavior described in the preceding paragraphs. A model has been proposed to explain similar behavior on the T-4 experiment.[11] It involves impurity transport due to current fluctuations in discharges similar to our type A.

11. V. A. Vershkov et al., "Plasma Behavior with Large Discharge Currents in Tokamak-4," Matt-TRANS-112 (IAE-2291), Princeton Univ., Princeton, N.J.

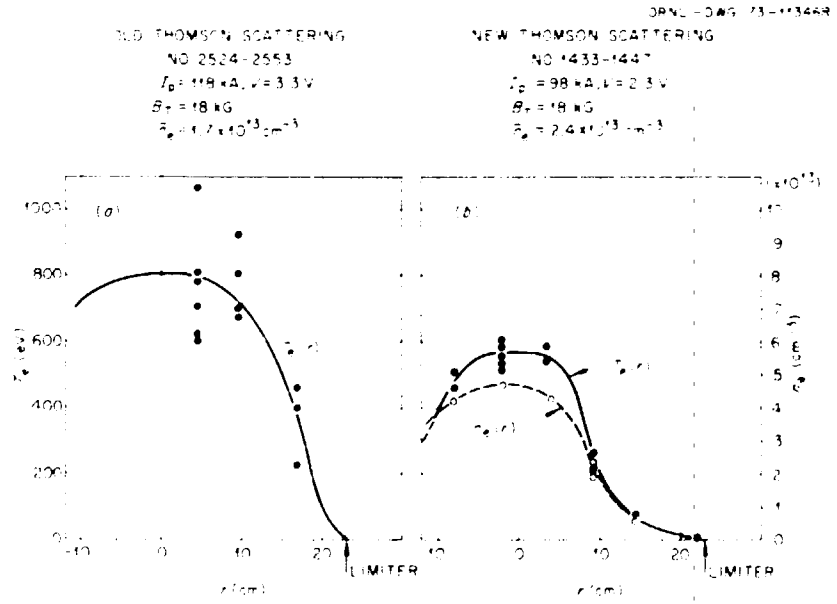

Fig. 1.1. Discharge profiles. The closed circles (T_e) represent individual experimental points. The open circles (n_e) are an average.

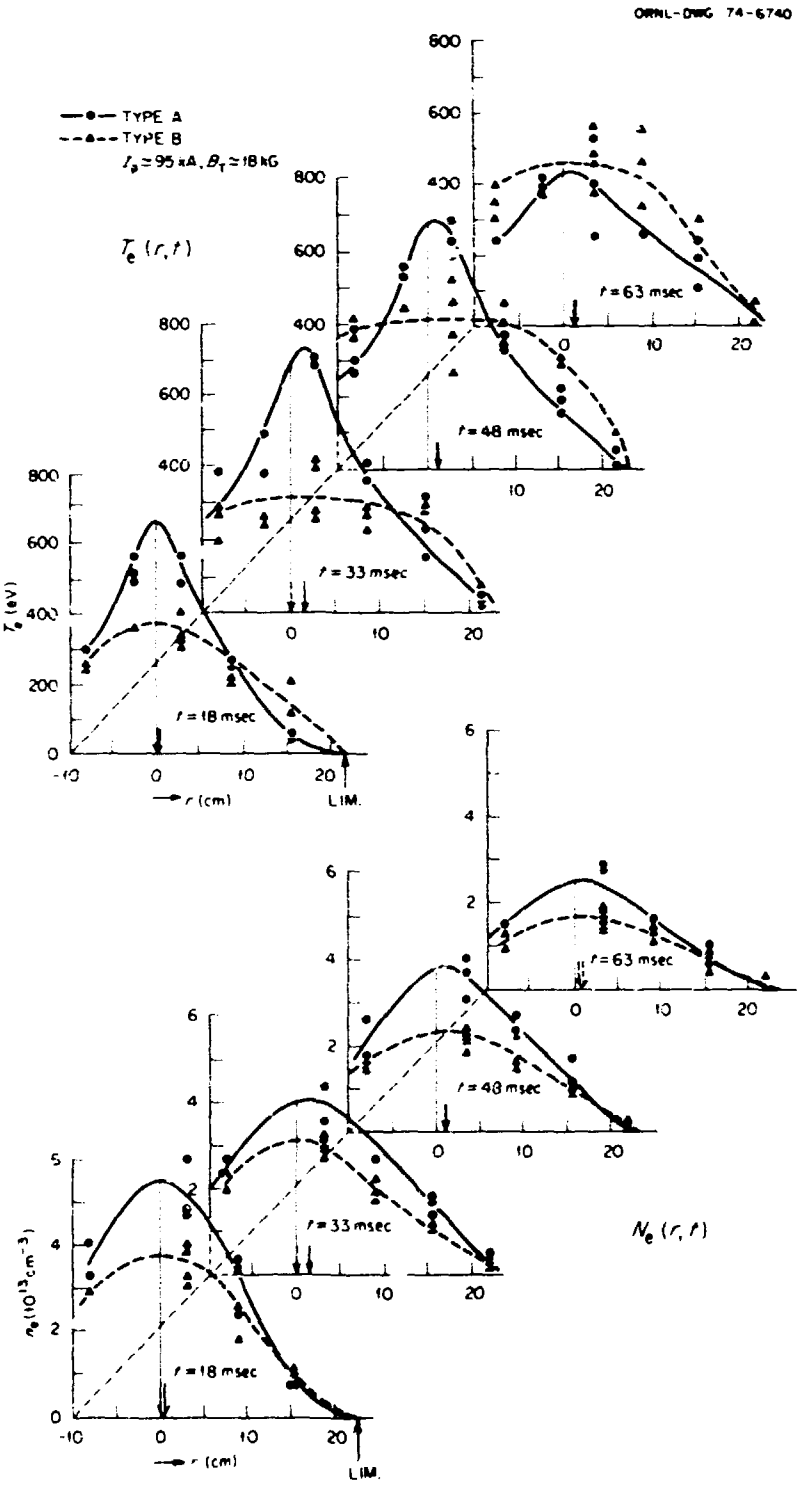

Fig. 1.2. Comparison of electron temperature and density profiles for a type A and a type B discharge. The solid (type A) and dashed (type B) arrows indicate the position of the discharge center as measured by a set of in-out loops. In both cases the plasma voltage drive was taken to zero at $t = 60$ msec.

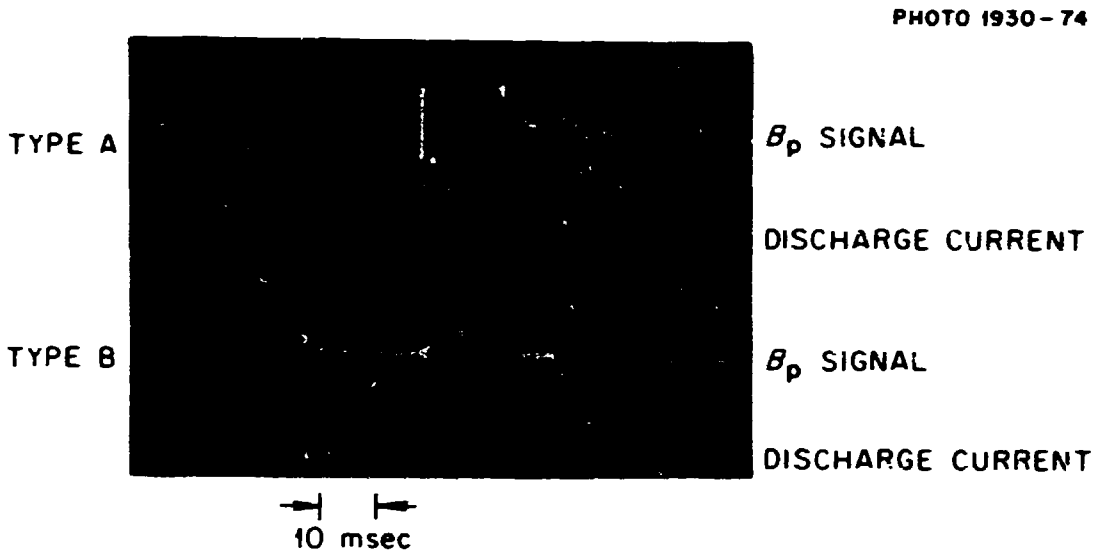

Fig 1.3. Extremes of MHD (poloidal field fluctuation) behavior. The upper traces in each photo are signals obtained from a small pickup loop near the discharge measuring $\dot{B}_p$.

It is apparent from the above discussion that our expanded diagnostic capabilities have initially created more questions than answers. During the coming year we will be able to expand the range of the available data in terms of plasma parameters and begin detailed comparison of the measured and the predicted plasma characteristics.

1.2 NEUTRAL BEAM INJECTION EXPERIMENTS

Two neutral beam injectors were installed and used to heat the ORMAK plasma. A description of the injectors, their interface with ORMAK, and details of machine modifications made at that time have been previously presented.[12-14] In this section a plasma neutral beam heating calculation will be discussed and the experimental results presented. It should be emphasized that both theory and experiment are not completed and the results presented here are preliminary.

1.2.1 Calculation of ΔT_i and ΔT_e Due to Injection Heating

A computer code has been written which combines various elements of injection heating theory developed previously.[15-17] Assuming that the temperature rise due to beam heating can be treated as a perturbation, one can write the proportions

$$\frac{\Delta T_i}{T_i} = \frac{2}{3}\frac{P_{\mathrm{inj},i}}{P_{e\text{-}i}} ,$$

$$\frac{\Delta T_e}{T_e} = \frac{P_{\mathrm{inj},e} + \frac{1}{3}P_{\mathrm{inj},i}}{P_{\mathrm{OH}} - P_{e\text{-}i}} ,$$

where $P_{\mathrm{inj},e}$ and $P_{\mathrm{inj},i}$ are the injection heating powers going to the electrons and ions, P_{OH} is the power input

12. L. D. Stewart et al., "Design of High Power Neutral Injection Heaters for the ORMAK System," to be published in the Proceedings of the Fifth Symposium on Engineering Problems of Fusion Research, Princeton University, Princeton, N.J., November 5-9, 1973.

13. D. C. Lousteau et al., "Mechanical Interfacing the High Power Neutral Injection Heaters to ORMAK," to be published in the Proceedings of the Fifth Symposium on Engineering Problems of Fusion Research, Princeton University, Princeton, N.J., November 5-9, 1973.

14. S. M. DeCamp and J. D. Rylander, "Development, Fabrication and Assembly of a Thin Wall, Low Aspect Ratio Liner and the Enclosed Tungsten Limiter for ORMAK," to be published in the Proceedings of the Fifth Symposium on Engineering Problems of Fusion Research, Princeton University, Princeton, N.J., November 5-9, 1973.

15. R. J. Colchin, J. D. Callen, S. Matsuda, and J. A. Rome, *Bull. Amer. Phys. Soc.* 18(10), 1271.

16. J. A. Rome, J. D. Callen, and J. F. Clarke, ORNL-TM-4332.

17. J. D. Callen, J. F. Clarke, and J. A. Rome, paper E-14 at the Third International Symposium on Toroidal Plasma Confinement, Garching, Germany, March 26-30, 1974.

from Ohmic heating, and $P_{e,i}$ is the power transferred from electrons to ions by collisions. The $^2/_3$ proportionality constant in the first equation arises from the fact that ions, heated by the beam, pass some of this added energy along to the electrons. This energy shows up as $^1/_3 P_{inj,i}$ in the second equation.

The power inputs to the electrons and ions via beam heating ($P_{inj,e}$ and $P_{inj,i}$) are complicated functions of the injection geometry,[15] the slowing-down time, and the charge-exchange loss time. Using electron heating as an example,

$$P_{inj,e} = \sum_{i=1}^{3} \frac{P_B(E_i)}{\pi a^2} \times \int_0^a H(r, E_i)\, G_e(r, E_i)\, 2\pi r\, dr ,$$

where a is the radius of the plasma and $P_B(E_i)$ is the input beam heating power at energy E_i. There are three energy components in the beam resulting from the acceleration of H^+ and the breakup of H_2^+ and H_3^+ molecules. The function $H(r, E_i)$ contains geometry parameters. The beam is assumed to have a radius of 6 cm and a (measured) current profile of the form

$$I = I_0 e^{-r_b^2/6.67} ,$$

where r_b is the local beam radius in centimeters. $H(r, E_i)$ also includes the effects of beam attenuation and trapping. The function $G_e(r, E_i)$ gives the fraction of the power imparted to the electrons in the face of charge-exchange losses. In both $H(r, E_i)$ and $G_e(r, E_i)$, full account is taken of the radial dependence of the density, temperature, plasma current, and neutrals. Neutral profiles are calculated in the same manner as by Hogan and Clarke.[16]

The quantity $P_{e,i}$ is given by

$$P_{e,i} = 3e \int \frac{n_e(T_e - T_i)}{\tau_s}\, dV ,$$

where τ_s is the slowing-down time and the temperatures are expressed in electron volts.

The temperature changes this calculation predicts are shown in Figs. 1.4 and 1.5 for a "low" and a "high" density case. Parabolic profiles have been assumed for $T_e(r)$, $T_i(r)$, and $n_e(r)$. A precise comparison with experiment requires a knowledge of n_0. Although our charge-exchange neutral measurements allow an estimate of the neutral density, it is sufficient here to note that ΔT_i *decreases* as n_e *increases* for fixed n_0. The dominant reason for this scaling is that at the higher electron densities there is less beam power *per ion*. Additionally, we see that for n_0 in the mid 10^8 cm^{-3} range (about what we expect)[4] an ion temperature increase of 25 to 40% would be expected for the lower value of n_e.

1.2.2 Ion Heating

The time-resolved ion temperatures shown in Fig. 1.6 are typical of the ion heating we have observed due to neutral beam injection. Perhaps more important than the magnitude of the ion temperature increase (at least from the viewpoint of understanding the heat processes) is how it scales with plasma parameters. Ion

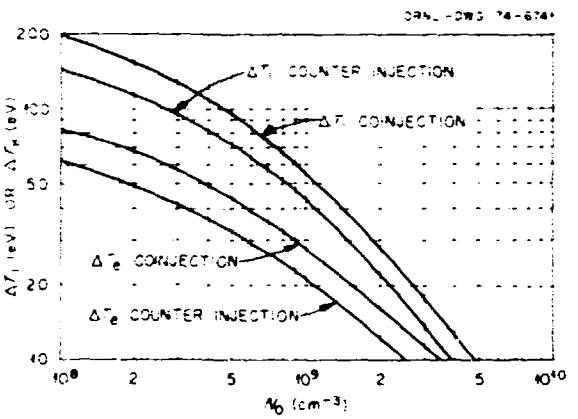

Fig. 1.4. Calculated electron and ion heating as a function of the central neutral density. The parameters used were $n_e(0) = 2 \times 10^{13}$ electrons/cm^3, $T_e(0) = 750$ eV, $T_i(0) = 250$ eV, $I_p = 120$ kA, $V = 3$ V, and 100-kW beam injection power.

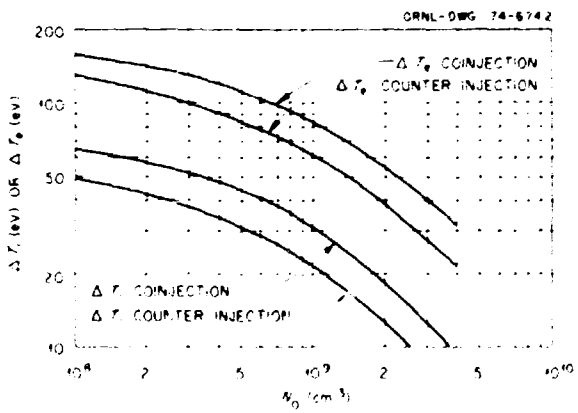

Fig. 1.5. Calculated electron and ion heating as a function of the central neutral density. The parameters used were $n_e(0) = 4 \times 10^{13}$, $T_e(0) = 750$ eV, $T_i(0) = 250$ eV, $I_p = 120$ kA, $V = 3$ V, and 100-kW beam injected power.

---

18. *Thermonuclear Div. Annu. Progr. Rep. Dec. 31, 1970*, ORNL-4688, p. 56, sect. 3.4.2.

temperatures with and without injection (the coinjector only) are plotted as a function of the average electron line density in Fig. 1.7.

We infer from the data presented in the two previous figures that

1. the coinjected (parallel to the plasma current) beam effects an ion temperature increase of from 10 to 40%, which saturates in 10 to 20 msec,
2. no further heating is observed when the counterinjected beam is added,
3. no heating is observed when the counter beam is used alone; additionally (not shown in the figures), a disruptive instability is sometimes instigated by this beam,
4. the general decrease of ΔT_i as n_e increases agrees with the trend predicted in Sect. 1.2.1.

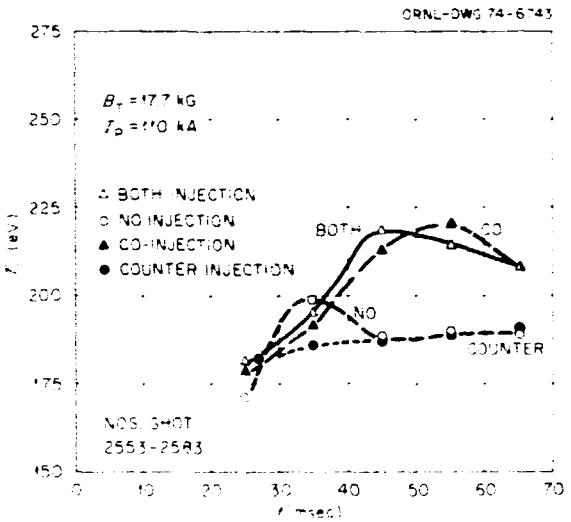

Fig. 1.6. Ion temperatures for different injection heating configurations. The plasma current was held flat from t = 20 to 60 msec, and the injection time was from t = 25 to 65 msec.

1.2.3 Electron Heating

Electron heating due to neutral beam injection has also been observed. The data are not simply interpretable because in addition to the electron temperature increase there is a density increase, as seen in Fig. 1.8. The situation is even more complicated for a type B discharge (Fig. 1.9) because even though the central electron temperature has increased, the profile has narrowed and the average temperature has actually dropped. The large increase in density more than compensates for this drop, however, and we find that β_p has actually increased. The results are summarized in Table 1.1 for t = 48 msec.

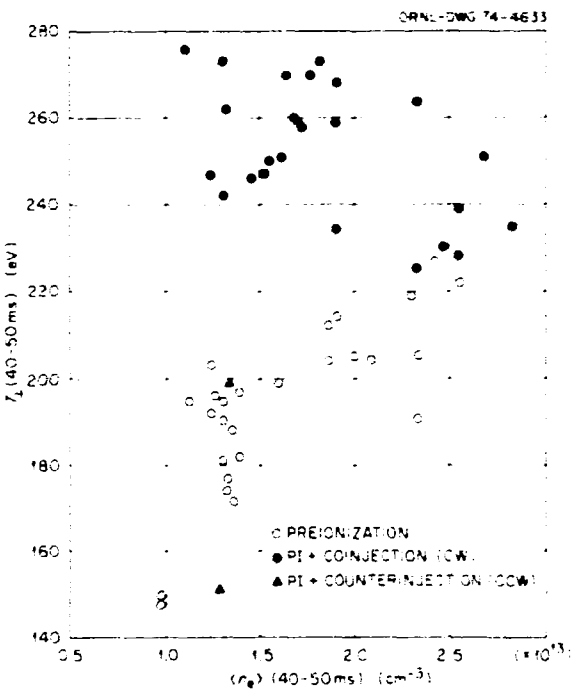

Fig. 1.7. Ion temperature as a function of average electron density (the *line* average) during the period t = 40 to 50 msec.

Table 1.1. Electron heating due to neutral beam injection and Ohmic heating

Discharge type	Injector power (kW)	Ohmic power (kW)	β_p	$\frac{\Delta\beta_p}{\beta_p}$	$\frac{\Delta\bar{T}_e}{\bar{T}_e}$	$\frac{\Delta T_{e0}}{T_{e0}}$	$\frac{\Delta\bar{n}_e}{\bar{n}_e}$	$\frac{\Delta n_{e0}}{n_{e0}}$
A	0	270	0.26					
A	100	250	0.29	0.12	0.27	0.11	0.10	0.18
B	0	340	0.26					
B	100	320	0.33	0.27	0.02	0.37	0.23	0.59

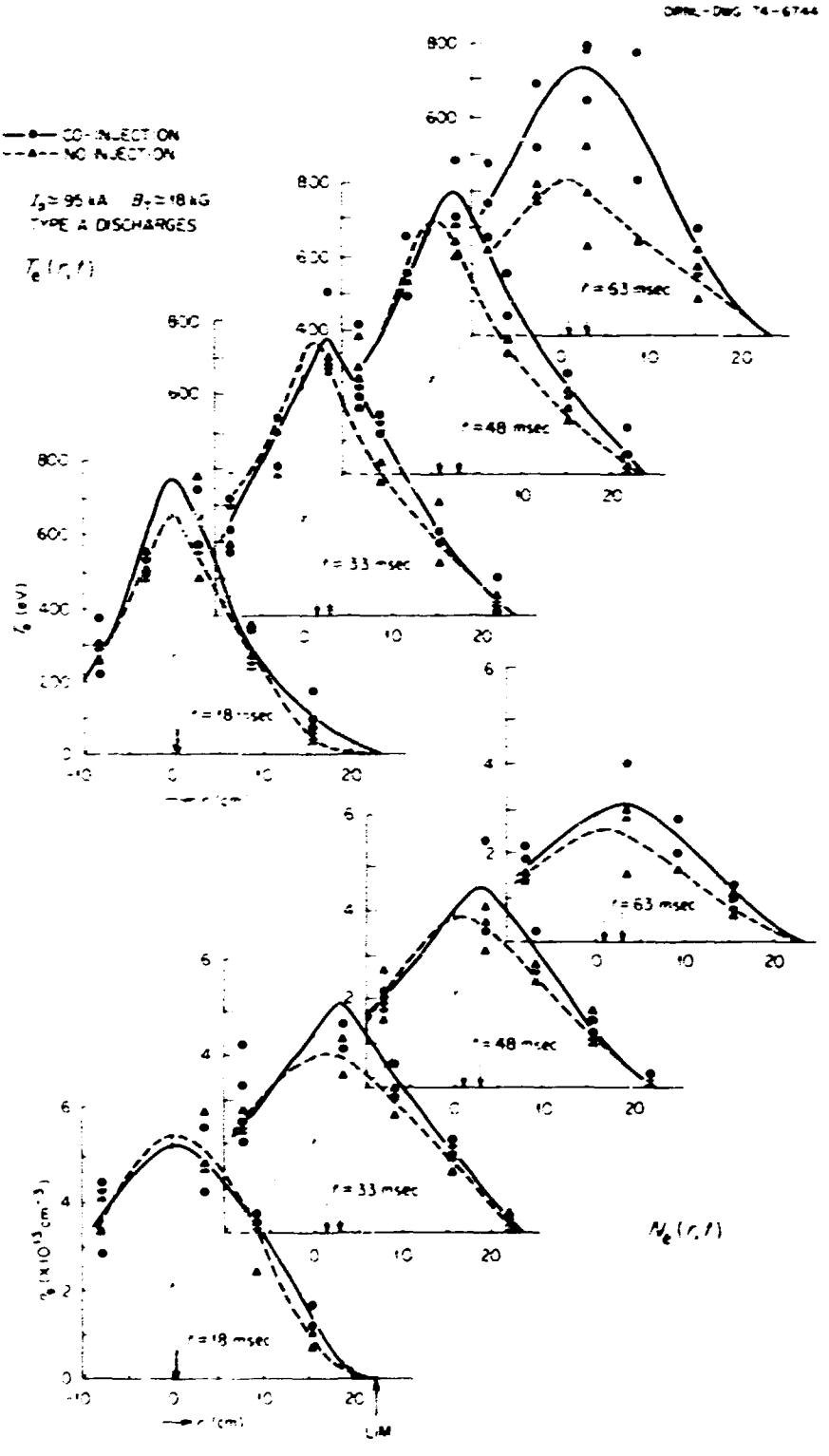

Fig. 1.8. Comparison of electron temperature and density profiles for discharges with and without coinjection for a type A discharge. The arrows refer to the plasma position as measured by a set of in-out loops. The injectors were on for the full duration of the discharge.

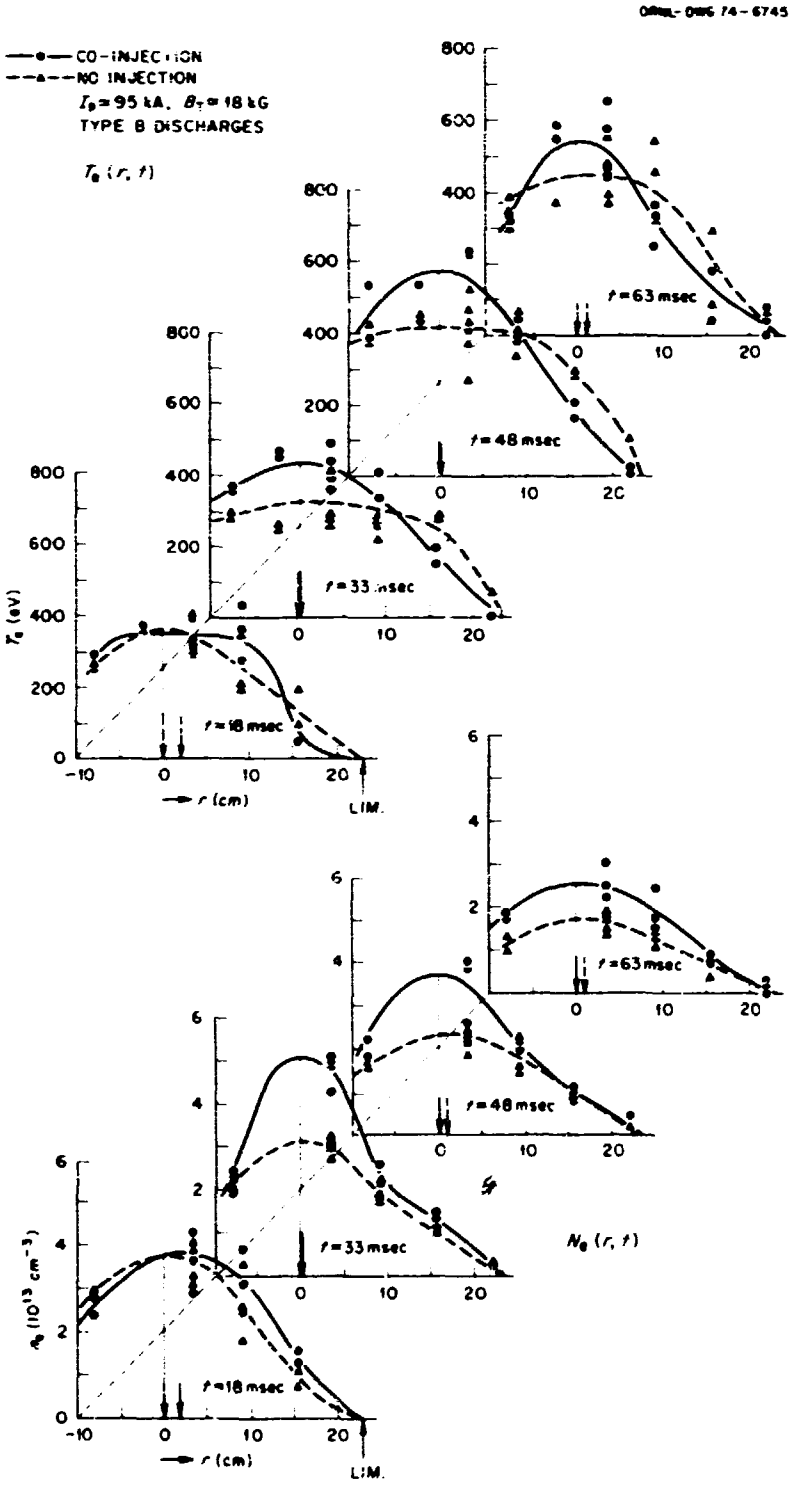

Fig. 1.9. Comparisons of electron temperature and density profiles for discharges with and without coinjection for a type B discharge. The arrows refer to the plasma position as measured by a set of in-out loops. The injectors were on for the full duration of the discharge.

It is obvious that the perturbation-type analysis used in Sect. 1.2.1 is not immediately applicable, because no allowance has been made for allowing the beam to self-consistently modify the plasma profiles. The overall magnitude of the electron effects which we see is, however, at the 10 to 20% level which this incomplete theory predicts (Figs. 1.4 and 1.5).

1.3 ORMAK PLANNING AND ENGINEERING GROUP

D. D. Cannon[2]
W. Halchin[2]
P. N. Haubenreich[19]
R. E. Hill[2]
M. H. Kunselman[2]
A. Legg[19]
S. O. Lewis[2]
R. S. Lord[20]
D. C. Lousteau[2]
D. G. McAlees[21]
R. McCarrell[2]
M. Roberts
J. D. Rylander[2]
L. M. Vinyard[2]
D. R. Wallace[2]

The engineering associated with the translation of the idea of injection heating into usable hardware centered about the control, in vacuum, of the neutral gas associated with the source as well as with the hardware connecting the source to the liner. Design of valves, actuators, housings, and attachments was followed by an abbreviated testing program conducted in vacuum at liquid nitrogen temperature that did bring to light a number of necessary changes in the design. Successful installation of first one and then a second injector in the middle of the year culminated the first phase of the injection modification program.

Recognition of the growing importance of the ability to have access to the injection valving and to the liner joint for tangential diagnostic purposes has led to a further design effort on injector systems 3 and 4. In these two later systems, the injector gas handling vacuum system that is presently integral with the main vacuum tank system will be separately pumped. This separation in topology will permit access without disturbing the main tank vacuum.

The idea of increasing the toroidal magnetic field in ORMAK as a technique of permitting large plasma currents and hence generating plasma significantly closer to fusion plasmas was given a positive push by the work of W. F. Gauster on asymmetric copper coils. The concept of introducing additional copper in the plane of the coil but not at the center constriction region gave rise to a scenario in which the existing generators could be used to drive the asymmetric coil to 50 kG. Further study revealed an alternate approach would be preferable, namely, develop a higher voltage, large power supply (when compared with the generators) and with it drive the existing (or modified) coils. This latter route was followed in preparing a detailed plan of action (UCCND Preliminary Proposal 564) for consideration by AEC-DCTR at the end of the year.

Evaluation by AEC-DCTR of the increasing level of confidence in the progress in confinement experiments and expected results in heating experiments led to the initiation of a study aimed at filling in the basic framework of SCORE – a feasibility D-T burning device conceived last year. At midyear, an eight-man-year effort was undertaken (ORNL-TM-4342) to determine the cost and time estimates, the development and requirements, the state of physics knowledge and expectations, and the general impact associated with the vast project aimed at feasibility and burning experiments (F/BX). By year's end a core of people had been trained and had produced a comprehensive first-draft coverage of a version 1 reference design, based in most areas upon conservative plasma parameters. This design centered about a 4-m-bore plasma of aspect ratio 3 and included feasible design solutions for each of the major components in the device itself and a first look at the entire plant as well.

The configuration chosen as the point of departure for the F/BX conceptual design study was, in most regards, a "conventional" tokamak – circular plasma, circular toroidal field coils, an iron-core transformer driving system, and a neutral-beam heating system. The most striking ways that it differs from earlier devices are its size and the use of superconducting toroidal field coils. The circularity of plasma and coil system is indicated as a means to provide a credible estimate; the noncircular option is also being considered for the next iterations in the study.

The large size is a consequence of present uncertainties in plasma loss scaling and the particular set of plasma assumptions chosen for use in sizing reference design version 1. The estimate of the size required to demonstrate power break-even with a D-T plasma is based on the cautious assumption that high losses associated with trapped ion effects will be encountered before the desired plasma conditions are reached. Other assumptions are that in the feasibility experiments the stability factor, $q(A)$, must not be less than 4 and that the maximum toroidal field (at the coil) will be limited to 75 kG. A "best guess" (neither particularly conservative nor especially optimistic) was used in the very

19. Reactor Division.
20. Physics Division.
21. On leave from the University of Wisconsin, Madison.

important but highly uncertain area of plasma impurities. (We assumed that impurities would be equivalent to $Z_{eff} = 2$.) These design bases and decisions led to large plasmas on the order of 1.9 m minor radius and 5.65 m major radius. A shield around 60 cm thick would be required. On this basis we selected 5.5 m as the bore diameter of the toroidal field coils for reference design version 1.

Conservatism in physics specifications inevitably imposed unprecedented demands on technology. One such area is plasma heating, where 8 to 16 MW must be delivered into the large plasmas. Another is the toroidal field coils, which are of unprecedented size. For the burning experiments a long pulse is desirable, and the reference design requires that the equipment be capable of maintaining the fields and plasma current for 100 sec (assuming that plasma losses will turn out to permit a pulse this long).

Consideration of the unusual requirements on the toroidal field coils led to the decision to use in the F/BX reference design NbTi in the form of multiple filaments embedded in a rectangular matrix of copper or aluminum; the operating temperature, current density, and magnetic field intensity are limited so that the NbTi operates in the superconducting mode. Material of this type has already been developed, and there is every reason to expect that sturdy coils meeting F/BX requirements can be successfully developed and fabricated. The decision to go this way in the reference design is basically a judgment that the chances of timely development and construction and reliable operation of F/BX are better with toroidal field coils of this material than with any other design. Liquid-nitrogen-cooled coils were ruled out because of pulsed fatigue problems and the lack of advantage over a long pulse. Water-cooled coils were considered in an alternate design but because of the pulsed high power requirements appeared to present a more expensive option.

In a number of critical physics areas, such as impurity control involving the magnetic limiter and liner wall, and large plasma current buildup, problems have been identified and specific active techniques and experimental programs are being prepared as solutions and are included in the cost estimate. Because their solutions stand as ideas rather than as demonstrated fact or thoroughly analyzed strategies, their efficacy is recognized to be unproved as yet.

Similarly, in a number of critical technology areas, such as superconducting coils, neutral beam injection, diagnostics, and vacuum, problems have been identified and work is in progress toward demonstrated solutions. In these cases, the development programs, either under way or suggested, involve lengthy progressions of technological investigation requiring intensive, creative work but do not depend upon achievement of any fundamental advances or breakthroughs.

As a result of the high cost involved with the large device implied by reference design version 1, the design study emphasis was refocused at year's end on a somewhat less conservative approach to somewhat lesser goals. This new reference design version 2 would be aimed at power break-even in D-T including beam-plasma interactions in addition to the less conservative parameters.

1.4 FUSION DYNAMICS OF LOSSY REACTOR SYSTEMS

J. Rand McNally, Jr. J. F. Clarke
R. D. Sharp[22] R. H. Fowler[22]

Nuclear fusion reactivity calculations have been made of various types of magnetically confined lossy reactor systems after the method of Etzweiler, Clarke, and Fowler.[23] Radiation-dominated D-T, D-D, D-^{3}He, and D-^{6}Li fueled plasmas reveal a positive reactivity above 5 keV, 50 keV, 50 keV, and 90 keV, respectively, in large reactor systems (a = 5 m) at densities of about 10^{14} electrons/cm^3 and higher.[24]

Beam-plasma reactions in a pulsed-mode F/BX device (a = 1.75 m, R = 6.00 m, $V \simeq 363$ m^3, B_θ = 46 kG, I_ϕ = 3.10 MA, $Z_{eff} = 1$, P_{INJ} = 8 MW at 180 keV D^0 into a D-T or T plasma, $T_0 \sim 1.5$ keV, $n_{e0} = 5.54 \times 10^{19}$ m^{-3}, $\bar{n}_0 \ll 10^{12}$ H^0/m^3) utilizing trapped-particle-loss-dominated,[25,26] radiation-damped conditions lead to about a 20% increase in plasma reactivity in the case 180-keV $D^0 \rightarrow$ D-T vs $H^0 \rightarrow$ D-T.

Large reactor systems (a = 5 m, R = 15 m) which are radiation-damped and trapped-ion-loss-dominated exhibit a plasma "blowout" phenomenon at about 5 - 10 sec when the injected particle energy E_0 is greater than about $\frac{3}{2}\gamma(T_+ + T_-)$. Since energy conduction and

22. Computer Sciences Division.

23. J. F. Etzweiler, J. F. Clarke, and R. H. Fowler, USAEC report ORNL-4083 (1973).

24. J. R. McNally, Jr., R. D. Sharp, R. H. Fowler, and J. F. Clarke, "Reactivity of Closed Fusion Reactor Systems for Advanced Fuels," submitted to *Nuclear Fusion*.

25. B. B. Kadomtsev and O. P. Pogutse in *Reviews of Plasma Physics*, vol. 5, M. A. Leontovich, ed., Consultants Bureau, New York, 1970, p. 249.

26. S. O. Dean, J. D. Callen, J. F. Clarke, H. P. Furth, T. Ohkawa, and P. Rutherford, *Status and Objectives of Tokamak Systems for Fusion Research*, USAEC report WASH-1295, to be published.

particle diffusion losses are about equal, γ is approximately 2. Plasma "blowout" is caused by the deposition of too much net power ($P_\alpha + P_{INJ} - P_R$) in the plasma from alpha particles and injection beam compared to the radiation power. This increased power deposition tends to drive the temperature up, but since the trapped ion losses increase as $T_e^{3.5}$, the plasma density decreases drastically (see Fig. 1.10). Injection of 300-keV D^0 and T^0 at 74 kW/m^3 into a 1.5-keV D-T plasma leads to plasma ignition at $T \sim 5$ keV after 2 sec of injection and then a positive reactivity (temperature and power excursion) for 3 sec. As T_e approaches 20 keV the plasma "blows out" during the next 5 or more seconds to a very low-density, high-temperature regime until equilibrium is established at

$$E_0 = \frac{3}{2}\gamma(T_i + T_e) - \frac{\tau}{n_e}(P_\alpha - P_R).$$

Here, P_α is the alpha power density produced from the D-T reaction, P_R is the radiation power density, and τ is the particle loss time, which is proportional to $T_e^{-3.5}$.

Alternatively, if E_0 is lowered to $E_0' = 10$ keV *after* ignition, a steady-state tokamak or orthogonal tokamak[27] is possible with $Q' = P_{out}/P_{in} \sim 70$. Charge-exchange losses will decrease this value of Q'; however, tailoring of the plasma density profile will reduce the trapped ion losses and thus may permit some increase of charge-exchange losses. The use of injection energies which are appropriately lower than that used here for ignition of the plasma (300 keV) will produce a flattening of the density profile as a result of the reduced penetration of the energetic neutrals into the plasma – this decreases the trapped ion losses, which vary as $[(1/n)(dn/dr)]^2$ according to Kadomtsev and Pogutse.[25] An injection energy of 50–100 keV would give quite good penetration for fueling, reduce the density gradients, and even eliminate the severity of the "blowout" in the absence of any reduced density gradient – for 100 keV, $Q = 3.8$, and for 50 keV, $Q = 9.7$.

27. J. R. McNally, Jr., Proc. Paris IAEA Symposium, *Nuclear Data in Science and Technology*, vol. 2, p. 41, 1973.

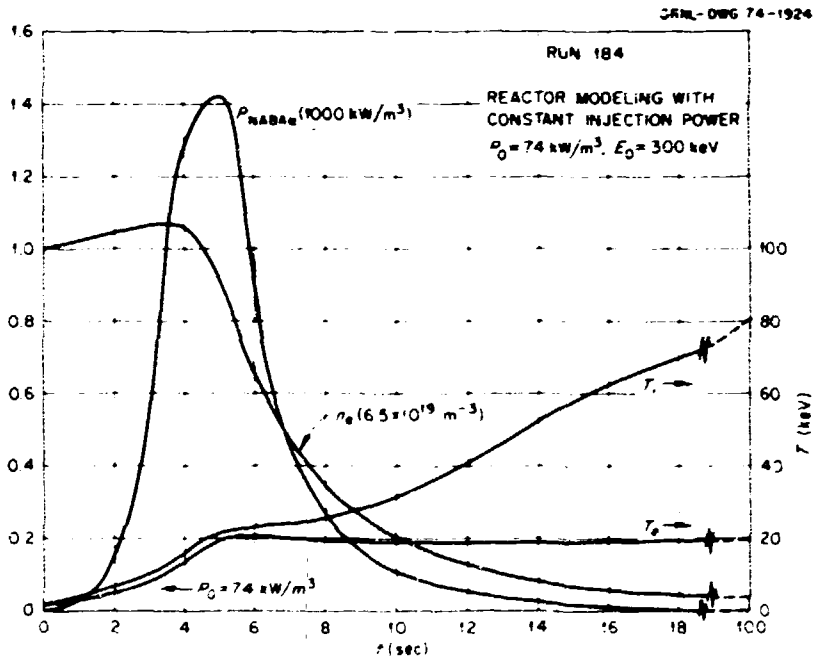

Fig. 1.10. Ignition, thermal runaway, power excursion and plasma "blow-out" characteristics of a large tokamak reactor heated by 74 kW/m^3 of 300-keV D^0 and T^0. Full trapped ion losses operating. $R = 15$ m, $a = 5$ m, $I_\theta = 8.9$ MA, $B = 43$ kG, $n_0 < 10^{12}$ m^{-3}, $n_{e0} = 6.5 \times 10^{19}$ m^{-3}, $T_0 = 1.5$ keV. $P_{NABA\alpha}$ = power output in neutrons, blanket (4.8 MeV/neutron), and alpha particles.

2. Plasma Theory and Computation

C. O. Beasley, Jr.
N. A. Betz[1]
P. D. Brooke[1]
J. D. Callen
P. Chrisman[2]
J. F. Clarke
E. C. Crume
R. A. Dory
J. L. Dunlap[3]
H. W. Eubank[4]
W. M. Farr[5]
R. H. Fowler[1]
J. E. Francis
G. E. Guest
C. L. Hedrick
H. R. Hicks[1]
J. F. Lyon[3]
H. K. Meier
D. G. McAlees[6]
J. E. McCune[7]
D. B. Nelson
C. E. Parker
J. A. Rome
G. O. Spies[8]
D. A. Spong[9]
O. C. Yonts

2.1. PLASMA CONFINEMENT AND HEATING IN TOKAMAKS

2.1.1 Impurity Effects on Tokamak Discharges

2.1.1.1 Radiation. R. A. Dory has surveyed the impurity radiation literature and provided codes for use in the one-dimensional, time-dependent transport code to follow the ionization state histories of carbon and oxygen impurities including ionization, recombination, and excitation processes, corona equilibrium generation where applicable, and dynamics where required.

2.1.1.2 Resistance anomaly. E. C. Crume has analyzed published data on tokamak discharges in hydrogen using various impurity models (with and without neoclassical modifications to the classical Spitzer resistivity) to assess the most plausible resistance anomaly values. The calculations give one-dimensional, self-consistent pictures of the discharge at specified times, usually chosen to coincide with the times at which temperature and density profiles are measured. The impurity ionization states are calculated in various ways including those mentioned in Sect. 2.1.1.1 under various assumptions as to the prior electron temperature and density. Resistance anomalies range from 2.3 to 10, relative to Spitzer, and 1.8 to 6, relative to neoclassical. Although different impurity models yield results which differ considerably in detail (and in some conclusions), there are some general similarities: (1) If only low-Z impurities are considered (e.g., carbon and oxygen), the relative impurity concentration must exceed 10% of the hydrogen density for Spitzer-based anomalies greater than 4. Less than 1% concentrations of high-Z impurities (e.g., tungsten or gold) have the same effect. (2) These impurities are predicted to be highly collisional throughout the discharge. (3) Models in which the impurity concentrations are peaked near the center of the discharge can yield q (safety factor) profiles predicted to be MHD unstable, in keeping with recent explanations of observations made on tokamak T-4.

2.1.2 Neutral Injection Heating in ORMAK

2.1.2.1 Neutral-beam injection into a tokamak: Part 1: fast-ion spatial distribution for tangential injection[10] (J. A. Rome, J. D. Callen, and J. F. Clarke). The production processes and spatial distribution of fast ions resulting from tangential injection of a diffuse neutral beam into a tokamak are discussed. The spatial distribution of fast ions for various injection trajectories and absorption mean free paths are calculated and discussed in detail. Maximum beam absorption for a parabolic density profile is shown to occur for injection

1. Computer Sciences Division.
2. Present address: Massachusetts Institute of Technology, Cambridge.
3. Formerly of Target Plasma Group, now in ORMAK Group.
4. Present address: Plasma Physics Laboratory, Princeton University, Princeton, N.J.
5. Present address: University of Arizona, Tucson.
6. On leave from University of Wisconsin, Madison.
7. Consultant, Massachusetts Institute of Technology, Cambridge.
8. Present address: Courant Institute of Mathematical Science, New York University, New York, N.Y.
9. On leave from University of Wisconsin, Madison.

10. Abstract of paper in *Nucl. Fusion* **14**, 141 (1974).

roughly halfway between the inner wall of the torus and the magnetic axis; however, since the fraction of beam absorbed is near unity and only weakly dependent on the injection trajectory, this is not an important optimization. Since the drift orbit surface area over which the fast ions are distributed is roughly proportional to the distance from the magnetic axis, the fast-ion density is found to be strongly peaked at the magnetic axis for present experiments where the absorption mean free path λ is comparable to the plasma radius, a. This geometric peaking effect is strong enough to overcome the exponential beam attentuation and cause the fast-ion density and consequent beam energy deposition to be peaked at the plasma center as long as $\lambda_0 \gtrsim a/4$. Charge exchange can deplete the fast-ion population, particularly near the plasma edge. When charge exchange is an important loss mechanism, beam injection nearly tangent to the magnetic axis is found to maximize the beam effectiveness in heating.

2.1.2.2 The power transferred to plasma ions and electrons from injected ions. J. D. Callen and J. A. Rome have improved upon earlier estimates of the fractional energy given up by injected ions to plasma ions and electrons by allowing for the loss of fast ions through charge exchange with hydrogen atoms. The results are displayed in Fig. 2.1, which shows the fractional powers G_i and G_e as functions of the initial energy E_0 relative to the energy E_c, for which the rates of energy transfer to ions and electrons are equal. Callen and Rome point out that impurities, included in the evaluation of E_c, have no significant effect on this calculation.

2.1.2.3 Plasma heating induced by neutral beam injection. Given the fraction of fast-ion energy transferred to the plasma ions and electrons in the presence of impurities and charge-exchange neutrals, Callen has developed procedures for calculating the ion and electron temperature increases caused by neutral beam injection. Procedures have also been developed for estimating the other plasma perturbations[11] (current, momentum, and density) produced by neutral beam injection. These calculations were illustrated for a particular ORMAK injection case and serve as the basis by which the theoretical results are compared with experiment as in Sect. 1.2.

2.1.2.4 Injected ion distribution in energy. Rome and Callen obtain the energy distribution function of the fast injected ions by solving a drift-kinetic equation

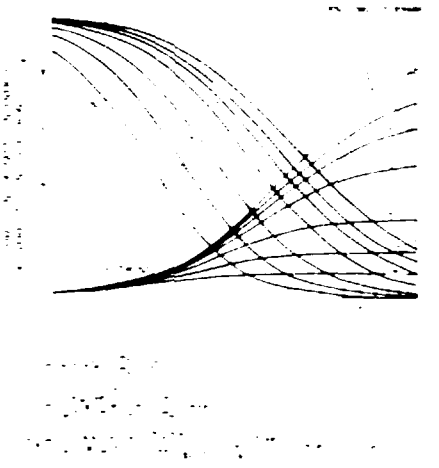

Fig. 2.1. Fraction of fast ion energy transferred to plasma ions (G_i) and electrons (G_e) in the presence of charge-exchange neutrals.

with a Fokker-Planck collision term using a multiple time scale analysis. If the fast-ion speed, v_b, is much greater than the plasma-ion thermal speed, v_i, but much less than the electron thermal speed, v_e ($v_i \ll v_b \ll v_e$), the appropriate Rosenbluth potentials may be expanded in an asymptotic series and the resulting kinetic equation averaged over the quasi-periodic bounce orbits, giving a complicated but tractable equation for $\partial f_b(v, \zeta)/\partial t$. Here $\zeta = (v_\parallel/v)_{\theta=0}$ is a convenient pitch-angle variable. This averaged Fokker-Planck equation has been solved analytically in limiting cases with $v_\parallel \gg v_\perp$ and neglecting the effects of the toroidal electric field and diffusion in speed (relative to dynamical friction) for a step-function source. More generally *the equation has been solved numerically for initial* conditions chosen to model experiments in ORMAK. Typical results at two different levels of impurity concentration, $\langle Z \rangle = 1$ and 10, are shown in Fig. 2.2. The addition of high-Z impurities greatly enhances the pitch-angle scattering, even if $E_0 \gg E_c$.

2.1.3 Diagnostic Application of Neutral Beams

J. A. Rome (in collaboration with H. W. Eubank, of Princeton) and G. E. Guest have proposed two different techniques for using neutral beams to measure the poloidal magnetic field in tokamak discharges. Rome's approach uses the shift of the guiding-center drift orbits of counterinjected ions. Part of a neutral beam which is counterinjected into a tokamak is scraped off by the limiter. The edge of the region of contained ions can be measured by a tangential charge-exchange analyzer. Using conservation of canonical angular momentum, the poloidal flux profile can be obtained, and from this

---

[11] *J. D. Callen, J. F. Clarke, and J. A. Rome, paper E-14* presented at the Third Int. Symp. on Toroidal Plasma Confinement, March 26–30, 1973, Garching, Germany.

the poloidal B field and heating current profiles can be easily calculated. Guest's technique utilizes the so-called stagnation orbit, that is, the guiding-center drift orbit which remains in the equatorial plane. Particles in the stagnation orbit satisfy a relation $e\,B_p(r_s) \cong Mv_b/R$, so that a measurement of the energy of such a particle determines the poloidal magnetic field at that point.

2.1.4 Two-Dimensional Tokamak Equilibria

R. A. Dory and R. H. Fowler have extended earlier work on two-dimensional, ideal MHD equilibria to include various elements of current interest, utilizing the extensive data on pressure profiles from ORMAK to narrow the range of parameters. For ORMAK (with

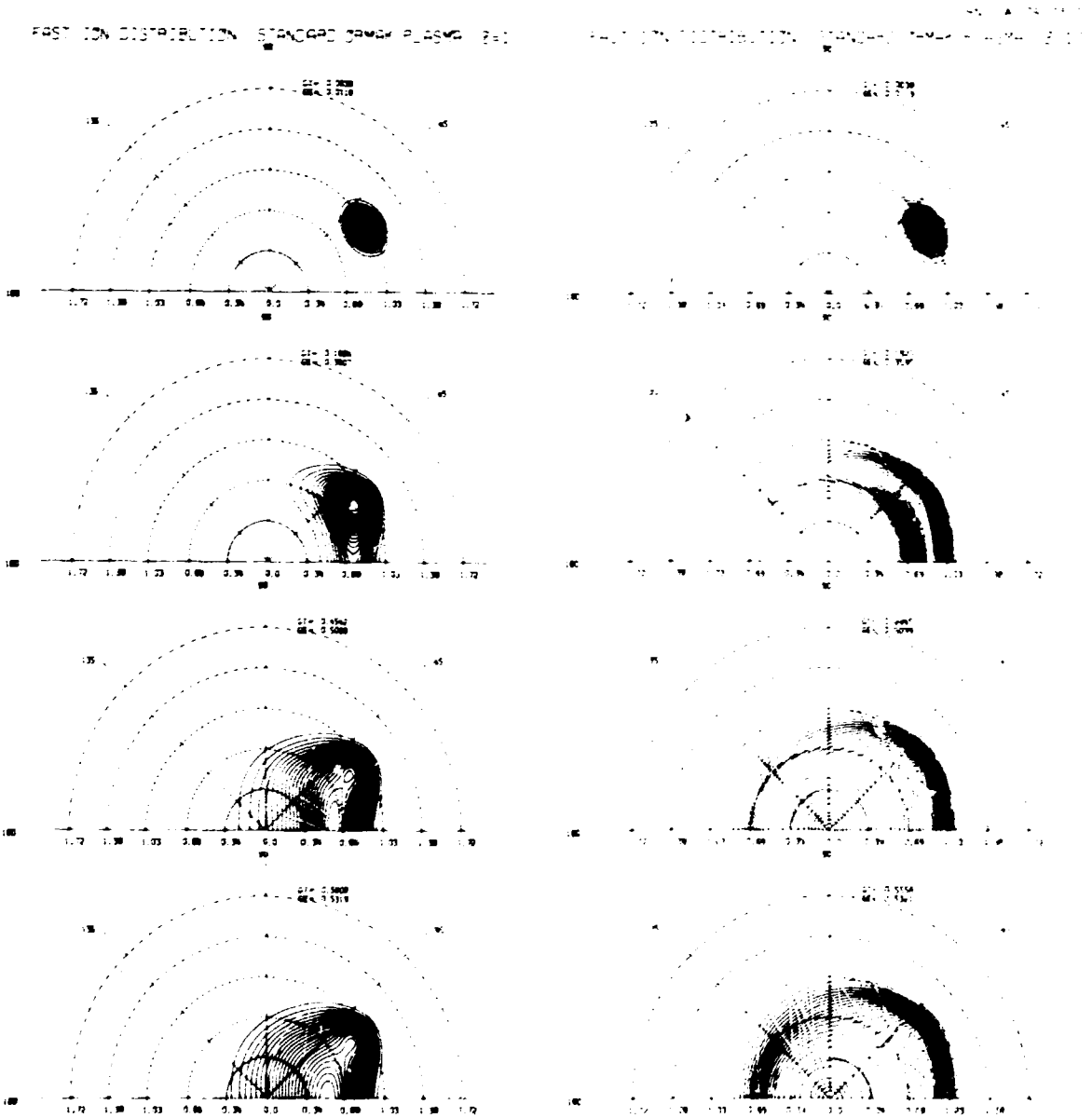

Fig. 2.2. Temporal development of the fast-ion distribution function for coinjection with $\ell/\ell_i = 1.10$.

circular cross section) they have studied perturbations of the magnetic flux surfaces caused by the vertical field coils, finding possibly significant effects as shown in Fig. 2.3. More generally they have examined equilibria with noncircular cross sections, ranging continuously from elliptical to D-shaped. Together with C. O. Beasley and G. E. Guest, Dory and Fowler have studied the guiding-center drift motions of trapped particles with special emphasis on the stability of collisionless trapped-particle modes. In interesting regimes (e.g., high $\beta_{poloidal}$), plasma diamagnetism is partially successful in providing favorable drifts to stabilize the collisionless trapped-ion modes and mitigate the dissipative trapped-ion modes. It is found, however, that the observed drift speeds, while in the stable sense for most of the plasma volume, are small enough to cause concern over enhanced transport from field errors, for reasons discussed earlier by Ohkawa.

2.1.5 MHD Stability of Two-Dimensional Tokamak Discharges

R. A. Dory, E. C. Crume, and H. R. Hicks have continued the development of a technique for solving the MHD equations of motion for two-dimensional models of the tokamak discharge, with realistic choices of pressure and current profiles. To date, the effort has centered on an Eulerian description of the fluid motions, but treatment of realistic boundaries has proved difficult. In related analyses, D. B. Nelson has obtained a simple one-dimensional reduction of the three-dimensional variational principle result for δW. The technique gives estimates of stability boundaries, growth rates, the stabilizing effects of shear, and magnetic field gradients which can be used to select initial conditions for examination via the numerical solution of equations of motion. This work is in progress.

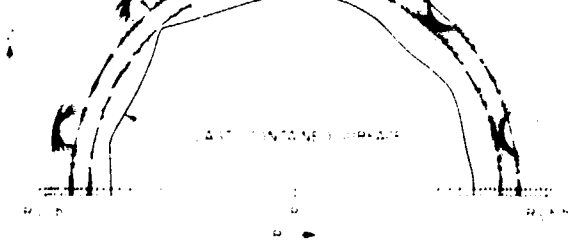

Fig. 2.3. Surface distortion from vertical field coils.

2.1.6 Runaway Electron Physics

D. A. Spong J. F. Clarke

Two aspects of runaway-dominated discharges which have been investigated are the evolution of runaway electron drift surfaces[12] and the stability of a toroidal relativistic electron beam against kink-type perturbations.[13] New results indicated by the drift surface analysis are a shrinkage of the runaway beam radius with time and a limitation on the maximum attainable γ, $\gamma_{max} \lesssim (\omega_{ce}/\omega_{pe})^2$. The kink mode stability analysis was motivated by a parameter study[14] made of ORMAK runaway discharges which indicated that values of q (the inverse rotational transform) less than 1 may have been reached. The stability analysis was fashioned after work done by Lee;[15] however, a velocity shear modification was added in order to make the analysis more applicable to runaway discharges. It was found that velocity profiles peaked on the outside tend to be less stable than a constant velocity profile, whereas those peaked in the center of the beam are somewhat more stable.

2.1.7 Magnetic Island Formation in a Tokamak Plasma from Helical Perturbations of the Plasma Current[16]

P. Clarisman J. F. Clarke J. A. Rome

We have studied the formation, structure, and some of the consequences of magnetic islands in a tokamak plasma, which may be produced from helical current perturbations in the plasma. The existence, structure, and magnitude of the current perturbations causing the island formation are deduced from experimental measurements of the time rate of change of the poloidal magnetic field in the ORMAK device.

The exact distribution of the current perturbations in the plasma causing these poloidal magnetic field variations is not known, but based on the experimental results and theoretical models of the resistive tearing mode instabilities, we chose what we believe to be a satisfactory model for the perturbations. We give physical justification for our model and show that it leads to the formation of magnetic islands of ~3-cm width in the plasma. We also give some physical insight

12. D. A. Spong and J. F. Clarke, ORNL-TM-4432 (1973).
13. D. A. Spong and J. F. Clarke, ORNL-TM-4512 (1974).
14. D. A. Spong, J. F. Clarke, J. A. Rome, and T. Kammash (to be published in *Nuclear Fusion*).
15. E. P. Lee, *Phys. Fluids* 16, 1072 (1973).
16. Abstract of ORNL-TM-4501.

as to the structure of the islands and how they break up into so-called ergodic regions as the perturbation strength increases. Finally we comment on the relevance of magnetic islands to tokamak phenomena.

2.2 PLASMA CONFINEMENT AND HEATING IN THE ELMO BUMPY TORUS

2.2.1 A Vlasov Theory of Ballooning Instabilities

G. E. Guest, C. L. Hedrick, and D. B. Nelson have considered a hot-plasma model whose density is uniform in two directions ($\hat{y}$ and $\hat{z}$) but decreases monotonically in the $\hat{x}$ direction. It is immersed in a $\hat{z}$-directed magnetic field which is uniform in the absence of plasma. With plasma present, a diamagnetic current flows in the negative $\hat{y}$ direction, balancing the force due to the pressure gradient and causing the magnetic field to increase in $\hat{x}$. For this model they have studied the stability of plasma waves which extend indefinitely in $\hat{z}$, propagate in the $\hat{y}$ direction, and are polarized with the wave magnetic field in the $\hat{z}$ direction (the analysis is localized in $\hat{x}$), using the linearized Vlasov equation to calculate the charge and current densities associated with the waves. Low-frequency ($\omega \ll \Omega_i$, the ion gyrofrequency) instabilities are found which have properties similar to those attributed to the ballooning modes predicted in variational analyses; in particular, the modes are not stabilized by the magnetic well produced by plasma currents. However, the characteristic frequency of the unstable wave is around the guiding-center drift frequency; and in a hot-electron plasma of moderate size (e.g., EBT) this frequency may easily exceed the ion gyrofrequency, thus invalidating the MHD description. From the Vlasov analysis, it is found that the modes are stabilized if the drift frequencies exceed the ion gyrofrequency, as shown in Fig. 2.4, where the characteristic frequency increases with β, the independent parameter of the model.

2.2.2 The Stability of Anisotropic Equilibria in Closed-Line Tori[17]

D. B. Nelson C. L. Hedrick G. O. Spies

In this memorandum we consider truly toroidal, nonaxisymmetric closed-line tori (bumpy tori). However, by studying only a subclass of equilibria we are able to achieve much of the simplicity of the axisymmetric problem.

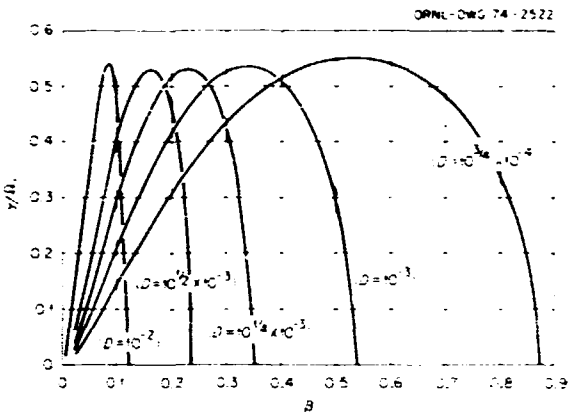

Fig. 2.4. Growth rate as a function of plasma pressure, β, for several values of the parameter $D \equiv c^2/(2r^2\Omega_i^2)$.

If we label magnetic lines by a pair of flux coordinates (α, β), then, in general, the functional form of the equilibrium pressure tensor is $P(B, \alpha, \beta)$. In this work we shall demand that P depend on only one flux coordinate, that is, $P(B, \psi)$, and we shall assume that the constant ψ contours form nested tori. Such equilibria are only partly two-dimensional because the magnetic field is assuredly not constant on a ψ contour. However, by employing an extension of Hamada coordinates to anisotropic equilibria, we arrive at a stability problem which closely resembles the two-dimensional axisymmetric case.

To determine the stability of these equilibria, we consider the second variation of potential energy, δW, and we define stability as positivity of δW for all allowable perturbations and instability as negativity for some allowable perturbation. We are unable to find a single condition on the equilibrium which is both necessary and sufficient for stability. By considering special perturbations, we determine necessary conditions for stability, while by relaxing constraints on the perturbations (i.e., considering unallowable perturbations), we find sufficient conditions for stability. The resultant expressions are presented in parallel forms which allow estimates of the uncertainty gap between the strongest necessary condition and the weakest sufficient condition.

The underlying model which we assume to describe the plasma is the zero-order guiding-center plasma, although some of the results are valid for the guiding-center fluid (or double adiabatic fluid) as well, and in the scalar pressure limit are comparable to infinite conductivity scalar pressure MHD. None of the analysis requires an assumption of low plasma pressure although

17 Abstract of ORNL-TM-4109.

in this limiting case certain of the expressions are simplified.

2.2.3 Some Techniques for Determining Tensor Pressure Equilibria[18]

C. L. Hedrick G. E. Guest D. B. Nelson

In this report we discuss several iterative techniques for computing finite-beta, tensor-pressure equilibria of guiding-center plasmas. These techniques have evolved in the course of investigations of the equilibrium and stability of plasmas confined in several existing and proposed experimental devices at ORNL: ELMO, the Canted-Mirror Facility, the ELMO Bumpy Torus, INTEREM, IMP, and the proposed Long-Field Experiment. These devices encompass magnetic configurations ranging from axisymmetric simple mirrors, through various forms of magnetic "wells," to a closed-line torus. For this reason the present review must deal with several distinct plasma models of varying complexity required to describe the experimentally observed equilibria in these different devices.

2.2.4 Sufficient Stability Criteria for Plasma Equilibria with Tensor Pressure[19]

G. O. Spies D. B. Nelson

Sufficient stability criteria are derived which are valid in all situations for which an energy principle holds: tensor or scalar pressure, collisionless or collisional dynamics, toroidal or open-ended geometry, conducting or insulating walls, closed or ergodic magnetic field lines. These criteria reduce to well-known ones in toroidal equilibria with scalar pressure. They are close to necessary criteria in low-beta equilibria, allowing for interchanges. Various well-known favorable properties (good curvature, magnetic well, negative V'', line-tying) are recovered by considering special classes of equilibria. But since none of these properties appears to be crucial in general, the present criteria are capable of yielding a variety of hitherto unknown stably confined equilibria.

2.3 CONFINEMENT AND HEATING IN MAGNETIC MIRRORS

2.3.1 Importance of Cold-Electron Drifts in Shallow-Well ECH Mirror Plasmas[20]

E. C. Crume J. L. Dunlap J. F. Lyon

Experiments on low-β, shallow-well ECH mirror plasmas show that favorable nonrelativistic electron drifts (vacuum $\partial J/\partial r < 0$ at the resonant heating contour are required for generation of the plasma and also determine the radial extent of the plasma.

2.3.2 Relativistic Electron Adiabaticity in the Finite-β Plasmas of ELMO and IMP[21]

E. C. Crume

Estimates of the maximum adiabatic energy of electrons heated by ECH in two ORNL mirror experiments have been made using primitive criteria and compared with results from experiments. The criteria are of the usual type based on guiding-center theory that provide estimates of the maximum particle energy for particle confinement in inhomogeneous magnetic fields. The criteria were evaluated along calculated field lines for both the vacuum fields and the finite-β modified fields of numerically calculated plasma equilibria. For the ELMO machine, a mirror machine in which the hot (relativistic) electron plasma forms a cylindrical annulus, the calculations indicate that the primary effect of finite β on adiabaticity is to reduce the plasma volume in which the highest energy electrons are adiabatic from that in the vacuum field. On the other hand, for the minimum-B IMP machine, the calculations indicate that the primary effect is to reduce the maximum adiabatic energy from that in the vacuum field. Experimental results from both machines are in agreement with these primitive estimates.

2.3.3 Microinstabilities in Inhomogeneous Plasmas II: Numerical Results[22]

C. O. Beasley, Jr. W. M. Farr
H. R. Hicks J. E. McCune

Results are presented from studies of microinstabilities in a model mirror plasma. The model has a Gaussian density distribution of ions and electrons along a varying magnetic field and a radial density gradient perpendicular to this field. Particles are contained self-consistently by a fictitious confining potential modeling mirror confinement. The ion velocity-space distribution is the finite-plasma equivalent of a

---

18. Abstract of ORNL-TM-4076.
19. Abstract of ORNL-TM-4452.
20. Abstract of paper submitted to *Physics of Fluids* for publication as a Research Note.
21. Abstract of paper 1A14 presented at the 1973 Annual Meeting of the Division of Plasma Physics (Philadelphia, Pa.).
22. Abstract of ORNL-TM-4523 and accepted for publication in *Nuclear Fusion*.

Guest-Dory loss-cone distribution, and the electron distribution allows for finite temperature effects, including Landau damping. Resonant and nonresonant loss-cone instabilities are discussed. It is found that resonant instabilities are stabilized when the plasma length is less than a critical length which is dependent upon electron temperature, but modes corresponding to flute modes in homogeneous plasmas (Dory-Guest-Harris and drift-cone) are found to remain unstable at all plasma lengths.

2.3.4 Program IPP6 – Microinstabilities in Inhomogeneous Mirror-Contained Plasmas[23]

C. O. Beasley, Jr. H. R. Hicks

A description of the program IPP6, the program for finding unstable loss-cone modes in a model mirror-contained plasma, is given. The input data are described, the output is explained, and the internal workings of the various subprograms are given. Connection is made with the previously published analytical derivation of equations used in formulating the model.

2.3.5 Subroutine CAUCHY - Complex Roots of a Function Using a Cauchy Integral Technique[24]

C. O. Beasley, Jr. H. K. Meier

A description of the subroutine CAUCHY, the program for finding zeros of an analytic function $f(z)$ within a contour in the complex z plane, is given. Calculations of zeros for several different examples are given.

2.4 DATA HANDLING GROUP

R. A. Dory J. E. Francis
N. A. Betz C. E. Parker
P. D. Brooke O. C. Yonts

The Data Handling Group was formed in July 1973 to coordinate the data handling needs of the Thermonuclear Division. Prior to this time, the same people carried on the same work without formal recognition of the scope of the project or an allocated budget for implementing the work.

Through December 1973, this group planned and acquired a computing network[25,26] to provide data acquisition facilities for the several CTR experiments and include provision for transfer of experimental and theoretical data to and from the Oak Ridge Computer Center facilities.

Interconnection of the data acquisition computers (DACs) through a remote entry station (RES) has been effected and testing of the communications hardware carried out. The control software for making data transmission a reality has been implemented but not yet fully checked out or placed into operation. Certain subsets of the network are operational in a provisional sense.

The RES function of providing input and output facilities between the Thermonuclear Division at the Y-12 site and the Computer Center at X-10 has been made operational.

The DAC function for the ORMAK facility[27] has been put into operation, including acquisition of 24 channels of time-resolved information through the main DAC, a Digital Equipment Corporation PDP-12, and through the "front-end" PDP-8/e's which provide the high data rates required. The data from the three computers are collected in the PDP-12 and stored permanently on small magnetic tapes for future reference, and analysis of those data whose processing is understood is carried out between experimental shots and displayed on a video screen. In the near future, the data will be transferred via the RES to the Computer Center, where the information will be available to scientists who will analyze it, using the time-sharing facilities of the PDP-10 and video output displays in the Thermonuclear Division.

A similar implementation of a data system for the ELMO Bumpy Torus experiment has been carried out by J. Reynolds of the Instrumentation and Controls Division, under the direction of R. A. Dandl. This system is now approaching completion.

A third system, originally acquired to handle data from the now-terminated IMP experiment, is used for advanced development of data acquisition systems for other experiments. Initial usage by the Magnetics and Superconductivity Development Group is expected shortly, and a first software implementation has been completed and is now in the testing stage.

---

23. Abstract of ORNL-TM-4475.
24. Abstract of ORNL-TM-4588.

25. N. Betz, R. A. Dory, J. E. Francis, and O. C. Yonts, *Proposal for Data System for ORNL Fusion Experiments*, ORNL-TM-3593 (1971).
26. O. C. Yonts and J. E. Francis, "Thermonuclear Division Data System," *Proceedings DECUS Conference Philadelphia, 1973*.
27. J. E. Francis, O. C. Yonts, and W. R. Wing, "ORMAK Data Handling System," Princeton Fusion Engineering Conference, 1973.

Data systems have been sketched out for advanced experiments under discussion in the Thermonuclear Division, namely, ORMAK-II and F/BX versions I and II.

Division needs in the area of large-scale computing have been anticipated through participation in three ad hoc committees[28] convened by the AEC Division of CTR to justify and specify the proposed CTR Computer Center to be based at Lawrence Livermore Laboratory with fast communication lines to four remote user service computers, one of which would be located in this division.

Codes have been generated for magnetic design of CTR experiments, including analyses of fields, flux surfaces, particle drift surfaces, and coil forces and stresses. These have been used in studying the ORMAK and EBT.

2.5 PLASMA ENGINEERING STUDIES

As experimental devices increase progressively in size and complexity, the need for a dedicated effort to interface the plasma physics and engineering areas during design will become more pronounced. In addition to synthesizing present-day plasma confinement and heating results for use in the engineering design of next-generation experiments, those involved in this activity will initiate and evaluate concepts applicable to future devices.

A prototype for such an effort was recently undertaken. As part of the feasibility-burning experiment conceptual design,[29] a plasma parameter study was made to determine the sensitivities of various plasma characteristics to engineering and physics constraints. The result was a set of plasma reference parameters, determined self-consistently from both the physics and engineering points of view, which were incorporated into a feasibility-burning experiment conceptual study.

The detailed orbit dynamics of ~3.5-MeV alpha particles in a tokamak geometry were analyzed.[30] Based on alpha particles produced isotropically in velocity space, guiding-center trajectories were used to determine the total fraction of alpha particles lost from the system due to excursions of orbits which intersect the limiter (or wall, in the case of a reactor). Results to date indicate that <20% of the alpha particles are lost from a device with a plasma current I = 2 to 3 MA and that <1% are lost from a reactor characterized by I = 15 to 20 MA. Implications of such losses are presently being analyzed. Results from the alpha-particle considerations are applicable to future deuterium-tritium–fueled devices.

---

28 Reports are forthcoming from AEC Division of CTR.

29. M. Roberts, *The ORMAK - F/BX Facility - Preliminary Considerations*, ORNL-TM-4342 (1973).

30. D. G. McAlees and H. K. Forsen, *Bull. Amer. Phys. Soc.* 18, 1305 (1973).

3. High-Beta Plasmas

R. A. Dandl[1] R. L. Livesey
H. O. Eason M. W. McGuffin
A. C. England J. W. Reynolds[1]
H. Ikegami[2] R. E. Wintenberg[1]

3.1 EBT

The ELMO Bumpy Torus (EBT) was in its final constructional phase during most of 1973, and on September 13, 1973 (at 4:20 PM) the first microwave plasma was formed in EBT, and the hot-electron annular rings were observed in the microwave-fed cavities. The facility has operated routinely since that time, and we have taken a considerable amount of reliable and useful experimental data.

The EBT is a specific toroidal array closely modeled after stable, steady-state, high-beta, hot-electron plasmas produced earlier in the ELMO open-ended trap by electron cyclotron heating. The EBT is expected to derive MHD stability from the average minimum B generated by the high-beta, mirror-confined, hot-electron shells typical of the ELMO plasma. Such annular hot-electron plasmas have been experimentally generated in each mirror section of EBT with only the outermost edges of the annuli line-tied against flutes by cold-plasma conduction to chamber walls.

We are encouraged by the observed stability in the present EBT, as well as in straight- and canted-mirror experiments, as long as the pressure exceeds a critical value. Although this stability is ascribed to some form of line-tying, there is evidence to indicate that conducting end plates may not be necessary. It is possible that the stabilization stems from the electrostatic confinement of a cold-electron component produced by ionization of the ambient background gas.[3]

Bumpy torus confinement of single particles has been shown by a number of authors[4] for a wide range of magnetic parameters. The neoclassical diffusion coefficient is given approximately by[5,6]

$$D \cong \frac{1}{2}\langle v_T^2 \rangle \frac{\nu}{\Omega^2 + \nu^2} ,$$

where Ω is the precessional frequency, v_T is the toroidal drift velocity, and ν is the effective collision frequency. The plasma confinement time in EBT of a collisionless, neoclassical plasma can be approximately given by

$$\tau = \left(\frac{R}{a}\right)^2 \tau_{ei} ,$$

where R/a is the aspect ratio of the torus. We expect plasma currents to significantly modify the magnetic field. These effects are being studied experimentally since it is difficult to obtain a unique pressure profile theoretically from first principles. Part of our program is, therefore, to optimize the vacuum field and to develop the analytical and experimental techniques for study and control of the equilibrium.

A schematic of EBT is shown in Fig. 3.1. The 24 coils are arranged in the bumpy torus configuration so as to give a mirror ratio of 2:1 with 15° cant angle between the planes of adjacent coils. This requirement is based upon experiments in the canted-mirror facility in which total stored plasma energy was observed to decrease by only 25% for 15° as compared with 50% for 22.5° cant angle. The major radius of the torus is 150 cm with an aspect ratio 10:1. The radius of the cavity sections

1. Instrumentation and Controls Division.
2. On leave from Institute of Plasma Physics, Nagoya University, Nagoya, Japan.
3. G. E. Guest and E. G. Harris, *Phys. Rev. Lett.* 27, 1500 (1971).
4. B. B. Kadomtsev and O. P. Pogutse *Nucl. Fusion* 11, 67 (1971).
5. L. M. Kovrizhnykh, MATT-TRANS-82 (October 1968).
6. L. M. Kovrizhnykh, *Soviet Phys. JETP* 29, 475 (1969).

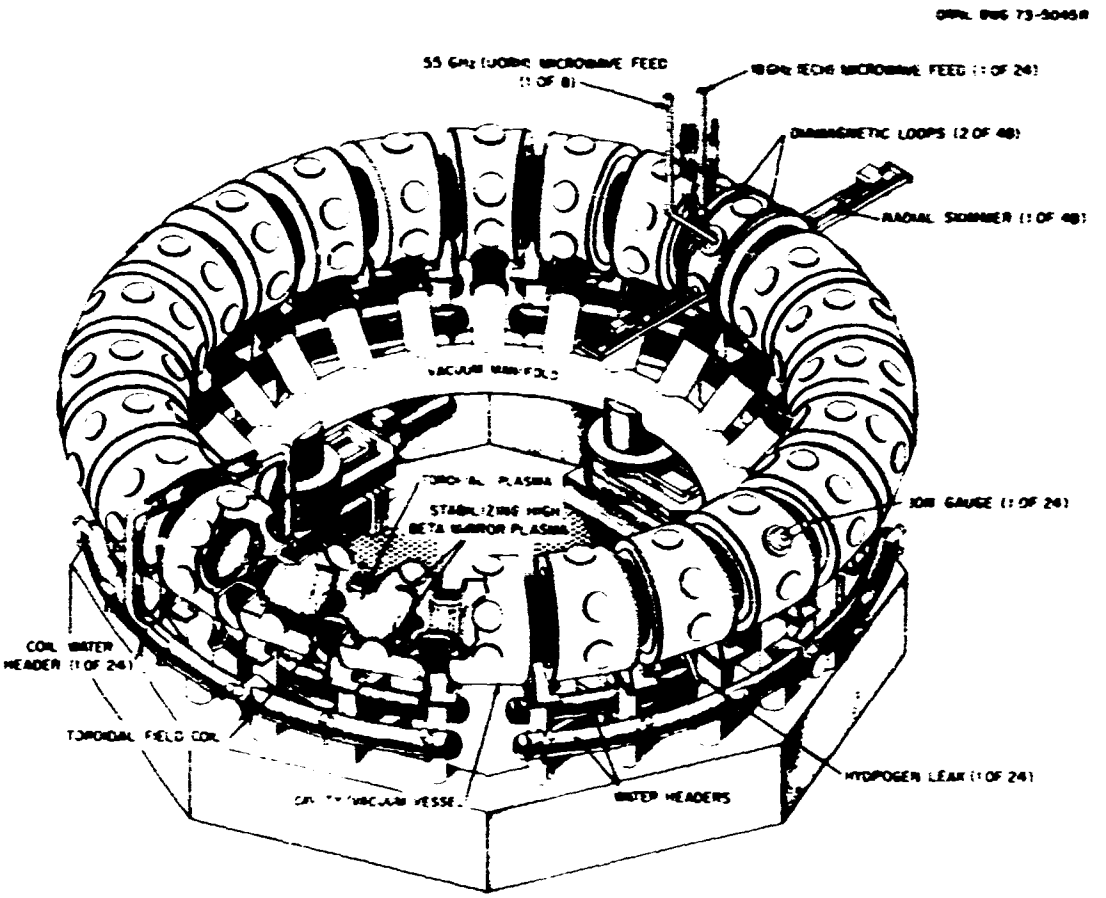

Fig. 3.1. ELMO Bumpy Torus.

enclosing hot-electron annuli is 30 cm with a maximum midplane magnetic mirror field of 6500 G.

The plasma is formed and heated by two 18-GHz klystron amplifiers with 30 kW (cw) divided into 24 equal parts in order to provide separate power feed to each individual mirror region of the torus. Resonant power feed to each mirror region is necessary for balanced excitation, because of the strong plasma absorption of power at the electron cyclotron frequency. Each klystron feeds alternate mirror regions in order to maintain overall power feed balance. A significant feature of the microwave technology is the degree of control of plasma parameters, such as density, temperature, amount of hot electrons, and, consequently, the location of drift surfaces, by the use of resonant and off-resonant frequencies. Two traveling wave amplifiers, at 55 GHz with 10 kW cw, generate the off-resonant power, which is almost entirely absorbed by the hot-electron annulus.

The average plasma density was determined by microwave interferometry and by measuring the perpendicular energy by diamagnetic loops coupled to the hot-electron shells, radial profiles, by skimmer probes; bremsstrahlung analysis allowed estimation of the hot-electron temperature and density, and Langmuir probes are used to determine the cold-plasma temperature and density profiles.

Magnetic field errors are known to destroy plasma confinement in closed-line devices, such as bumpy tori and multipoles, by causing the magnetic field lines to spiral out and strike the wall. In order to estimate the amount of error field in EBT, the shift of a pulsed electron beam trajectory caused by an artificially imposed error field was measured. The error field due to the asymmetry of the toroidal coil assembly (assumed to be uniformly distributed over the entire toroidal axis) was measured to be about 1.5×10^{-4} of the toroidal field. A more complete analysis of plasma

losses due to error fields shows them to be the dominant loss mechanism in EBT for a plasma of density less than 10^{12} cm^{-3} with the electron temperature 100 eV.

Preliminary experimental results were obtained with 4 out of the 24 cavities energized with 18-GHz resonant power (full-power operation will be under way in mid-March).

Although EBT in this initial phase was more like a vacuum bumpy torus than the high-beta EBT concept, we have made several important observations: the formation of stable annular plasmas (with significantly high beta) in each microwave-fed cavity with only edge stabilization by means of cold plasma line-tying, very efficient local power absorption (low-Q coupling) (90%) of the 18-GHz power in each fed cavity, nonlocal absorption (high-Q coupling) of the upper-off-resonance heating (UORH) power (55 GHz) shown in Fig. 3.2, and a toroidal plasma ($10^{11} < n_e < 10^{12}$) confined for several milliseconds. Figure 3.3 shows the dependence of two important plasma parameters as a function of microwave power: the total stored energy in the high-beta stabilizing relativistic electron plasma vs power and the cold toroidal density vs power. These curves show a power dependence very close to the

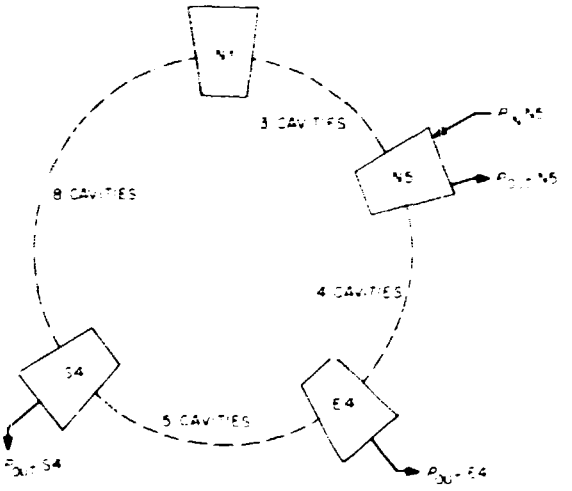

POWER SOURCE	$\frac{P_{OUT\,N5}}{P_{IN\,N5}}$	$\frac{P_{OUT\,E4}}{P_{OUT\,N5}}$	$\frac{P_{OUT\,S4}}{P_{OUT\,N5}}$
18 GHz ECH			
WITH PLASMA	1×10^{-4}	7×10^{-4}	7×10^{-4}
WITHOUT PLASMA	5×10^{-3}	0.2	0.4
55 GHz UORH			
WITH PLASMA	6×10^{-4}	0.35	0.35
WITHOUT PLASMA	1.1×10^{-3}	0.4	0.43

Fig. 3.2. EBT microwave attenuation measurements.

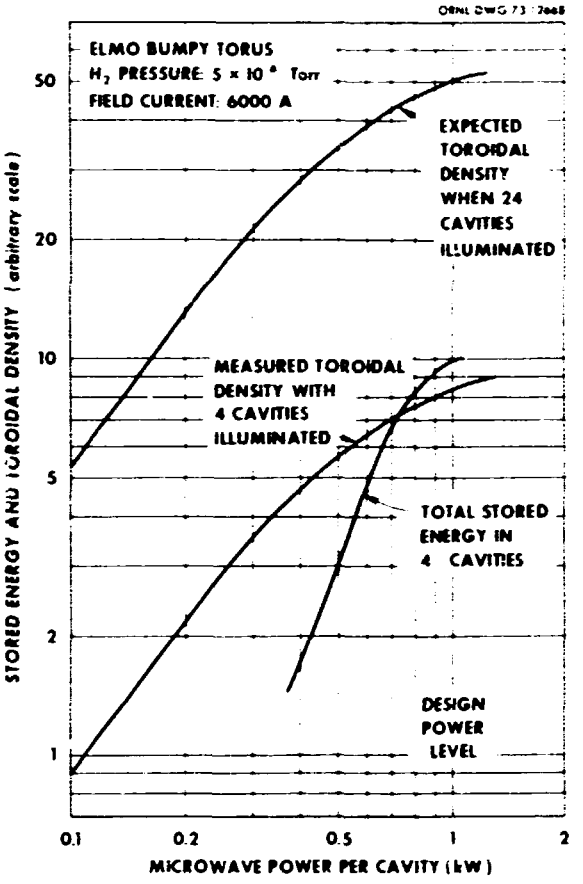

Fig. 3.3. EBT plasma parameters vs power.

calculated form. The uppermost curve shows the expected toroidal density vs power with all 24 high-beta annuli energized. Under some conditions the toroidal plasma profile is close to that predicted by the drift surface calculations preliminary to the machine design. The coupling between the mirror regions and the toroidal region by particles moving from one confinement regime to the other was sufficiently strong to cause all of the high-beta annuli being formed (i.e., 4) to have nearly the same diamagnetic strength without critical adjustment of the high-beta parameters in each mirror section.

Average plasma density is measured from the microwave interferometer to be 5×10^{11} cm^{-3}, and after turnoff of the microwave heating power, plasma density remains at 5×10^{11} cm^{-3} for about 1 msec (Fig. 3.4) then decreases to 3×10^{11} cm^{-3} in the next 1 msec, and about 7 or 8 msec later it again decays abruptly. At this time a sudden burst of x rays was observed, as shown in Fig. 3.4, indicating the destruction of the

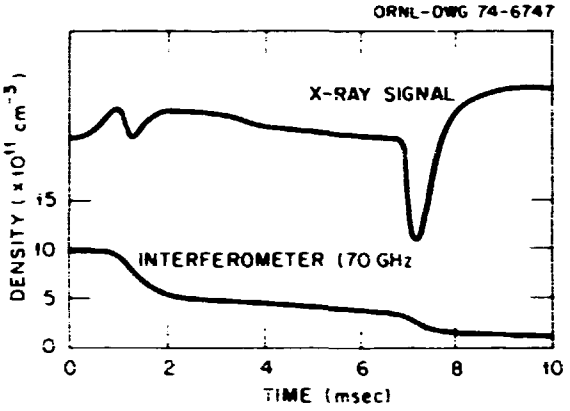

Fig. 3.4. Plasma density decay indicating high-beta annulus stabilization effect. The upper trace is x-ray-signal-detected by a small ionization chamber inserted on the inner wall of one of the four energized chambers (resonant power 18 GHz at 6 kW and off-resonant power 55 GHz at 2 kW). The lower trace is the 70-GHz microwave interferometer signal. Steady hydrogen gas feed at 3×10^{-6} torr.

hot-electron shells. These observations indicate some stabilization effects from the high-beta annulus with only four cavities energized.

The cold-electron temperature as measured by Langmuir probes indicates that the plasma outside the hot-electron shell has a temperature of about 4 eV, filling the region adjacent to the wall. The electron temperature shows a steep change across the hot-electron shell, that is, 10 V/cm, and the temperature of the toroidal plasma just on the inner edge of the hot-electron shell is observed to be more than 20 eV. The electron temperature of toroidally confined plasma cannot be conveniently measured by this probe method. We are preparing to use soft-x-ray detectors to measure the temperature of this component.

The electron density radial profile measured by the ion saturation current also delineated the confined plasma inside the hot-electron shell from the unconfined cold plasma outside the shell.

All of the basic machine functions, that is, microwaves, magnetics, vacuum, and controls, have been very satisfactory from the start, and the magnetic field lines of this 10-ft-diam torus closed to within 1.5 mm without corrector fields. One of the more pleasant experimental observations was macrostable annulus formation at a pressure considerably below the pressures usual for simple ECH mirror experiments.

The high-beta experiments starting in mid-January will be confinement oriented with special emphasis on the quantitative effects of average favorable $\int (1/B)dl$ stabilization of the toroidal plasma, so that the effect on confinement of such things as the magnitude and perturbed shape of the stabilizing annuli will be studied in as much detail as possible.

Later in the year we hope to obtain the following experimental information: (1) By controlling the microwave power and gas pressure, we hope to study the transport mechanisms of the EBT plasma from the medium collisional regime into the collisionless regime. (2) We also expect to control the plasma pressure in the hot-electron shell and to some extent its geometry so that MHD stabilization can be optimized. These results could provide insight into stable, high-beta toroidal confinement.

3.2 POLARIZATION OF FREE-FREE BREMSSTRAHLUNG FROM MAGNETICALLY CONFINED PLASMAS[7]

A. C. England

The polarization of bremsstrahlung from electron-ion collisions is calculated for magnetically confined electrons in the Born approximation. The polarization at high temperature is found to be of opposite sign to the low-temperature result and of smaller magnitude.

3.3 HIGH-β PLASMA BEHAVIOR IN A CANTED MIRROR[8]

R. A. Dandl A. C. England
H. O. Eason J. C. Sprott

A high-β hot-electron plasma was studied in an asymmetric magnetic mirror device with a variable cant angle. The plasma was produced by microwave heating at a frequency corresponding to cold-electron cyclotron resonance together with a higher frequency suitable for upper-off-resonance heating. The position of the high-β plasma annulus was studied as a function of cant angle and was found to correspond approximately to the position of a midplane modulus-B contour. High-β effects did modify the spatial location of the losses of energetic electrons into the loss cone but had little effect on the cold-plasma losses. Destabilization was not observed when the line-tying of the plasma center was reduced with glass end plates. An asymmetry of the cold-plasma loss with respect to the equatorial plane was observed at small cant angles, and an electric field model was conjectured to explain this behavior.

7. Abstract of ORNL-TM-4103, also *Phys. Rev. A* 8, 1475 (1973).

8. Abstract of ORNL-TM-4153, also *Nucl. Fusion* 13, 693 (1973).

4. Energetic Particle Injection

R. C. Davis
J. C. Ezell
R. R. Hall
T. C. Jernigan
O. B. Morgan
L. D. Stewart
W. L. Stirling
R. E. Wright

4.1 ORMAK INJECTION

The primary effort of the Energetic Particle Injection Group has been centered on fabrication and reliable operation of the ORMAK beam lines. A number of important factors have been stressed to ensure success in neutral-injection heating.[1]

Two neutral-injection heating units were installed on ORMAK. One of these units is shown in Fig. 4.1. The injector is thermally isolated from the ORMAK liquid nitrogen temperature environment. The neutralizing cell (not shown) is coupled directly to the ion source and uses the excess hydrogen gas coming from the source. A 3-in. valve is located in the beam line which allows the ion source to be removed while ORMAK is cold and under vacuum.

To significantly heat the plasma, the beam power input must be comparable to the Ohmic heating power input, typically 200 to 400 kW for ORMAK. Test stand measurements indicate that the plasma is receiving up to 100 kW of neutral-injected power per source. This is typically composed of 45% 25-kV H^0, 45% 12½-kV H^0, and 10% 8⅓-kV H^0.[1,2] The plasma attenuation of these neutral beam fractions is calculated to be 93, 97, and 99% respectively.[1]

1. L. D. Stewart, R. C. Davis, J. C. Ezell, T. C. Jernigan, O. B. Morgan, W. L. Stirling, and R. E. Wright, "Design of High Power Injection Heaters for the ORMAK System," Proceedings of Conference on Engineering Problems of Fusion Research, Princeton, N.J., November 1973 (to be published).

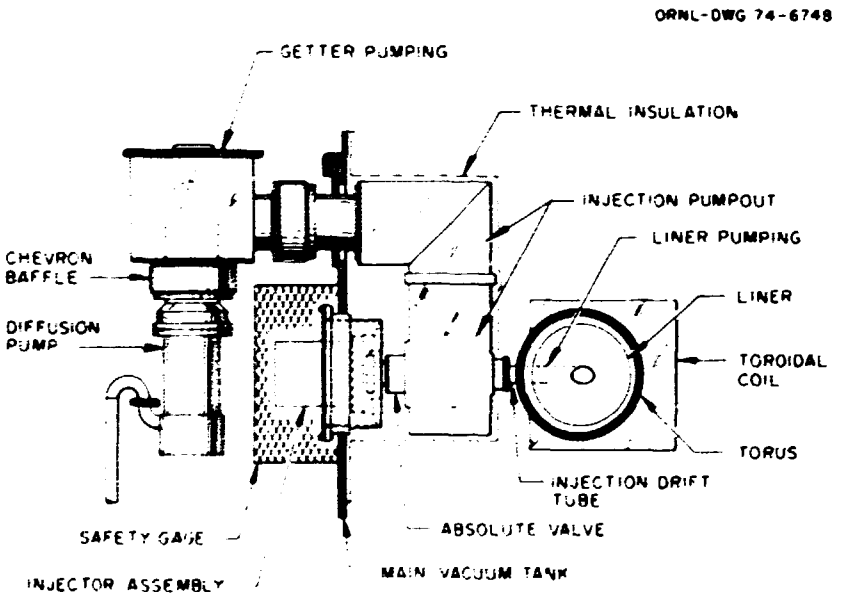

Fig. 4.1. ORMAK neutral injection unit.

Table 4.1. ORMAK cold gas input due to injectors

Injected power (kW)	Peak gas flow rate (atoms cm^{-3} sec^{-1})		Total gas input in 60 msec (atoms/cm^3)	
	Without gettering	With gettering	Without gettering	With gettering
71	1.9×10^{13}	1.1×10^{13}	8.5×10^{11}	4.8×10^{11}
235	5.1×10^{13}	2.9×10^{13}	2.3×10^{12}	1.3×10^{12}

T-3 data: τ_E affected when $Q > 2 \times 10^{15}$ atoms cm^{-3} sec^{-1}
Typical ORMAK filling density $\approx 6 \times 10^{13}$ atoms/cm^3

The injectors have been designed to have high gas efficiency and sufficient auxiliary pumping to keep cold gas streaming down to a level which should not perturb the tokamak plasma.[1,2] Up to 85% of the streaming gas can be pumped, with the remaining 15% going into the liner and plasma region.

Table 4.1 shows the magnitude of this remaining gas streaming to the plasma region. Shown are the peak flow rates, which are in atoms per second divided by the liner volume, for 71-kW operation on one injector, at which the data were taken, and for 235 kW, which represents optimization of the two installed injector systems. These flow rates can be compared with some Russian data for the T-3 tokamak which indicated that the energy confinement time was not affected until the cold gas input flow rate exceeded 2×10^{15} atoms cm^{-3} sec^{-1}. Also shown in Table 4.1 is the total atomic density added to the liner by this streaming during a 60-msec discharge. Note that these are the maximums attained at the end of a 60-msec pulse. For comparison, a typical ORMAK filling density is 6×10^{13} atoms cm^3, so the integrated streaming gas is a small perturbation on this.

Besides the cold gas streaming, another potentially bad side effect of injection is the increase of the tokamak plasma effective Z because of beam impurities. This is an increase in the effective charge number of the plasma ions and can cloud the interpretation of data. The ORMAK effective Z is 5 to 10, and we require that the increment in this due to injected impurities be small. A detailed study of beam impurity level has been made.[1,2] The dominant beam impurity is oxygen, and it can be maintained at <0.5%.[1,2] With a 0.5% beam impurity level of oxygen, which becomes fully stripped after entering the ORMAK plasma, we calculate a negligible increase in the effective Z with two injectors and the present 60-msec discharge, and we calculate a less-than-5% change for future operation with four injectors and a 100-msec pulse time.

A number of engineering problems have been solved in order to obtain successful operation.[3,4] These problems arose in the design and fabrication of the ion source and the beam line components and are important to the electrical stability, power dissipation, beam optics, beam quality, high efficiency, and reliability of the injector system.

4.2 SOURCE DEVELOPMENT

4.2.1 Geometry Effects

Studies of grid curvature, aperture displacement, and density gradients have increased our understanding of beam focusing. As a result, ion beam power on target in the simulated ORMAK beam line has increased from the 60 to 65% range to the 75 to 80% range of the total power supply output.

The ORMAK sources use grid curvature to match the density gradient and for thermal stability. Beam focusing is achieved by a programmed radially inward displacement of the apertures in the target cathode with respect to the positions of the corresponding apertures in the accel grid. With this type of focusing there are no undesirable side effects such as increased beam inter-

2. L. D. Stewart, R. C. Davis, J. T. Hogan, T. C. Jernigan, O. B. Morgan, and W. L. Stirling, "Neutral Beam Injection Heating of ORMAK," *Proc. Third Int. Symp. Toroidal Plasma Confinement, Garching, Germany*, March 1973.

3. R. C. Davis, T. C. Jernigan, O. B. Morgan, L. D. Stewart, and W. L. Stirling, "Engineering Considerations of the DuoPIGatron Ion Source," Proceedings of Conference on Engineering Problems of Fusion Research, Princeton, N.J., November 1973 (to be published).

4. D. C. Lousteau, S. M. DeCamp, W. Halchin, T. C. Jernigan, S. O. Lewis, O. B. Morgan, J. D. Rylander, and L. D. Stewart, "Mechanical Interfacing of the High Power Neutral Injection Heaters to ORMAK," Proceedings of Conference on Engineering Problems of Fusion Research, Princeton, N.J., November 1973 (to be published).

ception by the grids or beamlet profile spreading. Detailed experimental studies for single circular apertures on the 7-cm ORMAK source are summarized in Fig. 4.2. The deflection angle θ is given by

$$\theta = 18.4\ \Delta x/z \text{ degrees.}$$

where Δx is the aperture displacement and z is the extraction gap. Experimental studies were also done with slit apertures.

The results of operating a source with such an extraction system on the ORMAK beam line No. 2 are shown in Fig. 4.3. The significant improvement in power to the target can be seen.

4.2.2 Plasma Studies

The main effort has been to produce a plasma with sufficient density and uniformity to afford extraction

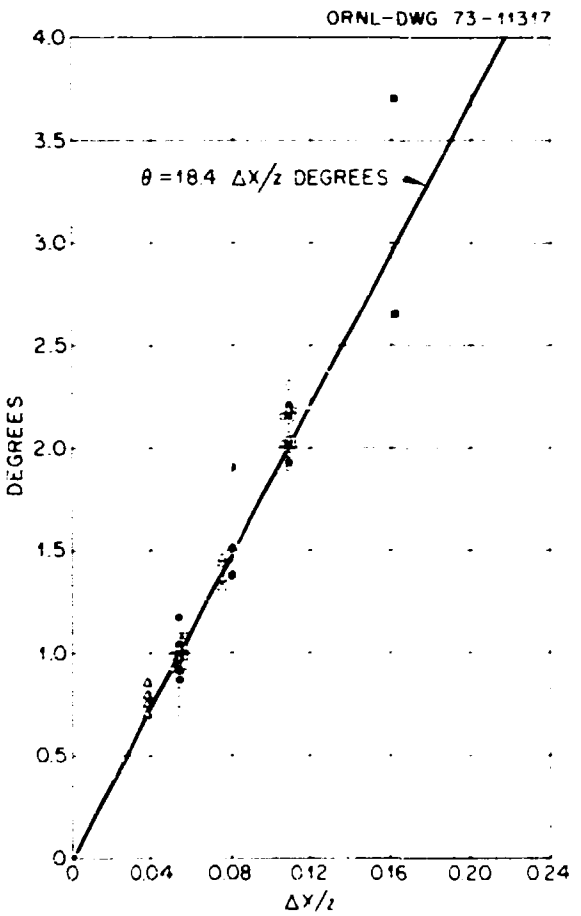

Fig. 4.2. Beam deflection as a function of $\Delta x/z$.

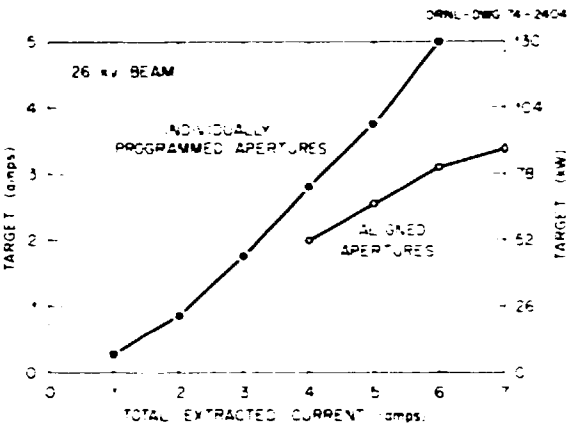

Fig. 4.3. Ion beam current and power delivered to the ORMAK test-stand mode target.

from a 10-cm-diam source. Figure 4.4 shows the electrode configuration for the profile shown in Fig. 4.5. The density distribution of the 7-cm ORMAK source is also shown in Fig. 4.5.

The source of Fig. 4.4 differs from the ORMAK source principally in three respects. First all components are radially larger; second, the plasma feed from the intermediate electrode to the PIG region is annular due to the axial "button"; and third, the epoxy insulator immediately above the target cathode permits an electrical connection employing two anode structures. One may electrically connect anode 2 to the target cathode and operate in conventional ORMAK fashion. Anode 1 receives about three-fourths of the arc current when operating as shown in the figure. The plasma is very quiet at low magnetic fields, $\Delta n/n \sim$ a few percent; the plasma uniformity is $\pm\sim 10\%$ at 5-cm radius but the average density is a factor of 2 to 3 too low with arc currents of 125 to 140 A. Increasing the source magnetic field rapidly increases the density. Simultaneously the density uniformity decreases to $\pm\sim 20\%$ and the noise level increases to $\Delta n/n \sim 20\%$ to 40%. In this operation mode the source is insensitive to utilizing anode 2 as an anode or as a part of the target cathode.

A total power supply current of 7 A at 20 kV has been extracted from this source with flat extraction grinds limited to 7-cm diameter. Increasing the open grid area to 10 cm and the accel voltage to 25 kV should increase this current by a factor of 2 to 3.

The continuing effort is to scale these sources to higher current, higher voltage, and longer pulse lengths. A new test stand is being built which will allow development and testing of sources of 40-A output current at 40-keV energy. These sources will be useful

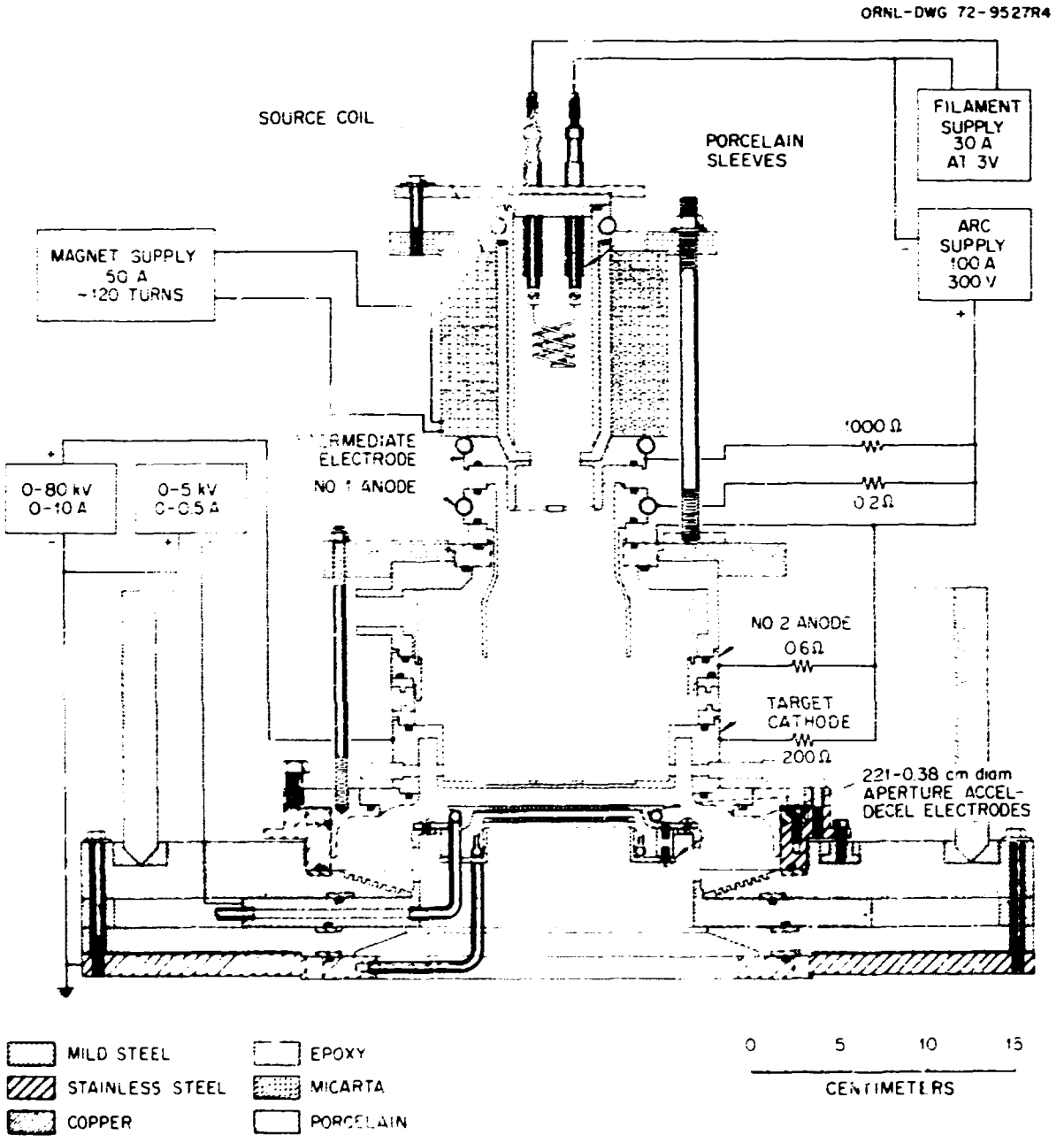

Fig. 4.4 DuoPIGatron ion source.

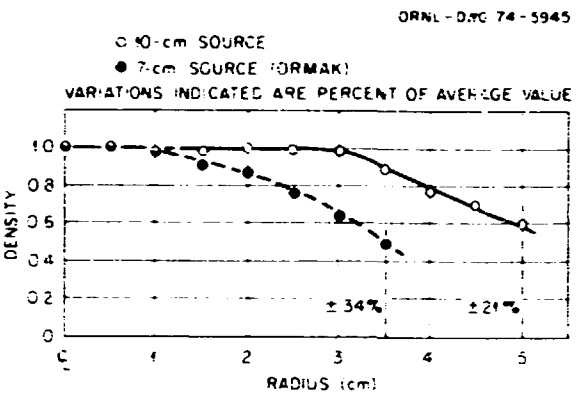

Fig. 4.5. Radial density profile.

for next-generation experiments such as PLT at Princeton, Doublet III at General Atomic, or a new tokamak proposed for ORNL. Pulse lengths of a few hundred milliseconds will be adequate, but the test stand will provide for pulses up to 1 or 2 sec. Also being proposed is a new test stand for development and testing of 10- to 40-A sources at energies between 150 and 200 keV. These sources will be necessary for the future two-component torus experiments being proposed both at Princeton and ORNL. This development program will of necessity include development of multistage extraction systems and negative ion source technology.

5. Atomic Cross Sections, Plasma Diagnostics, and the Controlled Fusion Atomic Data Center

Ignacio Alvarez[1] C. E. Bush
C. F. Barnett Carmen Cisneros[1]
J. A. Ray

5.1 ATOMIC PHYSICS

5.1.1 Angular Differential Scattering Cross Sections

5.1.1.1 (H, D) + N_2 → (H^+, D^+) + N_2 + e. Unlike nuclear physics, it is very difficult in atomic physics to measure the differential scattering cross section and then integrate over all space to obtain the total cross section that is in reasonable agreement with the total cross section measured directly. We have measured and compared the differential cross sections for the reactions: $H^0 + N_2 \rightarrow H^+ + N_2 + e$ and $D^0 + N_2 \rightarrow D^+ + N_2 + e$ in the energy range 0.5 to 4 keV. The results are shown in Fig. 5.1, where the differential scattering cross sections are plotted as a function of the scattering angle. From hard-sphere classical scattering theory, one would predict that the angular differential cross section would be the same for both H and D at the same center-of-mass energy. From Fig. 5.1 it is seen that the cross section for scattering of H in the inelastic collision is smaller than that for D at the corresponding center-of-mass energy. Integration of these cross sections over the spatial angles, θ and ϕ, results in the total cross section for electron loss or stripping, as shown in Fig. 5.2. The stripping cross sections for both H and D are the same at the same energy per nucleon or the same velocity. Comparison of these results with the total measurements of Stier and Barnett[2] and McNeal and Clark[3] indicates excellent agreement between the two methods of measurement. In Stier and Barnett's work, a beam attenuation method was used which was insensitive to scattering. In McNeal and Clark's work, the rate of increase of the H^+ was measured as the target pressure was increased. This method is sensitive to scattering in that all of the H^+ ions formed were probably not collected due to the geometry used. These measurements indicate that with proper precaution it is possible to determine differential scattering cross sections which, when integrated, yield total cross sections.

5.1.1.2 Differential scattering and total cross sections of D^+ in cesium vapor. One proposed method to obtain neutral deuterium beams at energies greater than 150 keV is to pass a D^+ beam through an alkaline vapor target, such as cesium, where electron capture and loss collisions at energies of 1 to 2 keV convert approximately 20% of the incident beam to D^- atoms. These D^- ions are accelerated to the desired energy and passed through a gas cell, where approximately 80% of the negative ions are converted to deuterium atoms. To estimate possible scattering losses in the previous measurements of Grubler et al.[4] and Schlachter et al.,[5] we have measured the differential scattering cross sections for formation of D^- from both D^0 and D^+ in cesium vapor in the energy range 0.5 to 2.5 keV. Results of these measurements are shown in Fig. 5.3 for the reaction $D^+ + Cs \rightarrow D^- + Cs^{2+}$. The cross sections decrease rapidly with scattering angle, which is typical of electron capture collisions. These results were integrated to obtain the solid line shown in Fig. 5.4, where the cross section for the double electron capture collision is plotted as a function of the incident D^+ energy. The present results are in reasonable agreement with Grubler et al.,[4] being a factor of 2 greater at 1.5

1. Visiting scientist, Institute of Physics, UNAM, Mexico, D.F.

2. P. M. Stier and C. F. Barnett, *Phys. Rev.* **103**, 896 (1956).

3. R. S. McNeal and D. C. Clark, *J. Geophys. Res.* **74**, 5065 (1969).

4. W. Grubler, P. A. Schnelzback, V. Konning, and P. Marmier, *Helv. Phys. Acta* **43**, 254 (1970).

5. A. S. Schlachter, P. J. Borkholm, D. H. Loyd, L. W. Anderson, and W. Haeberli, *Phys. Rev.* **177**, 184 (1969).

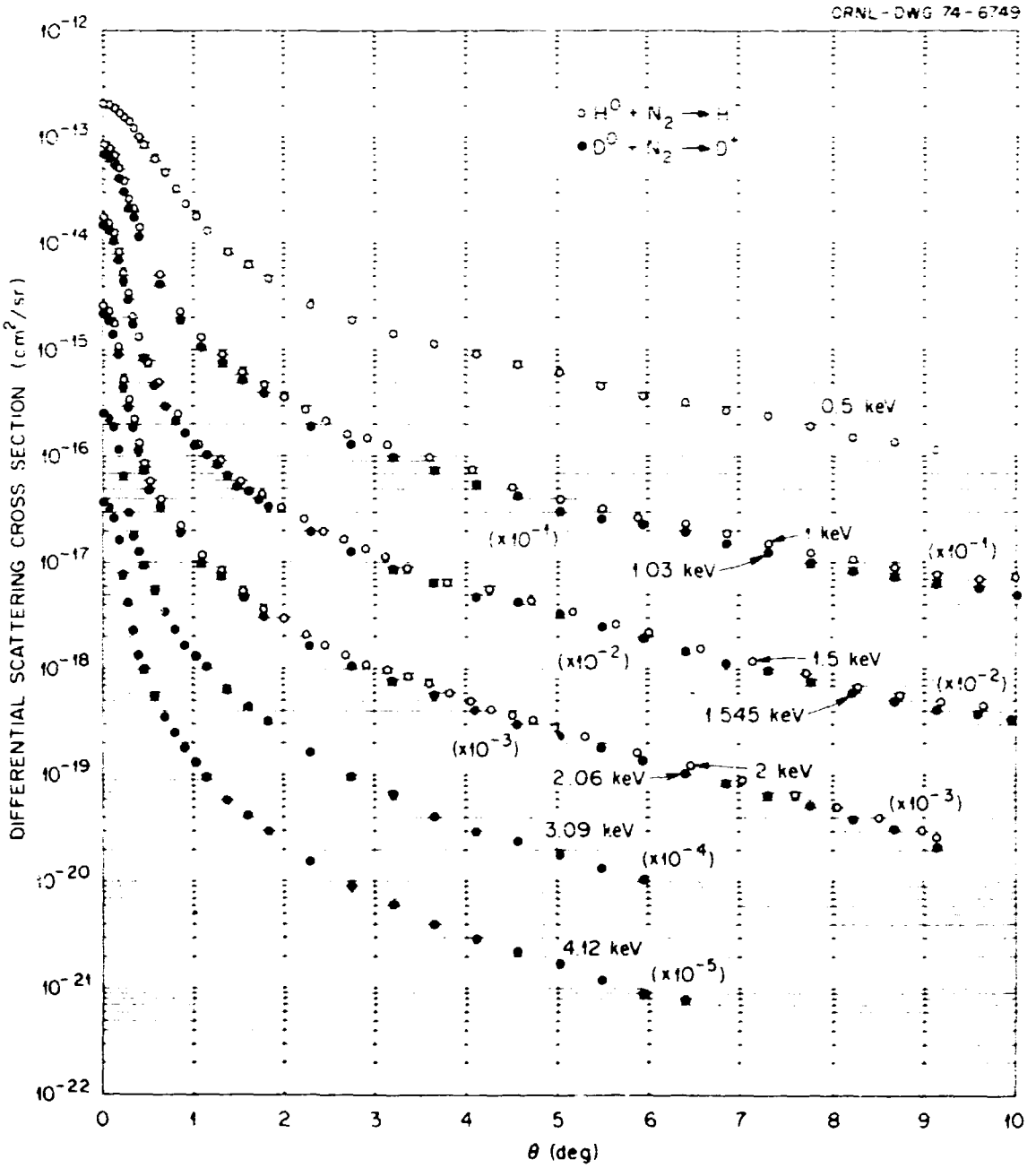

Fig. 5.1. Differential scattering cross sections for the reactions: $H^0 + N_2 \rightarrow H^+ + N_2 + e$ and $D^0 + N_2 \rightarrow D^+ + N_2 + e$.

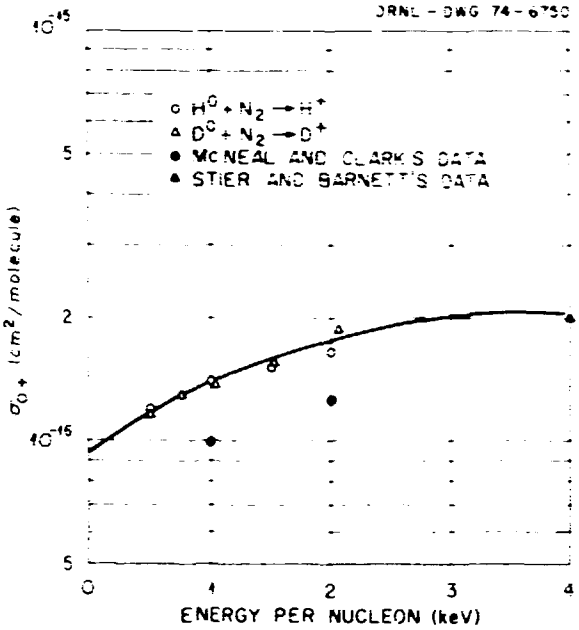

Fig. 5.2. Electron loss or stripping cross sections (σ_{0+}) for H^0 and D^0 in N_2 gas. The D^0 energy has been divided by two to compare to H^0 at the same velocity.

keV and a factor of 0.6 at 2.5 keV. Shown in Fig. 5.5 are the results obtained for energetic D^0 atoms incident on the cesium vapor. The results are consistently greater than those of Schlachter et al. by nearly a factor of 2. Of more importance to the physical process of forming a D^- beam is the equilibrium fraction obtained when sufficient collisions occur in the cesium vapor that a statistical charge equilibrium exists between the D^+, D^-, and D^0 particles leaving the cesium vapor cell. Shown in Fig. 5.6 are the angles in which 50% ($\theta.5$) and 90% ($\theta.9$) of the D^- beam were contained for both single collisions and multiple or equilibrium collision conditions. For D^+ incident on cesium vapor the scattering is less than 1° for most conditions. Shown in Fig. 5.7 is the equilibrium negative fraction for both D^+ and D^0 incident on the vapor cell. If true equilibrium conditions are established, then the fractions should be independent of the initial charge state. Within the experimental error this necessary condition is true, however, the incident D^+ values seem to be consistently higher. The present results are compared with those of Schlachter et al. The agreement is unsatisfactory in that the results of Schlachter et al. indicate a maximum at 1.5 keV, whereas the present values for the negative equilibrium fraction are still increasing at the lowest energy of 0.5 keV.

5.1.1.3 D_2^+ in cesium. For the formation of D^- from D_2^+ incident on a cesium target, the collision dynamics become more involved. The D^- can be formed either by electron capture into a repulsive state of D_2^-, which immediately decays, or by a two-step process in which D^+ or D^0 is first formed from dissociative collisions, with a second collision leading to D^-. The differential scattering cross sections, $d\sigma/d\Omega$, for the formation of D^+, D^0, and D^- are shown in Fig. 5.8 as a function of scattering angle for 2-keV incident D_2^+. Using the present techniques, it was impossible to separate the two components (D^0 and D_2^0) of the neutral beam. The curves for both D^0 and D^- formation exhibit structure at approximately 3.6° and also at 5°. This structure, plus the cross sections of formation of neutral particles, indicates either an electron capture into the $b\ ^3\Sigma_u^+\ 2p\sigma$ repulsive state of D_2 or the

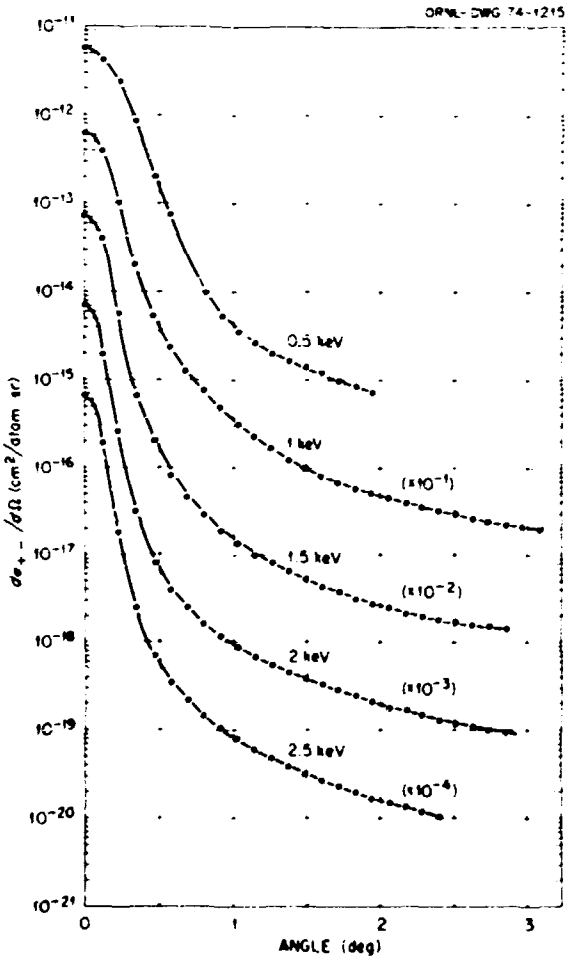

Fig. 5.3. Differential scattering cross sections for the inelastic collision: $D^+ + Cs \rightarrow D^- + Cs^{2+}$.

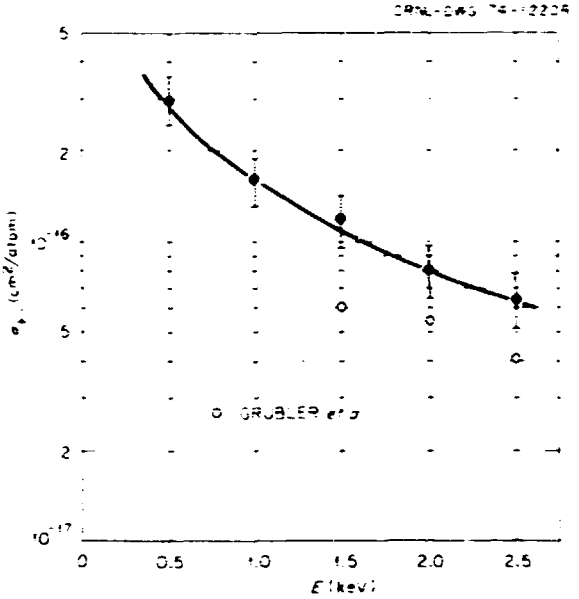

Fig. 5.4. Double electron capture cross sections for the reaction: $D^+ + Cs \rightarrow D^- + Cs^{2+}$.

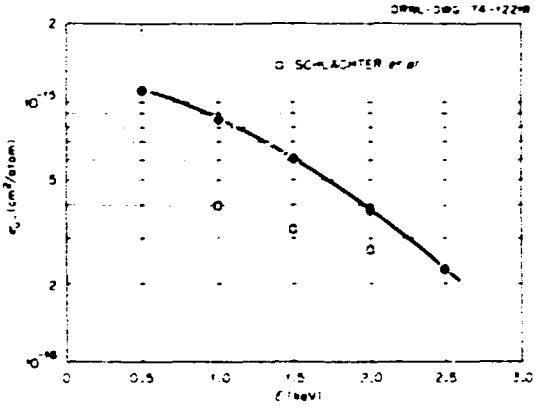

Fig. 5.5. Electron capture cross sections for the reaction: $D^0 + Cs \rightarrow D^- + Cs^+$.

capture of two electrons to form the $b + e^- \, ^3\Sigma^+_g$ repulsive state of H_2^-. The smaller peaks around 5° do not correspond to either a capture into a repulsive level or a Franck-Condon transition to a repulsive level. However, the D^+ curve shows no structure, which should be present if dissociative collisions are predominant. It is standard practice in the measurement of atomic collisions to verify that only single collisions are occurring in the vapor target to determine that the beam component being measured increases linearly with the target vapor density. Due to the scatter in the data, we were unable to determine if single-collision conditions were present. Thus, we cannot at the present time predict that D^- is formed through a single collision or through multiple collisions. The absence of structure in the D^+ component is not explainable from the data obtained.

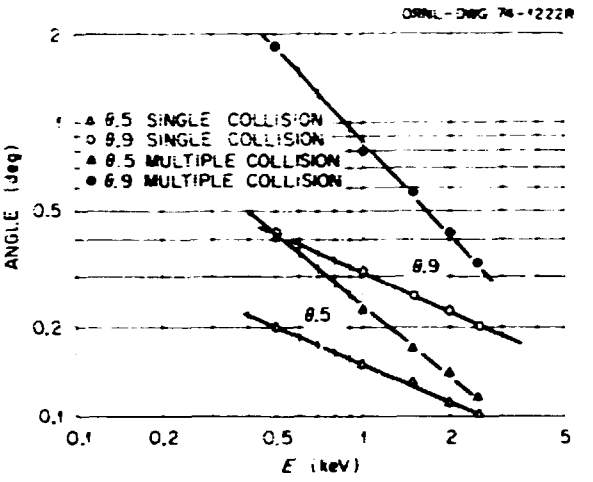

Fig. 5.6. The scattering angle in which 50% (θ.5) and 90% (θ.9) of the beam were contained for single and multiple collisions. Scattering results from formation of D^- from D^+ in cesium vapor.

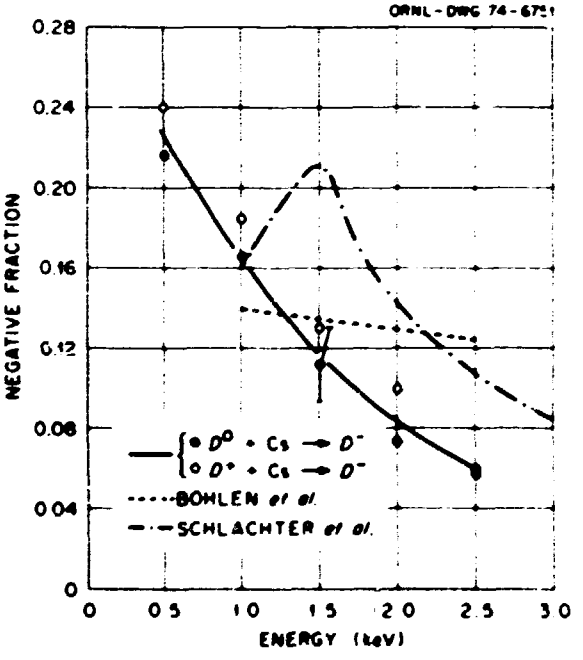

Fig. 5.7. Equilibrium fraction of D^- from the passage of D^+ through Cs vapor.

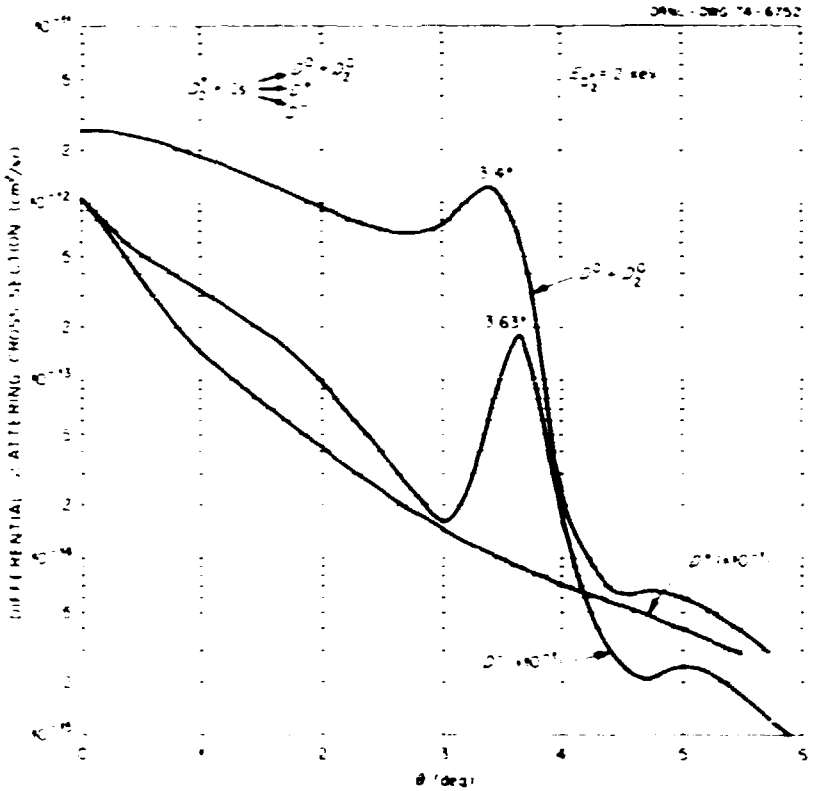

Fig. 5.8. Differential scattering cross sections for the formation of D^0, D^+, and D^- when D_2^+ passed through Cs vapor. Incident D_2^+ energy, 2 keV.

By multiplying the intensity of the beam at the angle θ by $\sin\theta$, we obtain the beam scattered into an angular ring at angle θ. This result is shown in Fig. 5.9, where $I(\theta)\sin\theta$ is plotted as a function of θ. Since $\sin\theta \to 0$ as $\theta \to 0$ the curve in the region less than 0.75° should be ignored. In presenting the scattering in this manner, the contribution due to the structure shows up very distinctively. Plotted in Fig. 5.10 is the half-cone angle (the angle into which 50% of the D^- is scattered) as a function of the instant particle energy. Two cases are shown: (1) formation of D^- from D^+ and (2) formation of D^- from D_2^+. The scattering is greater by more than an order of magnitude for incident D_2^+ than for D^+.

5.1.1.4 D_2^+ in cesium. With D_2^+ incident on cesium, the D^- formed has a broader distribution, as shown in Fig. 5.11, where $I(\theta)$ is plotted as a function of θ for 1.5-keV D_2^+ ions. At 4.5°, structure was found similar to that found in D_2^+. Since the energy levels are not well known for the triatomic ion, we were unable to determine the state responsible for this structure. If the intensity is multiplied by $\sin\theta$ to obtain scattering into an annular ring, we obtain the results shown in Fig.

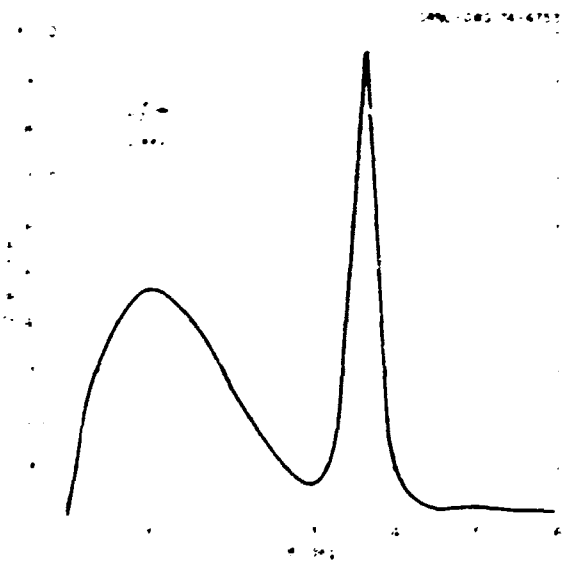

Fig. 5.9. The angular distribution of D^- scattered into an annular ring at angle θ. Results are for 2-keV D_2^+ passing through Cs vapor.

5.12. Again the curve is inaccurate as sin θ approaches zero. With D_3^+ we find that the structure present at 4.5° contributes only a small fraction to the scattering.

5.1.2 Formation of H^- from Dissociative Collisions of H_2^+, H_3^+, and HD_2^+

We have measured the H^- and D^- formation cross section from dissociative collisions of H_2^+, H_3^+, and

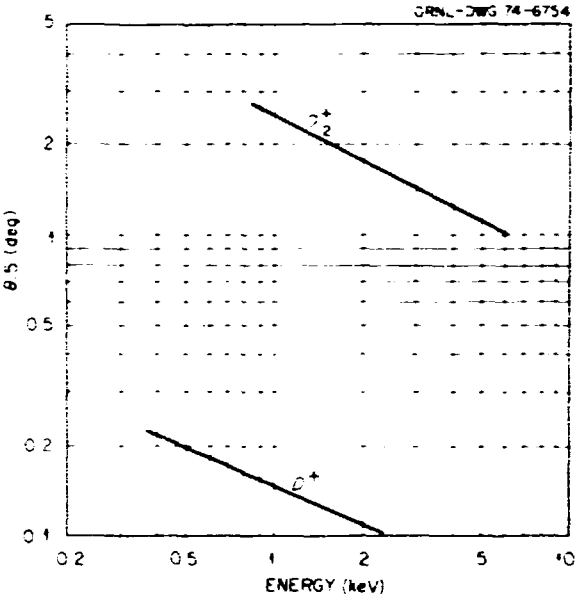

Fig. 5.10. Comparison of the scattering angles in which 50% of the beam was contained for the reactions $D^+ + Cs \rightarrow D^- + Cs^{2+}$ and $D_2^+ + Cs \rightarrow D^- + Cs^+ + D^+$.

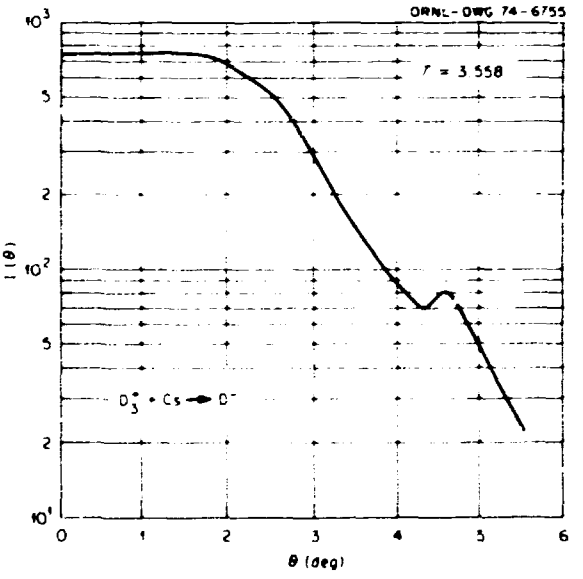

Fig. 5.11. Differential scattering cross sections for the formation of D^- as 1.5-keV D_3^+ was passed through Cs vapor.

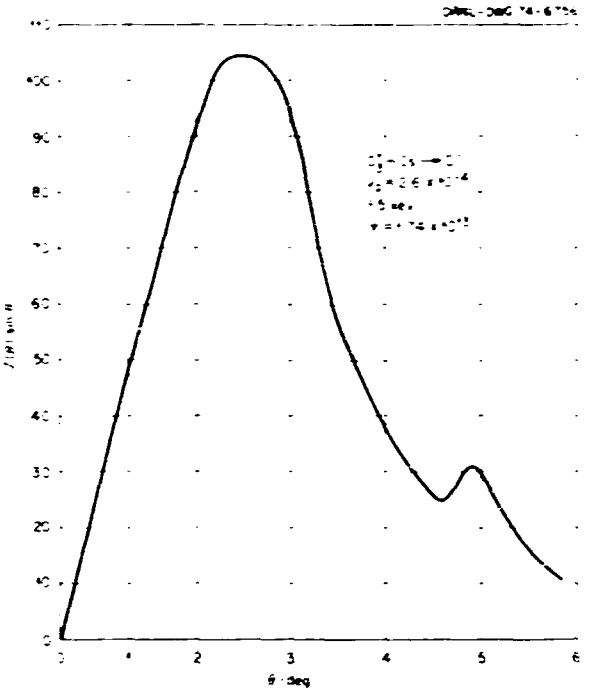

Fig. 5.12. The angular distribution of D^- scattered into an annular ring at angle θ. Results are for 1.5-keV D_3^+ passing through Cs vapor.

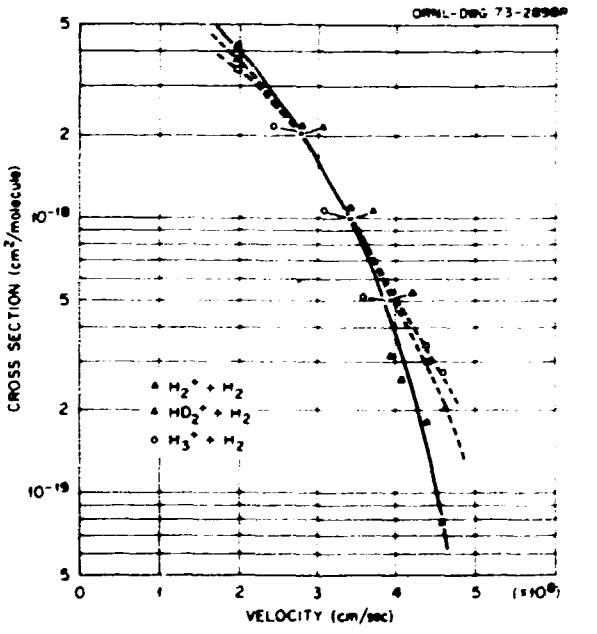

Fig. 5.13. Cross sections for the formation of H^- and D^- from the passage of H_2^+, H_3^+, and HD_2^+ in H_2 gas in the energy range 40–600 keV.

HD_2^+ in H_2. The measurements are straightforward in that the diatomic or triatomic ion beam is accelerated to the desired energy and passed through a gas cell where single collisions produced H^- or D^-, which were measured. Results of the measurements are shown in Fig. 5.13, where the cross section for negative ion production is plotted as a function of the particle velocity. The low velocity corresponds to a negative ion energy of 20 keV, while the upper velocity corresponds to 120 keV. The triatomic ions have the same cross sections within the accuracy of the experiment, while for H_2^+ there was a definite departure at higher energies. As expected the magnitude of the cross sections was small. Surprisingly, the H^- signal from HD_2^+ dissociation was less than background. As the gas cell pressure was increased, the fraction of H^- or D^- increased to a maximum value and then decreased to an equilibrium value which is the same as that for an equivelocity proton incident on the gas cell. The peak fraction or maximum fraction of the negative ion as a function of particle velocity is shown in Fig. 5.14. In no case was the peak fraction higher than a few percent. Presumably, xenon as a target atom produces a much greater fraction of H^- than an H_2 target. Preliminary measurements indicated that in this energy range, the fraction of negative ions using xenon in the gas cell was less than a factor of 2 more than when H_2 was used.

5.1.3 Electron Capture and Loss Cross Sections for Thallium and Potassium Particles

If various collision cross sections are known, a heavy-ion beam probe can be used to measure absolute spatial densities in high-temperature plasmas. To aid in the interpretation of density measurements in the EBMO Bumpy Torus (EBT), we have measured the electron capture and loss cross sections for K^+ and K^0 particles in H_2 gas. Other pertinent cross sections are the electron ionization of K^+ and the charge-exchange cross section of K^+ with H^+. The electron ionization cross sections are known from previous measurements, and R. A. Mapleton of the Cambridge Research Laboratories is presently computing the charge-exchange cross sections. Results of the measurements are shown in Fig. 5.15, where the cross sections are plotted as a function of the incident potassium energy. Four cross sections are shown: (1) single electron loss (σ_{01}) for K^0; (2) double electron loss (σ_{02}) for K^0; (3)

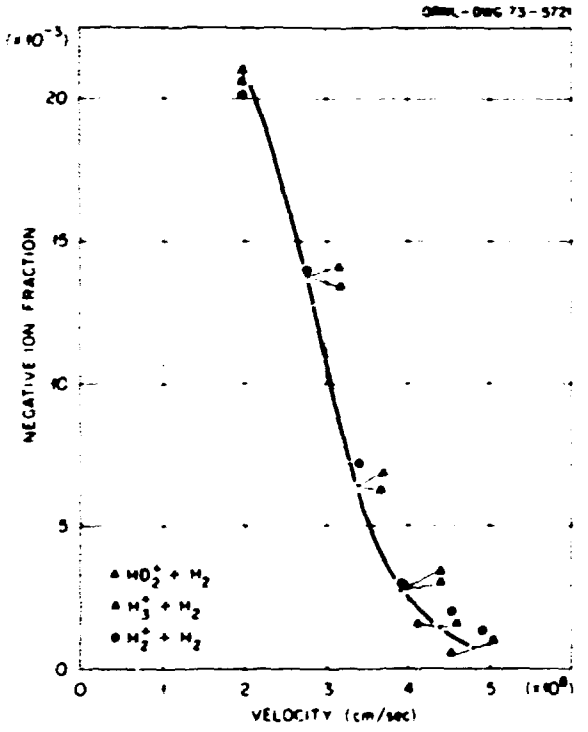

Fig. 5.14. Equilibrium fraction of H^- or D^- formed from collisions of H_2^+, H_3^+, and HD_2^+ in H_2 gas.

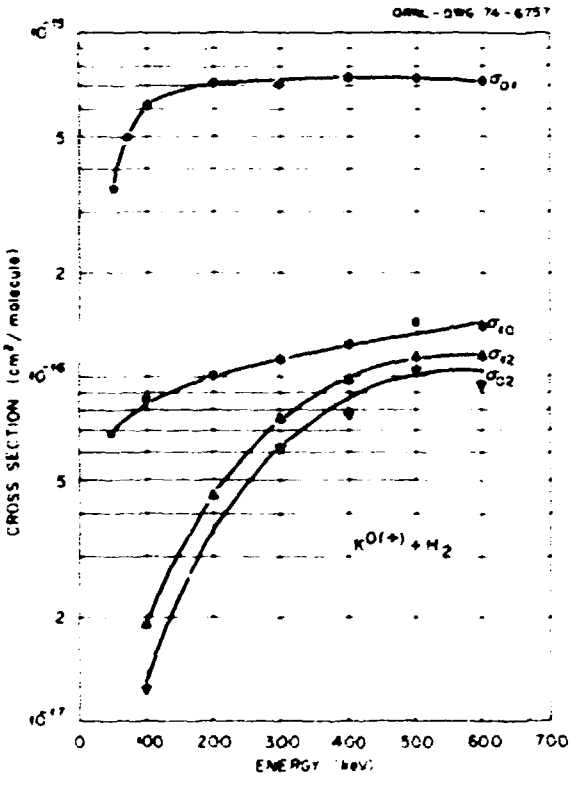

Fig. 5.15. Electron capture and loss cross sections for potassium particles passing through H_2 gas.

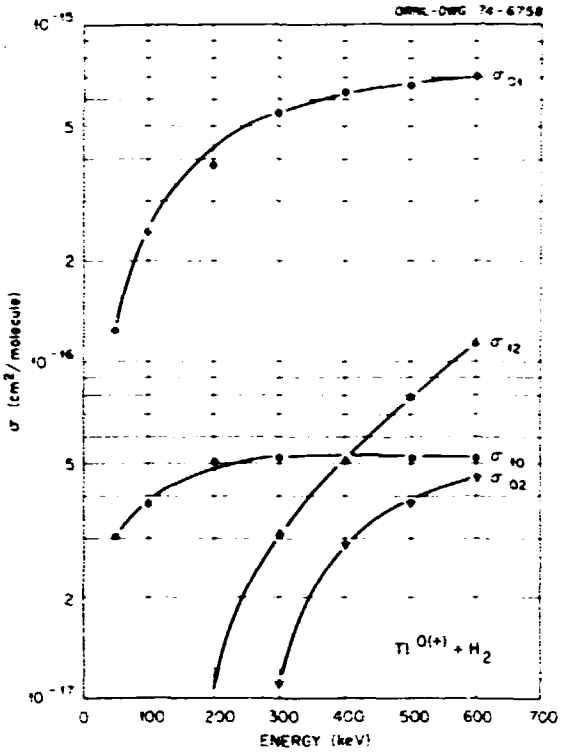

Fig. 5.16. Electron capture and loss cross sections for tellurium particles passing through H_2 gas.

single electron loss (σ_{12}) for K^+; (4) single electron capture (σ_{10}) for K^+. The single electron loss or stripping cross sections are relatively constant above 100 keV, while the other charge-changing cross sections increase monotonically with energy in the region 50 to 600 keV. Similar measurements have been made for thallium beams in H_2, and the results are shown in Fig. 5.16. The σ_{01} cross sections exhibit a more pronounced energy dependence than that for K^0, although the magnitude is approximately the same at 600 keV. If the decision is made in the future to install the Tl^+ ion beam diagnostic apparatus on ORMAK, then these results will aid in data reduction.

5.2 PLASMA DIAGNOSTICS

5.2.1 Tangential Neutral-Particle Spectrometer

A seven-channel neutral-particle spectrometer has been designed and constructed to determine the energy dispersion of neutral particles escaping ORMAK in a direction tangential to the toroidal magnetic field. An analyzer similar to that described previously[6] was mounted on a rail such that the particles escaping in the horizontal plane could be scanned in the energy region 1 to 30 keV. By mounting the analyzer on a low-energy accelerator, an absolute calibration of the efficiency was obtained. In Fig. 5.17 the results of the calibration are shown where the analyzer efficiencies (ions counted/neutrals in) are plotted as a function of the particle energy. N_2 gas was used in the conversion cell. For the channel (No. 7) furthest away from the N_2 cell, curves are shown for N_2 pressures of 1, 5, and 10 millitorr. During the course of the calibration, we discovered the analyzer efficiency varied for different channels. The cause of this variation was traced to collisional scattering at the higher pressures of 10 millitorr. The magnitude of this effect is shown in Fig. 5.17 as the dashed line where the efficiency was plotted for the channel nearest the gas cell.

The analyzer has been installed on the ORMAK apparatus, and preliminary results indicated: (1) the tangential ion temperature was equal to the perpendicular ion temperature, indicating thermodynamic equilibrium, (2) scans along the horizontal plane indicate constant ion temperature, (3) with 25-keV H injection the ion energy spectrum was as shown in Fig. 5.18. A broad peak was found in the region 8 to 14 keV. Without a knowledge of the energy composition of the neutral beam used for heating, it was impossible

6. *Thermonuclear Division Annual Progress Report*, ORNL-4896, p. 35 (1972).

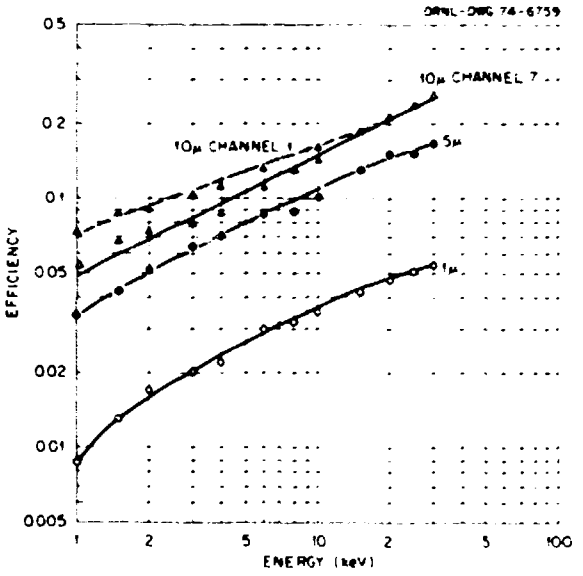

Fig. 5.17. Calibration of the tangential electrostatic analyzer for H^0 energies in the range 1–30-keV N_2 conversion gas.

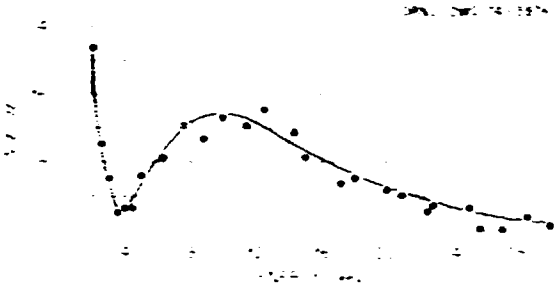

Fig. 5.18. Energy spectrum obtained with the tangential particle spectrometer for 25-keV neutral beam heating.

to calculate the energy exchange or equilibration time between the fast ions and the thermal plasma particles.

5.2.2 Pyroelectric Detector

A pyroelectric crystal has been used to measure the energy flow in the form of photons and neutral particles from the ORMAK plasma. In the past, when the energy incident on the probe was summed over the plasma surface, it was found the measurement indicated that the energy lost by these channels was several times the input energy. During the past year the thickness of the front electrode has been decreased, resulting in an increase in sensitivity by a factor of 2, and the time constant decreased to less than 1 msec. Also, electrons were being lost from the front electrode of the crystal by secondary or photoelectric emission. This emission added to the polarization current as measured by the operational amplifier. This emission has been suppressed by a bias electrode, but the probe response is still a factor of 5 too large. This may be the result of two factors (1) nonuniform radiance over the plasma surface and (2) the crystal has been calibrated with an He-Ne laser, and the response may be different for neutral particles. These two sources of trouble will be examined in the near future.

5.2.3 Potassium Ion-Beam Probe

A K^+ ion beam will be used to probe the spatial density and space potential in the ELMO Bumpy Torus. In addition we anticipate being able to measure the beta in the hot electron ring plasma by determining the deflection of the K^+ beam with and without the electron plasma. During the past year, all components have been procured and assembled. Preliminary tests will be made on a solenoidal magnetic field with gaseous ionization to simulate plasma electron ionization.

6. Magnetics and Superconductivity

C. A. Berry[1]	K. Koyama[3]	E. C. Moore
R. W. Derby	H. M. Long	J. E. Simpkins
C. M. Fitzpatrick	M. S. Lubell	W. C. T. Stoddart[4]
W. F. Gauster[2]	J. N. Luton	P. L. Walstrom

6.1 MAGNETICS

The analysis of resistance-optimized asymmetric coils to produce toroidal fields was continued with consideration of circular bore coils having circular, rectangular, and rounded-corner external shapes. The calculated resistance was checked with some coil shapes cut from resistance paper and found to agree within ±1%. The asymmetric coil study culminated in the design and fabrication of a 50-kG coil for ORMAK with a 66-cm bore and a 152.4-cm by 91.4-cm external dimension with rounded corners. The copper coil shapes were machined from 0.95-cm-thick plate using a numerically controlled machine and were fitted with a hollow copper cooling tube by soft soldering. Four such shapes were insulated with fiber glass and are to be vacuum potted in a steel restraining frame to form the 24-turn coil. The per-turn resistance of these coils is only one-fourth of that of the present ORMAK coils, so that the present generators can be used to provide a 50-kG toroidal field. Vacuum potting and final tests of these coils are scheduled for next year.

A code for calculating the magnetic field components of an arbitrary collection of axisymmetric solenoids has been developed from the rectangular solenoid routines published by Garrett.[5] The only requirement for these coils is that their axes lie in a plane. The code also provides for vertical field coils, the only restriction being that their axes are perpendicular to the axes of the horizontal-axis coils. This code includes the full torus case as a subset. The code is being incorporated into a finite-element stress code and is being used in the preliminary magnetic design of coil test facilities for the superconducting coil development program and for the High Field ORMAK Program.

A code for the calculation of self- and mutual inductances of collections of rectangular-cross-section axisymmetric coils has been developed. This code provides us with the essential tools for designing protection circuits, calculating charging time, and other transient conditions for collections of coils.

Strain-gage-signal-conditioning modules for dynamic coil testing were designed and are under construction. Investigations were made, and continue to be made, into the problem of magnetic field effects on strain gages and lead wires.

A finite-difference procedure was employed to analyze the thermal performance of cryogenic coils such as those used in ORMAK and proposed for High Field ORMAK.

The maximum permissible current in a pulsed magnet coil will usually be determined by the maximum permissible temperature increase, which, in turn, depends on the power supply, the cross-sectional area of conductors, and the specific heat of the conductor material. The time between pulses or the time needed to cool the coil back to its original temperature is more complicated to calculate. The obvious variables include the thermal properties of the coolant as well as those of the conductor. In addition, the velocity of the fluid and the size and shape of the coolant passages play important roles. More subtle is the influence of the electrical insulation between the turns of the coil. If the layer of insulation is thin or ineffective as a thermal insulation, the coil will tend to be a uniform temperature throughout, and no moving cold front will be established. Hence, heat will be removed rather sluggishly. If, on the other hand, the turns are well

1. Co-op student, University of Tennessee.
2. Consultant.
3. On leave of absence from Electrotechnical Laboratory, 5-4-1 Mukodai-cho, Tanashi-city, Tokyo, Japan.
4. Engineering Analysis.
5. M. W. Garrett, ORNL-TM-3575.

insulated from each other, a moving cold front is set up and efficiently sweeps the heat out of the conductor. This investigation, based on ORMAK coils, showed that the thermal linking of the turns does indeed increase the cooling time between pulses by as much as a factor of 2. The results of this analysis and previous calculations of a 6°K heat exchanger were employed by the ORMAK group to initiate the design of an addition to the ORMAK cryogenic system to allow operation down to 6°K. The design and installation of this addition will be completed next year.

Engineering for magnet laboratory alterations and additions has begun. A control room will be constructed in the center of two large laboratory rooms. The east laboratory room will remain largely unchanged. The minimum goals for next year will be to complete the control room, relocate the generator controls, and install sufficient utilities to begin superconducting tests in the west laboratory.

A program was undertaken to develop a method for vacuum impregnating thick magnet coils containing impermeable sheet insulation and to determine some properties of the cured epoxy such as tensile and bond strengths. No attempt was made to find the "best" epoxy; we restricted ourselves to the mixture used on the ORMAK toroidal field coils, which has proven satisfactory through several years' use in other apparatus in the Thermonuclear Division. The first coil to be impregnated is the asymmetric high-field prototype for ORMAK. This coil has 5-mil smooth Kapton film between turns and between each of the four layers and dry glass cloth or tape on each side of the Kapton. It was therefore deemed necessary to impregnate successfully samples of glass cloth bounded by copper on one side and Kapton on the other (which represent a coil section) to show that the properties of the cured insulation would be satisfactory.

A test section 155 cm high with glass cloth between a heated copper plate and a transparent plastic cover was impregnated. The conditions for impregnation were investigated, and electrical and mechanical tests showed that a satisfactory impregnation scheme for the High Field ORMAK coils could be prescribed. This impregnation is scheduled for the coming year.

The coils[6] for the ELMO Bumpy Torus have been completed and tested and are in service. During the safety test of the full 24-coil torus, the current was raised to 7850 A, 10% above the design value, and the magnetic forces were further increased by deenergizing selected coils to simulate fault conditions. The largest observed stress was 6000 psi (in the aluminum flanges), and all voltages, fields, temperatures, etc., were normal. It appears from the test data that if more power were available and if care were taken to pretighten the mechanical structure so that it would be symmetrically stressed, the coil system could be operated successfully at 9300 A, 30% above the design value. The High-Beta Plasmas Group has inferred from their electron beam measurements[7] that the field error averaged along the minor torus axis is 1.5×10^{-4} times the unperturbed field. This value is the net result of all field errors and includes the effects of coil manufacturing inaccuracies, coil misplacement and misalignment, imperfect lead compensation, and the ambient field.

6.2 VACUUM COATING AND THIN FILMS

Investigations concerning the effectiveness of the platinum diffusion barrier that limits the diffusion of many of the constituents of stainless steel from migrating through the gold film on the ORMAK liner have been completed. The liner coating operation, which consisted of the application of 2 μ of gold with a 500-Å platinum underlayer by means of ion plating, is also complete. Various other components that "see" the plasma, such as microwave guides, laser parts, and several hundred seals and plugs, were also coated. Photomultiplier tubes used in the Thomson scattering system (SCAT-PAK) were coated with silver, increasing sensitivity by a factor of 2.

Large sputtering targets were designed and constructed to demonstrate the feasibility of sputter-coating large substrates (e.g., coating an ORMAK liner in situ). A sample sector of the ALCATOR vacuum wall was coated with this system. This technique would also facilitate the application of coatings, such as refractories, which could not be applied easily by vacuum evaporation.

Considerable effort has been exerted toward development of a thin-film bolometer with fast response to be used as an energy analyzer in ORMAK. Sputtered Ge (Ga) films have shown promising results, although more work in this area is required.

A small vacuum deposition system was constructed for the deposition of beryllium films but was not used for this purpose, since aluminum films were substituted. However, this vacuum system was utilized to deposit thin gold films from a neutron-irradiated source. These films were used to measure the sputtering rate of the liner wall surface in ORMAK under actual operation.

6. *Thermonuclear Div. Annu. Progr. Rep. Dec. 31, 1972*, ORNL-4896, pp. 45–46.

7. Sect. 3, this report.

A program has been prepared to conduct a systematic investigation of various promising materials (e.g., vanadium, niobium) for coating the High Field ORMAK liner, and these investigations are now under way.

6.3 SUPERCONDUCTIVITY

The diamagnetic code, developed in 1972, was applied to a 100-kG niobium-tin superconducting solenoid.[8] The calculated and measured field values agreed well. With this code, we now have the capability of calculating central fields of superconducting solenoids exactly for design or other purposes.

Magnetic design of a 150-kG superconducting solenoid for the Physics Division (ORNL) was carried out. Experiments on the flux-jump stability of niobium-tin superconducting ribbon with various amounts of aluminum interleaving were performed to qualify the material for use in this 150-kG solenoid.

The 106-kG, 7.5-cm bore magnet wound with Nb_3Sn conductors and damaged by internal arcing has been rebuilt. The new design replaced the perforated load-bearing stainless-steel spool with an unperforated non-load-bearing epoxy glass spool. This greatly reduces the possibility of heat propagating and arcing damage between the windings and devices mounted in the bore. A thin 0.5-cm perforated stainless-steel outer sleeve, maintained in tension by large Bellville spring washers at either end of the solenoid, compresses the windings axially. Thus, thermal and magnetic breathing are permitted. The sleeve also serves as electrical shielding between the windings and metal dewar. Since the spool is not perforated, helium is supplied to windings by lengthwise-milled channels on the outside surface of the spool. A removable transfer tube can be plugged into a manifold at the top of the solenoid. This routes helium through the windings for efficient cooldown.

During this year the emphasis of our work in superconductivity has shifted from small-scale experiments on short samples and coils to considerations involved in scaling up from present-sized magnets to those anticipated for fusion feasibility experiments. A number of memos were prepared and many talks were presented to show first that superconducting magnets were superior to copper coils; second, to provide a conceptual design of a superconducting toroidal system for a fusion feasibility and burning experiment-size machine; and third, to emphasize the need for a development program. All three of these programs were successfully carried out during the year. The advantages of superconducting magnets and comparisons between superconducting and cryoresistive coils will be covered further in papers prepared by the F-BX group and technical memos prepared by members of the Engineering Science Group. Our design efforts on a feasibility-sized toroidal system will be included in the *ORMAK F/BX, a Tokamak Fusion Test Reactor* (ORNL-TM-4634). Our reason for the details about the development program for superconducting magnets will be covered in a program proposal being prepared for evaluation by the DCTR office.

6.4 DIAMAGNETIC EFFECTS IN A TAPE-WOUND SUPERCONDUCTING SOLENOID[9]

P. L. Walstrom

The effect of diamagnetic shielding currents on the magnetic field in a tape-wound superconducting solenoid is calculated on the basis of the isothermal critical state model and compared with measured values. The calculation is found to be in reasonable agreement with the data. Additional calculations showing the effect of the tape width on the diamagnetic correction to the central field are presented.

6.5 ON THE INFLUENCE OF THE BETWEEN-THE-TURNS THERMAL INSULATION ON THE DUTY CYCLE OF A LARGE LIQUID-COOLED PULSED COIL FOR USE ON ORMAK AND HIGH FIELD ORMAK[10]

R. W. Derby

The maximum permissible current in a pulsed magnet coil is usually determined by the maximum permissible temperature. This temperature is, in turn, dependent on the available power supply, the specific heat, and the cross-sectional area of the conductor. The allowable time between pulses is considerably more complicated. The obvious variables include the thermal properties of the liquid coolant as well as those of the conductor. In addition, the velocity of the fluid and the cross-sectional area of the coolant passage play important roles. More subtle is the way in which the turns are connected to each other. If the layer of insulation is poor the coil tends toward a uniform temperature, and

8. ORNL-TM-4456 (accepted for publication in the *Journal of Applied Physics*, May 1974).

9. Abstract of paper submitted for publication in the *Journal of Applied Physics*; available as ORNL-TM-4456 (January 1974).

10. Abstract of paper in *Proceedings of the Fifth Symposium on Engineering Problems of Fusion Research, Princeton, N.J., November 6–9, 1973*, IEEE Pub. No. 73 CH0843-3-NPS, p. 376.

hence the steepness of the moving cold front is greatly decreased. The resulting rate of heat removal is thus smaller than it would be if all turns were well insulated from each other.

The problem described in the previous paragraph has been investigated in a quantitative way using finite-difference methods. The possibility of improving the heat removal rate of future machines is discussed. Finally, the numerical methods were checked by comparing several degenerate or extreme cases with certain closed-form solutions.

6.6 CRYOGENIC ENGINEERING FOR ORMAK[11]

H. M. Long J. N. Luton, Jr.

A liquid nitrogen circulating system is employed to maintain a base temperature of 80°K within the vacuum chamber and to remove the Joule heating from the coil systems of ORMAK. The heat exchange components are arranged to facilitate controlled cool-down of the system, and the flow control valves allow pressurization of the liquid within the coil system to suppress nucleate boiling. Under pulsed operation to fields of 25 kG, 9.4 MJ are deposited in the copper coils in 1.5 sec. The cooling system is designed to limit heating of the toroidal field coils to 110 K and to restore them to 80 K in 10 min. A new heat exchanger is being designed to allow a base temperature of 67°K in order to allow either higher field or shorter duty cycle.

6.7 DEVELOPMENT OF THE 50-kG TOROIDAL FIELD COIL FOR HIGH FIELD ORMAK[12]

J. N. Luton, Jr. R. W. Derby
R. L. Brown W. C. T. Stoddart

The main (toroidal) field of ORMAK of 25 kG on-axis is produced by 56 copper coils pulsed from motor-generator power supplies and cooled with liquid nitrogen. It is desired to replace the present toroidal field system with one which produces twice the field strength but does not require the replacement of such major machine components as the plasma liner, aluminum torus, or outer vacuum shell. Such a doubling of the field strength with the same pulse shape would normally imply more than a fourfold increase in power consumption, as well as a fourfold increase in the magnetic forces. However, by (1) using a novel and more efficient shape of the individual coils, (2) reducing the initial temperature of the coils by subcooling the nitrogen, and (3) modifying the force-restraining structure to allow more room for coil conductor near the major axis, it is possible to produce the required 50 kG with the same power supply. The new coil configurations are not axisymmetric but are radially thicker at some azimuths than others. Two methods of constructing such coils are described: one involves winding with nonuniform hollow conductor, the other involves machining of copper plates and the subsequent insertion of a cooling tube. Preliminary tests and the production of a full-sized prototype coil are discussed.

6.8 ANALYSIS OF THE 50-kG TOROIDAL FIELD COIL FOR HIGH FIELD ORMAK[13]

W. F. Gauster P. L. Walstrom

Due to space limitations on the windings, the power efficiencies of toroidal field coils for tokamak experiments are in general rather poor. Very substantial improvement can be achieved by using asymmetrical magnet coil designs. Mathematical analysis and electric current flow plotting of various types of asymmetrical coil designs are discussed, and results of resistance measurements with the High Field ORMAK prototype coil are presented.

6.9 PASSIVATION OF THE ORMAK VACUUM LINER[14]

J. E. Simpkins

The inner vacuum liner in ORMAK, which was constructed of type 304 L stainless steel, has been coated with a 1- to 2-μ gold film. The resultant surface is considerably more inert than the bare stainless surface and reduces plasma-wall interactions. We found, however, that some of the constituents of the stainless

11. Abstract of paper in *Proceedings of the Fifth Symposium on Engineering Problems of Fusion Research, Princeton, N.J., November 6–9, 1973*, IEEE Pub. No. 73 CH0843-3-NPS, p. 380.

12. Abstract of paper in *Proceedings of the Fifth Symposium on Engineering Problems of Fusion Research, Princeton, N.J., November 6–9, 1973*, IEEE Pub. No. 73 CH0843-3-NPS, p. 370.

13. Abstract of paper in *Proceedings of the Fifth Symposium on Engineering Problems of Fusion Research, Princeton, N.J., November 6–9, 1973*, IEEE Pub. No. 73 CH0843-3-NPS, p. 367.

14. Abstract of paper in *Proceedings of the Fifth Symposium on Engineering Problems of Fusion Research, Princeton, N.J., November 6–9, 1973*, IEEE Pub. No. 73 CH0843-3-NPS, p. 385.

steel diffuse through the gold film when the couple is heated to about 300°C. Further investigation indicated that a 500-Å platinum film between the gold and stainless acts as a diffusion barrier for many of these constituents. Diffusion profiles of oxygen, silicon, sulfur, and carbon suggest that platinum acts as a barrier to prevent diffusion of all these elements. Mass scans of the gold surface with platinum underlayer show greatly reduced peaks for most of the impurities found on the bare stainless surface.

6.10 DIFFUSION THROUGH GOLD FILMS ON STAINLESS STEEL[15]

J. F. Simpkins

Gold-coated type 304 stainless steel has been used for the liner of the plasma chamber in thermonuclear experiments at this laboratory. To be most effective, these coatings should provide an inert, sorption-free surface, have good heat reflecting properties and strong adherence, and produce the minimal increase in electrical conductivity. Thin films of gold on stainless satisfy most of these requirements, except that after a short heat treatment, many of the constituents in the stainless were found to diffuse through the gold film. Mass scans of a gold-coated stainless steel surface and of a bare stainless surface showed almost identical impurity distributions. Tison et al. reported that, for a platinum film on titanium, diffusion through the platinum was suppressed by the formation of the intermetallic compound Ti_3Pt at the interface. We have found that a 500-Å film of platinum between the gold and stainless also acts as a barrier to the diffusion process in this system and greatly reduces the amount of contamination at the gold surface. Mass scans of the gold surface with platinum underlayer after heat treatment revealed very little diffusion through the gold. In addition, the ion microprobe mass analyzer was used to monitor $^{16}O^+$, $^{32}S^+$, $^{28}Si^+$, $^{29}Si^+$, and $^{56}Fe^+$ intensities as a function of depth into the film cross section. This technique also indicated that the platinum acts as a barrier to diffusion through the gold.

6.11 SAFETY WITH HIGH MAGNETIC FIELD SYSTEMS[16]

J. N. Luton, Jr.

This paper first reviews the magnetic forces within and between coils, forces on coil leads and iron, eddy currents, coil heating, and energy stored in the magnetic field. Four quite different magnet systems are qualitatively and quantitatively compared to give an indication of the variation encountered in laboratory magnet systems. Commonly occurring hazards are discussed and illustrated, including insulation failure of resistive and superconducting coils, loss of coolant, structural collapse, and ancillary equipment failure. We next consider the ability of the human body to resist mechanical abuse, electric shock, and magnetic fields. Finally, based on the foregoing technical discussion, the paper considers personnel safety and suggests specific safety precautions that should be taken during design and operation of high-field coil systems.

6.12 MAGNETIC INSTABILITY IN HARD SUPERCONDUCTORS[17]

K. Koyama

By considering the electric field induced by flux motion, the requirement for stabilization of a hard superconductor against flux jumps has been found to be $J_c^2 < k^2 C_v T_0 [1 + (D_t / D_m)]\mu_0^{-1}$, where C_v is the heat capacity per unit volume of the superconductor, T_0 is given by $J_c(\partial J_c/\partial T)^{-1}$, D_t and D_m are the thermal and magnetic diffusivities of the superconductor, respectively, and k^2 is the smallest number satisfying the following time-independent temperature equation: $\nabla^2(\Delta T) = k^2 \Delta T$. Using the above criterion, we derive the stability requirements in both adiabatic and dynamic stability limits. We then discuss the stability of commercial superconductors covered by normal metal. The stability criteria can be obtained by replacing D_m in the inequality with the average magnetic diffusivity of the normal metal and superconductor.

6.13 CALCULATION OF RADIAL MAGNETIC FIELDS FOR AXISYMMETRIC SOLENOIDS WITH RECTANGULAR CROSS SECTION[18]

P. L. Walstrom M. S. Lubell

The ratio of maximum radial field to maximum axial field has been calculated numerically for axisymmetric

---

15. Presented at the New Mexico Chapter A.V.S., 9th Annual Symposium, Albuquerque, N.M., April 9–11, 1973; available on video tape from A.V.S., 335 E. 45th St., N.Y.C. 10017.

16. Abstract of paper presented at the Southern Area Research and Development Symposium, April 1973. Conference proceedings to be published. Available as ORNL-TM-4313.

17. Abstract of paper in *J. Appl. Phys.* **44**, 5531 (1973).

18. Abstract of paper in *J. Appl. Phys.* **43**, 4195 (1973).

solenoids of rectangular cross section and constant current density over a wide range of coil configurations. It is also shown that for a certain range of coil shapes the maximum modulus of the magnetic field occurs on the end faces of the windings. These considerations are pertinent in the design of superconducting magnets for two reasons: (1) Many superconductors have lower critical current in a field normal to the wide surface than in a field parallel to the surface, and (2) large radial fields can cause catastrophic flux jumps.

7. Cryogenic Dielectric Measurements

W. F. Gauster[1] H. M. Long
R. H. Kernohan[2] W. J. Schill
S. W. Schwenterly[2]

7.1 CRYOELECTRIC RESEARCH[3]

W. F. Gauster S. W. Schwenterly

A literature search on the dielectric strength of cryogenic liquids and gases has revealed the limitations of existing data with respect to gap length, test voltage, and power. Consequently, a more complete program of experiments has been instituted which includes breakdown, flashover, and partial discharge tests under dc, ac, and impulse voltages. Auxiliary tests have been carried out to assist in the design of experimental equipment. Considerable attention has been devoted to the statistical evaluation of the experimental data.

An intermediate-voltage test facility with 130 kV dc, 5 mA and 80 kV rms ac, 70 mA supplied has been put into service and provided with appropriate instrumentation. A Hipotronics 700 kV ac, 1.5 A resonant test set has been set up, tested, and approved by the ORNL Accelerator Review Committee. The high-voltage facility, now under construction, will utilize this resonance transformer and the already existing Haefely 600 kV dc, 5 mA supply. Several manufacturers have been contacted regarding the purchase of an impulse generator rated at about 1.5 MV. A sensitive Biddle bridge-type detector has been purchased for the partial discharge experiments.

A cryostat incorporating a vacuum bushing has been constructed for the intermediate-voltage facility and successfully operated up to 120 kV. Information gained from experiments with this cryostat is being used to design a much larger version for higher voltages and operation with pressures up to 10 bars and temperatures up to 10°K. Although lack of funds slowed progress on this project, the large dewar for this cryostat is expected to be completed during the present fiscal year.

The experimental program has concentrated on the intermediate-voltage cryostat. A large amount of dc breakdown data[4] have been obtained in slowly boiling liquid helium using sphere and plane electrodes. After various improvements were made in the cryostat design, the heat leak to the electrodes became so low that recent data agree well with values published by Gerhold[5] for nonboiling helium and are much higher than values published by Meats[6] for boiling helium. In agreement with these other investigations, variation of the voltage ramp rate from 0.08 kV/sec to 10.0 kV/sec gave no significant change in the breakdown electric fields, which ranged from 327 kV/cm at 3.0 mm to 500 kV/cm at gaps of less than 1.0 mm.[4] Some future subjects for investigation will include the influences of helium boiling rate and contamination, electrode geometry, and electrode surface conditions, with dc voltages of both polarities and ac voltages. Furthermore, two major projects for the coming fiscal year will be the acquisition of an impulse generator and completion of a bushing for the high-voltage cryostat.

The programs on cable conductor materials measurement and development being carried out in the Metals and Ceramics Division have proceeded to an initial characterization of materials. Since no funding for these studies was included in the FY 1974 budget, they are now in standby status. It is expected that they will resume in FY 1975.

---

1. Consultant.
2. Solid State Division.
3. ORNL-TM-4187, Appendix A (March 1973).
4. ORNL-TM-4476, January 1974.
5. J. Gerhold, *Cryogenics* 12, 370 (1972).
6. R. J. Meats, *Proc. Inst. Elec. Eng.* 119, 760 (1972).

7.2 DIELECTRICS FOR SUPERCONDUCTING SYSTEMS[7]

W. F. Gauster R. H. Kernohan
H. M. Long S. W. Schwenterly

An investigation of the dielectric properties of fluids and solids for use in superconducting systems is under way at the Oak Ridge National Laboratory as part of the AEC program in superconducting power transmission. The investigation initially will encompass ac and dc breakdown and prebreakdown phenomena in liquid helium and in a variety of solids in liquid helium. Extension to impulse measurements is expected in the near future. A prime objective of the investigation is to determine scaling laws applicable to various models of superconducting cables and other cryogenic apparatus. The experiments are being devised with this objective in mind. Experimental facilities have been set up for ac testing with a series resonant transfer to 700 kV rms and for dc testing to 600 kV. A high-voltage cryostat has been designed for service to 1000 kV with provision for optical as well as electrical recording of both breakdown and prebreakdown phenomena. Other apparatus for testing to lower voltages is also available. Instrumentation for partial discharge measurements by multichannel pulse-height analysis, high-speed oscilloscope, and bridge detection is available.

The influence of electrode surfaces and impurities as well as pressure and temperature on the dielectric properties of liquid helium will be determined. The behavior at large gaps is of particular interest. Breakdown and surface flashover of bulk and laminated solids in liquid helium and in vacuum at liquid helium temperatures are to be included in the investigations.

---

7. Abstract of paper presented at the Annual NAS/NRC Dielectric and Insulation Conference, Montreal, Canada, October 29–31, 1973, to be published in the Annual Report of the Conference and the annual *Digest of Literature in Dielectrics*.

8. Fusion Reactor Technology

R. G. Alsmiller[1] J. R. DiStefano[4] L. H. Jenkins[5] N. Nozawa[9] J. L. Scott[4]
J. Barish[2] L. Dresner[6] C. E. Klabunde[5] E. M. Oblow[1] F. J. Smith[3]
D. E. Bartine[2] C. K. H. Dubose[4] R. L. Kluch[4] O. S. Oen[5] D. Steiner
J. T. Bell[3] W. P. Eatherly[4] J. T. Kriese[8] J. K. Redman[5] R. A. Strehlow[3]
E. E. Bloom[4] K. Farrell[4] D. B. Lloyd[7] R. E. Reed[5] M. L. Tobias[7]
S. Cantor[3] L. M. Ferris[3] R. E. MacPherson[7] M. T. Robinson[5] J. J. Tudor[7]
R. R. Coltman, Jr.[5] R. C. Forrester[3] F. R. Mynatt[1] M. J. Saltmarsh[10] J. S. Watson[3]
W. H. Cook[4] A. P. Fraas[7] J. Narayan[5] R. T. Santoro[1] F. W. Wiffen[4]
J. H. DeVan[4] T. A. Gabriel[1] T. S. Noggle[5] H. C. Savage[3] F. J. Young[11]

8.1 MAGNETOHYDRODYNAMIC EFFECTS IN FUSION REACTOR BLANKETS

8.1.1 Effects of a Strong Magnetic Field on Boiling of Potassium[12]

A. P. Fraas D. B. Lloyd R. E. MacPherson

One of the most promising ways to cool the lithium blanket of a full-scale fusion reactor is to employ a once-through potassium boiler in the blanket. A question has been raised as to whether this approach might have the disadvantage that magnetohydrodynamic effects might inhibit nucleate boiling. An analysis of the problem indicates that this is not the case, and an experiment has been run in which potassium has been boiled in magnetic fields ranging from 0 to 50,000 G. This work indicates that the presence of a strong magnetic field will have small effects on nucleate boiling of potassium, but there should be no serious effects so far as the operation of the boiler is concerned. The principal effects noted in the course of the experiment were some small changes in the boiling sounds and some small changes in the boiler temperature distribution. The change in sound is believed to result from an inhibiting effect of magnetohydrodynamic forces on the rate of implosion of bubbles, and the change in temperature distribution is believed to have stemmed from small changes in the thermal convection flow pattern in the boiler so that there was a small change in the distribution of energy input between nucleation sites in going from a zero magnetic field to a strong magnetic field.

8.1.2 Magnetohydrodynamic Blanket Scaling in a Toroidal Fusion Reactor[13]

F. J. Young

The blanket region of a toroidal fusion reactor is a vital link in the chain of energy conversion processes necessary for the generation of electricity from thermonuclear fusion. In a typical full-scale reactor the blanket would contain 2800 metric tons of lithium, which would be pumped along the toroidal magnetic flux tubes. Even in a well-designed blanket, it is not possible to avoid having some regions in which the lithium would be channeled perpendicular to the magnetic field lines. The resulting magnetohydrodynamic phenomena cause increased viscous and eddy-current losses. It is important to understand and to be able to predict the

1. Neutron Physics Division.
2. Computer Sciences Division.
3. Chemical Technology Division.
4. Metals and Ceramics Division.
5. Solid State Division.
6. Chemistry Division.
7. Reactor Division.
8. Present address: Westinghouse Electric Corporation, Bettis Atomic Power Laboratory, West Mifflin, Pa.
9. Visiting Scientist, JAERI, Japan.
10. Physics Division.
11. Visiting Scientist, Westinghouse Research Laboratory, Pittsburgh, Pa.

12. Abstract of ORNL-TM-4218 (February 1974).
13. Abstract of paper prepared for presentation at the Topical Meeting on the Technology of Controlled Nuclear Fusion, San Diego, California, April 16–18, 1974.

requisite pumping power. Although the pumping power appears as heat, large amounts of pumping power flowing into the blanket aggravate formidable intrinsic heat transfer and thermal stress problems present in the blanket region. Estimates of pumping power have been made on the basis of one- and two-dimensional laminar magnetohydrodynamic studies, but it is realized that turbulence may play a major role, and this implies the need for experimental data. The lithium blanket envisioned is hard to simulate with one- or two-dimensional models and operates in a range of parameters exceeding past experiments by almost two orders of magnitude.

In this paper the magnetohydrodynamic scaling of a full-sized blanket is investigated with a view to specifying an experimental-scale model blanket, the smaller the better, that will be magnetohydrodynamically similar to the lithium blanket of a full-sized prototype reactor. The equations of magnetohydrodynamic channel flow and heat transfer were subjected to a dimensionless analysis. Of all the possible dimensionless parameters describing MHD channel flow and heat transfer, the most important were identified. For the present lithium blanket design, they are given by: Reynolds number, 210,000; magnetic Reynolds number, 0.34 (in pumping region) and 11.34 (in field-flow-aligned region); magnetic Mach number, 0.00425 (implying a Hartmann number of 63,000); and Peclet number, 4000.

The properties of many liquid metals were studied as possible candidates for the scale-model liquid. It was determined that either NaK (44% Na) or NaK (78% Na) can be used to obtain MHD similarity provided the fluids are heated to temperatures of 180°C and 135°C respectively. If it is assumed that the magnetic field is supplied by a superconducting niobium-titanium magnet producing a field of 7.5 T, the model scale factor for NaK (44% Na) is 1/2.77, and for NaK (78% Na) it is 1/2.58. Thus the model can be about one-third the size of the full-scale lithium channel.

8.2 MATERIALS COMPATIBILITY STUDIES

8.2.1 Corrosion of Vanadium by Lithium[14]

J. H. DeVan R. L. Klueh

The partitioning of oxygen between liquid lithium and α-vanadium was investigated between 600 and 1000°C. At all test temperatures the interstitial oxygen content of the vanadium was decreased by contact with lithium, even when the lithium contained excess Li_2O. Vanadium containing as much as 2200 ppm O resisted lithium attack at 815°C. Additions of oxygen to the lithium did not enhance the dissolution of vanadium. The oxygen content of V–20% Ti also was decreased by exposure to lithium at 800 and 1000°C; however, the decrease at 800°C was apparently slowed by the diffusion kinetics of oxygen in the alloy.

8.2.2 Corrosion of Niobium and Tantalum by Lithium[15]

R. L. Klueh

The effect of oxygen on the corrosion of niobium and tantalum by liquid lithium at 600°C was studied with static capsules. An increase in the oxygen concentration of the lithium from 100 to 2000 ppm had no measurable effect on the dissolution of either refractory metal, a result that is contrary to the effect of similar oxygen concentrations in sodium and potassium. Exposure to lithium reduced the oxygen content of niobium and tantalum to ≤20 ppm regardless of the oxygen concentration of the lithium. These results agree with thermodynamic calculations that predict that the equilibrium distribution coefficient (i.e., the ratio of the oxygen concentration in the refractory metal to that in lithium) is very much less than unity.

When the oxygen concentration of niobium and tantalum exceeded a threshold level, lithium (with no oxygen added) penetrated the refractory metal. Penetration resulted from the formation of a ternary oxide on grain boundaries or preferred crystallographic planes and proceeded by a wedging mechanism, caused by stresses generated by the corrosion product.

Penetration was along grain boundaries at low oxygen concentrations, the attack depth and number of affected boundaries increasing with increasing oxygen concentration. At higher oxygen concentrations, transgranular attack also occurred. The threshold oxygen concentrations for attack (grain-boundary penetration) were determined to be 400 and 100 ppm for niobium and tantalum respectively.

8.2.3 Corrosion of 2¼ Cr–1 Mo Steel by Lithium

J. H. DeVan J. R. DiStefano

A promising alloy for lithium containment at 500°C or below has the base composition 2¼ Cr–1 Mo–bal Fe. A modification of this alloy has been developed for

14. Abstract of "The Effect of Oxygen on the Corrosion of Vanadium and V–20% Ti by Liquid Lithium," paper presented at ANS Winter Meeting, San Francisco, California, November 11–16, 1973, to be published in *Nuclear Applications*.

15. Abstract of ORNL-TM-4069 (March 1973), to be published in *Met. Trans.* 5 (April 1974).

sodium service that contains 1% Nb to retard decarburization. We constructed a small thermal convection loop of the niobium-stabilized 2¼ Cr–1 Mo steel and operated it with lithium for 10,000 hr at a hot-leg temperature of 600°C. The weight loss occurring at the hottest point in the loop corresponded to 0.1 mil/year surface removal. This corrosion rate is five times lower than that for austenitic stainless steels under comparable conditions.

8.3 NEUTRONICS

8.3.1 Analysis of a Bench-Mark Calculation of Tritium Breeding in a Fusion Reactor Blanket[16]

D. Steiner

A fusion reactor operating on the deuterium-tritium fuel cycle will require a tritium-breeding blanket. Tritium production in the blanket will be accomplished through interactions between the fusion neutrons and the isotopes of lithium, via the $^6Li(n,\alpha t)$ and the $^7Li(n,n'\alpha t)$ reactions. The tritium breeding performance of conceptual blanket models has been calculated by a number of groups. However, since these calculations have generally been based on different cross-section sets, it has been difficult to compare results obtained by different groups. At the Neutronics Session of the International Working Sessions on Fusion Reactor Technology (held at Oak Ridge National Laboratory, June 1971), it was agreed to undertake a bench-mark calculation of tritium breeding using version 3 of ENDF/B (ENDF/B-3) as the reference for cross-section data.

Calculations were carried out with discrete-ordinates codes and with Monte Carlo codes. Analysis of the calculations identified deficiencies in the cross-section processing codes and differences in calculational details which resulted in discrepancies among the calculated results. Correction of these deficiencies and a more precise specification of calculational details will lead to improved agreement in future fusion bench-mark problems. The following observations are made regarding future calculations.

1. For the assumed blanket geometry, approximating the flux with a fourth-order angular quadrature (S_4) gives a system tritium breeding value which is within about 0.5% of the Monte Carlo system value. Thus the S_4 approximation is adequate for survey calculations on system tritium breeding.
2. An S_{12} approximation is recommended in those cases where accurate spatial information is desired.
3. More attention should be given to the choice of mesh spacing. The effect of mesh spacing in the vacuum region was discussed in this paper. However, additional mesh-spacing problems are most likely present in the bench-mark model; for example, the mesh spacing in the lithium regions near the graphite may be too coarse.
4. Future bench-mark calculations should involve magnet shield models as well as breeding blanket models.

8.3.2 Magnet Shield Design for Fusion Reactors[17]

J. T. Kriese D. Steiner

Current concepts of mirror and tokamak fusion reactors employ superconducting magnet coils in order to minimize the power requirements of the magnet system. Since most fusion fuel cycles of interest involve the production of high-energy neutrons, adequate shielding must be provided for the cryogenically cooled coils. The magnet shield must limit both nuclear heating and radiation damage in the coil region. We have surveyed alternate shielding materials with regard to their nuclear engineering characteristics in deuterium-tritium fusion reactors. The topics considered include (1) nuclear heating, (2) radiation flux levels, (3) estimates of shield material costs, and (4) chemical compatibility considerations.

8.3.3 The Nuclear Performance of Vanadium as a Structural Material in Fusion Reactor Blankets[18]

D. Steiner

Several early conceptual designs of fusion reactors employed niobium as the structural material for the blanket. Subsequent neutronic analyses of these designs indicated that the neutron-induced activity and associated nuclear afterheat of the niobium structure reached significant levels during reactor operation. Although the engineering requirements imposed by activation of the niobium structure appear to be less stringent than those imposed by the radioactive inventories associated with fission reactors, it is desirable to identify alternate structural materials which ameliorate the engineering requirements imposed by neutron activation. Preliminary investigation of several potential structural materials indicated that vanadium would

16. Abstract of ORNL-TM-4177 (April 1973).
17. Abstract of ORNL-TM-4256 (June 1973).
18. Abstract of ORNL-TM-4353 (October 1973); also *Nucl. Fusion* **14**, 33–44 (1974).

exhibit excellent activation characteristics in a fusion reactor.

We have examined the nuclear performance of vanadium as a structural material in a deuterium-tritium fusion reactor. For comparison, calculations are also presented for niobium. The areas considered include (1) tritium breeding, (2) nuclear heating, (3) radiation effects relating to material damage, and (4) neutron-induced activity. It is concluded that (1) the tritium breeding characteristics of vanadium are somewhat superior to those of niobium, (2) nuclear heating in the first wall of the blanket will be substantially lower with vanadium than with niobium, (3) helium and hydrogen production in the first wall will be significantly greater with vanadium than with niobium, and (4) vanadium will exhibit an afterheat and biological hazard several orders of magnitude lower than those of niobium for times after shutdown of about 100 days and greater.

8.3.4 Cross-Section Sensitivity of Breeding Ratio in Fusion Reactor Blankets[19]

R. G. Alsmiller, Jr. | F. A. Gabriel
J. Barish | F. R. Mynatt
D. E. Bartine | E. M. Oblow
R. T. Santoro

For several proposed fusion reactor blanket configurations, the changes in the tritium breeding ratio due to changes in nuclear cross-section data are being calculated on the basis of linear perturbation theory. Results are being obtained for the changes in the breeding ratio due to changes in specific energy ranges of various partial cross sections of the major constituents of the blankets. In the specific configuration for which the studies have been completed, the breeding ratio was found to be most sensitive to changes in the $^7Li(n,n'\alpha)t$ cross section, but the sensitivity to changes in this cross section was not large.

8.3.5 Cross-Section Sensitivity of Tritium Breeding in a Fusion Reactor Blanket: Effects of Uncertainties in Cross Sections of ^6Li, ^7Li, and ^{93}Nb[20]

D. Steiner | M. L. Tobias

We have examined the cross-section sensitivity of the tritium breeding ratio in a fusion reactor blanket model which is representative of a large class of blanket configurations under current investigation. This blanket model exhibits the following tritium breeding and neutronic characteristics: (1) liquid lithium of natural isotopic abundance is used for breeding, (2) the tritium breeding ratio is in the "high" range, i.e., (3) graphite is employed for neutron moderation, and (4) the neutron leakage from the blanket is relatively low, about 4% of the source neutrons. The sensitivity of the breeding ratio was evaluated by altering reference cross-section sets to reflect estimates of the uncertainties in the cross sections of the $^6Li(n,\alpha)t$, the $^7Li(n,n'\alpha)t$, and the $^{93}Nb(n,2n)$ reactions. Our analysis leads to the following observations:

1. The status of the $^6Li(n,\alpha)t$ cross-section data appears adequate for accuracies of the order of about 1% in tritium breeding calculations. We emphasize that this observation applies to the class of blanket configurations considered here and that other classes must be examined to determine the generality of the observation.

2. Uncertainties in the cross section and secondary-neutron energy distribution of the $^7Li(n,n'\alpha)t$ reaction attach uncertainties in excess of 5% to the tritium breeding ratio. A reevaluation of the relevant data in the energy range above about 10 MeV might provide a smaller uncertainty, and we recommend that such a reevaluation be undertaken. Additional measurements may be required to reduce the uncertainty in the tritium breeding ratio to the order of 1 to 2%.

3. Uncertainties in the $(n,2n)$ cross section of ^{93}Nb attach uncertainties of about 2.4% to the tritium breeding ratio. New experimental data on the $^{93}Nb(n,2n)$ cross section are available, and a recent evaluation of these data suggests that the variations adopted here may reflect too pessimistic an estimate of the uncertainty. This point will be pursued in future studies.

4. When the cross sections of the $^6Li(n,\alpha)t$, the $^7Li(n,n'\alpha)t$, and the $^{93}Nb(n,2n)$ reactions are varied simultaneously, the calculated uncertainty in the tritium breeding ratio is about 7% to 8%. This uncertainty approaches 10% when uncertainties in the secondary-neutron energy distribution of the $^7Li(n,n'\alpha)t$ reaction are included.

8.3.6 Coupled Neutron and Gamma-Ray Cross-Section Sets for Fusion Reactor Calculations[21]

J. T. Kriese

Coupled 37-energy-group P_3 (third-order Legendre coefficient expansion) neutron (52 groups) and gamma-

---

19. D. E. Bartine, R. G. Alsmiller, Jr., F. R. Mynatt, E. M. Oblow, and T. T. Santoro, "Cross-Section Sensitivity of Breeding Ratio in a Fusion-Reactor Blanket," *Nucl. Sci. Eng.* 53, 304–314 (1974).

20. Abstract of paper in *Nucl. Fusion* 14, 153–163 (1974).

21. Abstract of ORNL-TM-4277 (August 1973).

ray (21 groups) cross-section sets have been developed for calculating fluxes in conceptual fusion reactor designs. These cross-section sets are suitable for use with either the discrete-ordinates code ANISN or the Monte Carlo code MORSE. This library includes data for H, ^{6}Li, ^{7}Li, B, ^{12}C, O, Mg, Al, V, Fe, Cu, Nb, Ta, and Pb. *These data sets can be obtained on request from the Radiation Shielding Information Center (RSIC) at ORNL.* The cross-section sets will be updated as new data and evaluations become available.

8.4 RADIATION DAMAGE STUDIES

8.4.1 The Tensile Properties of Fast Reactor Neutron-Irradiated BCC Metals and Alloys[22]

F. W. Wiffen

Rod tensile samples of niobium, molybdenum, tantalum, one alloy based on each of these metals, and two vanadium-base alloys have been irradiated in EBR-II at temperatures between 390 and 1140°C to neutron fluences in the range 1.5 to 6.1 × 10^{22} neutrons/cm^2 (>0.1 MeV). The effect of neutron irradiation at these fluences and temperatures on the strength and ductility properties was determined in tensile tests at temperatures between 20 and 800°C at strain rates of 0.02 min^{-1} or slower. The effect of irradiation is most severe in molybdenum-base systems. Irradiation near 400°C renders Mo–50% Re brittle to at least 800°C. Similar irradiation of molybdenum and Mo–0.5% Ti produces a high concentration of small dislocation loops in the microstructure and raises the strain-rate-dependent tensile ductile-brittle transition temperature from below room temperature to the range 400 to 550°C. Brittle failures occur with a mixed cleavage and grain boundary separation fracture mode. Specimens of tantalum, T-111, and Nb–1% Zr exhibited zero uniform elongation but had total elongations in the range 4 to 10% with ductile-mode fractures for most test conditions. Niobium, V–10% Cr, and VANSTAR-7 had 5 to 17% total elongation and uniform elongations in the range 1.5 to 10%. Marked strength increases over control values were found in all samples. The results are discussed in terms of the microstructures and fracture modes. It is concluded that dislocation channeling is the process responsible for the complete loss of uniform elongation where loop hardening predominates.

22. Abstract of published paper, p. 176 in *Defects and Defect Clusters in B.C.C. Metals and Their Alloys*, ed. R. J. Arsenault, *Nuclear Metallurgy*, vol. 18 (1973).

8.4.2 Effect of High Helium Content on Stainless Steel Swelling[23]

F. W. Wiffen E. E. Bloom

Type 316 stainless steel specimens have been irradiated in the HFIR reactor at temperatures between 380 and 680°C to displacement damage levels up to 120 displacements per atom and transmutation-produced helium contents up to 6000 ppm. Swelling in solution-annealed samples was found to be larger than predicted by either helium swelling models or fast reactor irradiation results, and the temperature dependence of swelling was also not in agreement with either model. Cold work was effective in reducing swelling for irradiation temperatures up to 600°C but was ineffective at 680°C. For both annealed and cold-worked materials the swelling was nearly temperature-independent between 380 and 600°C but increased markedly at 680°C. Present models are inadequate to explain the swelling results in the presence of these high helium concentrations.

8.4.3 Neutron Irradiation Damage in Niobium and Nb–1% Zr[24]

F. W. Wiffen

The favored candidate structural material in several CTR conceptual designs is a niobium alloy, possibly Nb–1% Zr. These designs give operating temperatures between 400 and 1000°C and total neutron flux at the first wall of 1.6 to 20 × 10^{14} neutrons cm^{-2} sec^{-1}. A probable choice of the first-wall neutron loading is 1 MW/m^2. This corresponds to a flux of 2.8 × 10^{14} neutrons cm^{-2} sec^{-1} (>0.1 MeV), and continuous operation for one year will result in 22 displacements per atom (dpa) and transmutation reactions yielding 1200 ppm Zr, 90 ppm H, and 26 ppm He. Of these, the displacement damage and helium accumulation will have the most important effects on the structural material properties. Specimens irradiated in fission reactors are being tested to examine the effects of displacement damage in the absence of transmutation products.

Fully recrystallized samples of commercially pure niobium and Nb–1% Zr were irradiated in EBR-II in

23. Abstract of paper presented in "Fusion Reactor Materials" session at the American Nuclear Society meeting in November 1973 [*Trans. Amer. Nucl. Soc.* 17, 143 (1973)] and submitted for publication in *Nuclear Technology*.

24. Summary of paper presented in "Fusion Reactor Materials" session at the American Nuclear Society meeting in November 1973 [*Trans. Amer. Nucl. Soc.* 17, 140 (1973)].

the range 390 to 1000°C, up to 34 dpa, and fluences up to 3.7×10^{22} neutrons/cm^2 (>0.1 MeV). These irradiations produced 1 to 2 ppm He. At 2.5×10^{22} neutrons/cm^2 (26 dpa), electron microscopy established swelling due to void formation in niobium for irradiation temperatures of 425 to 1000°C. The maximum void swelling was 4.8% at 585°C, suggesting a swelling vs temperature curve for niobium with a peak near 600°C. The limits on the temperature range for void formation were not established by this work. In Nb–1% Zr irradiated under identical conditions, appreciable void swelling (about 1%) was found only at 790°C, although the results were not definitive at 1000°C. At lower temperatures, voids could not be detected in the complex microstructure of dislocation loops. Void suppression in Nb–1% Zr was confirmed for irradiation at 390 and 450°C in samples where geometry and density measurements were used to supplement the microscopy observations. Postirradiation annealing the samples to 900°C simplified the microstructures in the two materials and confirmed the void suppression in the Nb–1% Zr for irradiation at 450°C.

Buttonhead specimens of niobium were irradiated near 450°C to a fluence of 3.0×10^{22} neutrons/cm^2 (34 dpa) and were tensile tested at 25, 400 and 650°C. All tests showed ductile behavior. At all test temperatures the results were qualitatively similar; yield and ultimate strengths in the irradiated samples were 2 to 5 times the control specimen values, and total elongations of irradiated samples ranged from 12 to 17% in niobium and from 8 to 12% in Nb–1% Zr. An important difference between the two materials is in the uniform elongation: while the niobium had 2.5 to 10% uniform elongation, the Nb–1% Zr was plastically unstable with only 0.1% uniform elongation. Fractography showed ductile-mode failure surfaces in both materials. The difference between the two materials can be explained by the different microstructures. In the irradiated Nb–1% Zr, the first moving dislocations sweep up the irradiation-produced dislocation loops and leave defect-free channels or "soft" paths for further deformation. In the niobium, the voids produced by irradiation cannot be removed by dislocation motion and produce some work hardening during deformation. Electron microscopy showed some evidence of this channeling in the Nb–1% Zr, but none was observed in the niobium.

8.4.4 Graphite for Controlled Thermonuclear Reactor Applications[25]

W. P. Eatherly J. L. Scott W. H. Cook

Graphite has appropriately been selected as one of the blanket materials in the designs of several controlled thermonuclear (fusion) reactors (CTRs). We examined in some detail the operating conditions of CTRs as they affect the graphite during the normal 20 to 30 years central power station life. We restricted the examination to the effects of neutron fluence and temperature as they determine the potential lifetimes of current and advanced grades of graphite under anticipated operating conditions in CTRs. The problem areas are delineated, and recommendations for solving them are given.

The operating temperatures for graphite in CTRs range from 200 to 1000°C. Below 300°C the total stored energy in the neutron-irradiated graphite is a serious problem; we emphasize the need for attention to this. We concentrated the major part of our examination on an Oak Ridge National Laboratory design of a tokamak fusion reactor that uses graphite as the center part of its blanket. The graphite is 40 cm thick in the radial direction, and the calculated temperatures across it range from 650 to 970°C. The fluence across the 40 cm of graphite for typical central station power plants operating for 30 years with a plant factor of 85% would normally be 10×10^{22} down to 0.4×10^{22} neutrons/cm^2 (>50 keV). (The energy for all neutrons referred to in this report is >50 keV.) The greatest fluence acquired to date in studies of various grades of graphite is 4×10^{22} neutrons/cm^2 at temperatures in the vicinity of 700°C. Fast-neutron irradiations at high temperatures have been made up to 1300°C, but the fluences generaliy range from only 1.5×10^{22} to 2×10^{22} neutrons/cm^2.

We use temperature profiles, flux distribution, and existing irradiation data to predict lifetimes of commercial grades of graphite. We conservatively assume that the lifetime is equivalent to the fluence at which the net parabolic volume distortion of the graphite returns to zero. The volume distortion is strongly affected by the irradiation temperature. The lifetime curves that were developed showed that the "best" existing grades of graphite are inadequate for more than half of the radial thickness of the graphite for 20 to 30 years of operation. It appears that the graphite lifetime could be as short as four years under the severest conditions.

Oak Ridge National Laboratory has been developing new experimental grades of isotropic graphite that have shown improved unirradiated and irradiated properties. These include techniques that involve green coke (calcined below 1000°C) and unconventional fabrication techniques. Although these new experimental

25. Summary of paper presented in "Fusion Reactor Materials" session at American Nuclear Society meeting, November 1973 [*Trans. Amer. Nucl. Soc.* 17, 146 (1973)].

grades are in the early developmental stages, they show promise of significantly longer lifetimes and improved performance characteristics.

This study showed that (1) there is an extreme lack of basic and critical engineering design data for graphite for the nuclear environment of CTRs, (2) there is a need for and promise of significantly better grades of graphite, and (3) the orderly development of CTRs requires that advanced fundamental and engineering studies on the irradiation and development of graphite be begun without delay.

8.4.5 Development of Ion Irradiation Facilities

E. E. Bloom C. K. H. Dubose M. J. Saltmarsh

The neutron energy spectrum of a fusion reactor will be different from that available in fission reactors. To investigate the effects of this fusion reactor neutron spectrum on the properties of potential CTR first-wall materials, a number of simulation techniques are being used. One technique is the irradiation of materials with self-ions. To make use of this technique a 5.5-MV Van de Graaff has been equipped with a multiple ion source which will allow the injection of transmutation products (e.g., helium), followed by irradiation with self-ions to create displacement damage. In the past year the facility was made fully operational. A number of improvements beyond the initial design were made: (1) an x-ray analyzer was added to the system for continuous analysis of composition of the ion beam; (2) additional devices were added for both continuous and intermittent measurement of beam current; and (3) modifications were made to allow samples to be changed more rapidly. Initial experiments to correlate damage in ion-irradiated and neutron-irradiated samples are now under way.

We have also initiated the design of a facility to study radiation creep deformation. Approximately 60-MeV alpha particles accelerated by the Oak Ridge Isochronous Cyclotron will be used to create displacement damage as they pass through thin (about 0.125 cm thick) uniaxially stressed samples. It is expected that displacement rates about a factor of 10 higher than those attainable in the Experimental Breeder Reactor II core can be achieved. The facility will be used to study mechanisms of radiation creep as well as provide information on the behavior of engineering alloys.

8.4.6 Ion Radiation Damage[26]

O. S. Oen J. Narayan T. S. Noggle

The relation of ion damage to equivalent reactor neutron damage is dependent on theoretical treatments of the stopping of energetic (MeV) particles in solids. The theory is largely untested by experiment, particularly with respect to the nuclear component of the stopping, which produces the atomic displacements responsible for the damage in metals. The present work represents initial results of a combined theoretical and experimental program to relate the predicted and observed damage in copper irradiated with 1-MeV protons at room temperature. The nascent displacement damage was calculated as a function of proton penetration depth, including such factors as straggling of the proton beam. Experimental targets were sectioned parallel to the range of the ions. The damage was observed in the electron microscope as dislocation loop structures formed by the clustering of interstitials. Measurements of the damage density and the size distribution of the loops as functions of distance from the surface allow estimates to be made of the number of point defects as a function of depth. Experiment and theory are in quantitative agreement with respect to the range of the protons and in semiquantitative agreement with respect to the damage density as a function of penetration depth. This study shows both qualitative and quantitative differences between proton and fast-neutron damage in copper. First, only interstitial-type dislocation loops have been detected here, although approximately equal numbers of vacancies and interstitials are observed in dislocation loops in fast-neutron-irradiated copper. Second, only about 1% of the calculated number of displaced atoms is observed in the proton irradiation, whereas approximately 5 to 10% of the calculated number of displaced atoms is observed in the neutron irradiations.

8.4.7 Low-Temperature Damage Rate Studies[27]

R. R. Coltman, Jr. J. K. Redman
C. E. Klabunde R. E. Reed

In order to provide a basis for quantitative estimation of 14-MeV neutron damage from observations of fission neutron or ion damage, a program has been initiated to measure the damage production rate in electron, proton, fission-neutron, and 14-MeV-neutron irradiations of dilute alloys of vanadium, niobium, and molybdenum. Changes in electrical resistance will be measured during irradiations at 4°K. The program involves the cooperation of two other laboratories in this country

26. Summary of paper published in *Proceedings of the International Conference on Applications of Ion Beams to Metals*, Plenum Press, April 1974.

27. Abstract of paper in *Solid State Div. Annu. Progr. Rep., Dec. 31, 1973*, ORNL-4952, p. 29.

and two in Europe, each providing special irradiation facilities. Experimental samples, consisting of 25-μm-thick foils of alloys of vanadium, niobium, and molybdenum containing 0.03 percent zirconium, have been prepared, analyzed, and characterized at ORNL. These samples have recently been distributed to the other laboratories for damage production experiments. The fission-neutron irradiations will be performed in the ORNL Low Temperature Irradiation Facility using a ^{235}U converter especially designed to operate within a superconducting magnet.

8.5 SURFACE STUDIES

8.5.1 Remarks on the Theory of Fast-Neutron Sputtering[28]

M. T. Robinson

Theoretical estimates of neutron sputtering yields are in serious disagreement with experiment, unlike the situation with ion sputtering. Possible reasons for the discrepancy are sought without success. It is shown that chunk ejection by neutrons is not due to single neutron events nor to the dynamic interference of cascades. The need for more complete experimental data to guide development of the theory is emphasized.

8.5.2 CTR Surface Physics

L. H. Jenkins M. T. Robinson
T. S. Noggle M. J. Saltmarsh

Investigations have begun in two areas of surface physics of interest in CTR devices. The surprising neutron sputtering results obtained recently by Kaminsky[29] have prompted us to design a neutron sputtering experiment using a neutron beam from ORIC, produced by deuteron stripping reactions in beryllium or lithium. Neutron spectra have been measured in these targets, and other necessary apparatus is under construction. Targets of gold and niobium will be used. The ORIC source will allow neutron flux densities near 10^{12} cm^{-2} sec^{-1} and doses greater than 10^{16} cm^{-2}, both numbers considerably exceeding those used heretofore.[29]

Theoretical investigations of the reflection of low-energy (about 10^2 eV) hydrogen atoms from metal surfaces have begun using the computer program MARLOWE,[30] designed for studies involving atomic collisions in solids. Calculations to date for copper (001) surfaces show the crucial importance of inelasticities in the collisions as well as expected crystallographic effects. It seems likely that experimental studies of inelastic energy losses will be necessary to provide normalizations for more extensive calculations.

8.6 SYSTEM STUDIES

8.6.1 An Assessment of the Power Balance in Fusion Reactors[31]

M. Nozawa D. Steiner

A general formalism has been developed for analysis of the energy balance in fusion reactors. This formalism has been applied in a detailed and consistent fashion to four current D-T fusion reactor concepts: the laser fusion, the mirror fusion, the theta-pinch fusion, and the tokamak fusion reactor concept. On the basis of a critical examination of the reactor plant subsystems, sets of reference parameters were adopted for each concept. The requirements for power break-even and net power production were then derived for each concept using these reference parameters. The sensitivity of the power break-even and the net power requirements to variations from the reference points was examined in detail. We note the following points with regard to the results of this study.

1. The fusion energy multiplication factor Q, the ratio of fusion energy to heating energy absorbed by the plasma, appears to be a more fundamental measure of fusion power achievement than the Lawson number, $n\tau$. This is particularly true for pulsed systems, where $n\tau$ is a time-averaged quantity.
2. The power break-even value of Q, Q_e, is a measure of the inherent energy handling and conversion efficiency of the reactor plant. In this sense the mirror reactor has relatively high inherent efficiency, while the laser fusion reactor has relatively low inherent efficiency. When the power break-even requirement is cast in terms of the fractional burnup of fuel, the tokamak and theta-pinch reactor exhibit

28. Abstract of paper presented at a conference on Surface Effects in Controlled Thermonuclear Fusion Devices and Reactors, Argonne National Laboratory, January 10–12, 1974.

29. M. Kaminsky and S. K. Das, paper presented at a conference on Surface Effects in Controlled Thermonuclear Fusion Devices and Reactors, Argonne National Laboratory, January 10–12, 1974.

30. M. T. Robinson and I. M. Torens, *Phys. Rev. B* (1974), in press.

31. Abstract of ORNL-TM-4421 (January 1974); to be published in *Nuclear Fusion*.

the least demanding requirements, about 1% fractional burnups.

3. The ratio of Q to Q_c, Y, for a given overall plant efficiency, is a measure of the extent to which fusion performance must be extended beyond the power break-even (feasibility) point. In order to achieve overall plant efficiency to about 40% at modest Q to Q_c ratios (Y about 3 to 4), it appears to be necessary to develop advanced thermal conversion systems with efficiencies approaching 60%. With conventional thermal conversion systems (efficiency about 40%), Q to Q_c ratios of at least 10 will be required to achieve overall plant efficiencies of about 40%.
4. For a given overall plant efficiency, (*a*) the mirror reactor requires the lowest value of Q, while the laser fusion reactor requires the highest value of Q, and (*b*) the tokamak and theta-pinch reactors require the lowest values of fractional burnup.
5. The theta-pinch reactor requires relatively high values of supply energy but relatively low values of circulating energy. This behavior is a consequence of direct energy recovery by induction.
6. The sensitivity of the energy handling and conversion characteristic, Q_c, to variations in subsystem efficiencies is a useful measure of cost-benefit with respect to fusion technology research and development. The theta-pinch reactor exhibits high sensitivity coefficients that exceed those of the other reactor concepts by an order of magnitude.

Future progress in fusion reactor technology as well as in plasma physics will yield more detailed and accurate information on the fusion plant subsystem and operating conditions. This will refine the values of the reference parameters and will allow a more precise determination of the power-balance characteristics. The basic formalism developed in this study should prove useful in future assessment of fusion power requirements and implications.

8.6.2 Mechanical Engineering Design Considerations for a Tokamak Scientific Feasibility Experiment and Plasma Test Reactor[32]

A. P. Fraas J. J. Tudor

A substantial fraction of the cost of both the design and the construction of a fusion facility will be dependent on the structure of the facility, the auxiliary equipment required, and the building in which it is installed. This memo is intended to indicate how some of these problems might be handled, what the equipment might look like, and what its cost might be. The effects of a number of different design choices for major components are given particular attention.

8.6.3 Relations between the Major Size and Cost Parameters of Tokamaks[33]

A. P. Fraas

A set of preliminary estimates of the effects of torus size on major design and cost parameters has been made for a series of tokamak reactors with superconducting coils for the toroidal field. The three sets considered include essentially zero-power scientific feasibility experiments, low-power reactor systems for plasma physics experiments, and full-scale power reactors. The prime concern is with the cost of the superconducting magnet coils, but allowances for the blanket and magnet shield systems are also included, as well as the system for heating the plasma to the ignition temperature. The prime objective was to show trends for major parameters, not absolute values for costs.

The results of the study indicate that the cost of a superconducting coil system for the toroidal field increases relatively little with torus diameter for a scientific feasibility experiment, is quite insensitive to torus size for a plasma physics test reactor, and actually falls off with increasing size for a full-scale power reactor. These effects stem from the reduction in the required magnetic field associated with an increase in torus size together with the increase in the allowable current density in the superconductor material associated with a reduction in the design value for the magnetic field. The results indicate further that, for a modest increase in the cost of superconducting magnets for the toroidal field, it should be possible to build a feasibility experiment so that it can be converted readily into a plasma physics test reactor.

8.6.4 Conceptual Design of the Blanket and Shield Region and Related Systems for a Full-Scale Toroidal Fusion Reactor[34]

A. P. Fraas

An effort has been made to delineate the many boundary conditions that must be met in the design of a full-scale toroidal fusion reactor power plant, with particular emphasis on the problems associated with the

32. Abstract of ORNL-TM-4371 (November 1973).
33. Abstract of ORNL-TM-4080 (January 1974).
34. Abstract of ORNL-TM-3096 (May 1973).

blanket and magnet shield region. These have included provisions for cooling, fuel injection, spent plasma scavenging, magnetohydrodynamic pumping power and heat transfer problems, reactor safety considerations, materials compatibility, fabrication, assembly, maintenance, and costs. In short, an effort was made to take into account all of the boundary conditions that could be envisioned and evolve a well-balanced design with reasonable compromises throughout.

8.6.5 Mechanical Stress in the Pressure Vessel of a Lithium-Filled Exploding-Pellet Thermonuclear Reactor[35]

Lawrence Dresner

Lubin and Fraas have proposed a thermonuclear reactor powered by a laser-ignited pellet of solid deuterium-tritium (D-T).[36] In their device, fusion energy in the form of bursts of x rays, fast neutrons, and D-T plasma is captured in a pool of molten lithium surrounding the exploding pellet. The molten lithium then delivers the fusion energy to a heat engine that generates electricity. The nearly instantaneous absorption of bursts of fusion energy in the lithium creates outgoing pressure waves which eventually load the wall of the pressure vessel. In this report, we estimate the maximum strain produced in the vessel by the impact of the pressure waves. We also discuss the effect of including voids (gas bubbles) in the lithium.

About three-fourths of the energy yield of the thermonuclear reaction is carried off by fast neutrons; the remainder is carried off by x rays and plasma fragments. The x-ray pulse and the neutron pulse occur simultaneously, and the pressure waves to which they give rise overlap. Because we are in a range of strongly nonlinear phenomena, we cannot simply add their effects. The mathematical difficulties of treating both pulses at the same time are great, and we must perforce study them separately. Another reason for studying the neutron pulse and the x-ray pulse separately is that the physical phenomena involved in the production and propagation of the pressure waves are quite different in the two cases.

8.7 TRITIUM HANDLING AND RECOVERY

8.7.1 Systems Evaluations

J. S. Watson R. C. Forrester

During the past year, our engineering evaluations of tritium processing techniques and problems have concentrated on methods for handling the plasma exhaust for recycle. Conceptual studies of tritium handling systems have been made for near-term plasma physics experiments (especially ORMAK F/BX), and the relationship of these systems to those for eventual fusion power reactors has been examined. Many of the techniques needed for tritium management in the physics experiments are similar to those needed for power reactors, although scaling of equipment to much larger sizes will be required for power reactors. Accordingly, many of the development programs that support the near-term plasma experiments will be applicable to ultimate commercial systems. Some real differences do exist. Power reactors will require isotopic separation of protium from tritium and deuterium, while ORMAK F/BX, which is expected to have minimal protium contamination, will require separation of deuterium and tritium. Power reactors (but not ORMAK F/BX) may incorporate diverters of as yet unspecified designs. However, the basic techniques for tritium recovery will apply, with minor alteration, to many possible diverter designs. Major changes in our present tritium processing concepts therefore appear unlikely.

Major process steps required for plasma recycle from a power reactor are: (1) removal of "gases" from the reaction zone; (2) removal of helium, oxygen, nitrogen, etc.; and (3) isotopic removal of hydrogen. Cryosorption pumps appear best for the initial step. The large tritium inventory in such pumps and their necessarily cyclic operation are disadvantages, but their pumping speeds are unlikely to be matched by other pumping systems of comparable cost. Sorption on and desorption from beds of uranium chips will apparently serve to separate the hydrogen isotopes from helium, oxygen, nitrogen and other volatiles for ORMAK F/BX; whereas palladium diffuser membranes may prove superior for larger reactor systems. Several demonstrated methods exist for the separation of hydrogen from deuterium; these methods could, apparently, be applied with moderate cost to the hydrogen-tritium separation required for power reactors. Present plans for ORMAK F/BX are to feed pure deuterium through the injectors into tritium-deuterium mixtures in the active plasma region. Therefore the resulting plasma exhaust will become enriched in deuterium, and deuterium removal will be required. For a relatively short-term experiment such as ORMAK F/BX (but not, of course, for a power reactor), it may prove desirable to use separation services available at other AEC sites.

35. Abstract of ORNL TM-4050 (July 1973).

36. M. J. Lubin and A. P. Fraas, "Fusion by Laser," *Sci. Amer.* **224**(6), 21 (June 1971).

8.7.2 Experimental Studies

J. T. Bell H. C. Savage
S. Cantor F. J. Smith
L. M. Ferris R. A. Strehlow
R. C. Forrester J. S. Watson

An experimental study of the sorption of tritium from liquid metals (e.g., potassium or lithium) has been made using hydride-forming metals as sorbents. Extrapolation of available equilibrium data indicates that some metals, especially yttrium, should be effective sorbents; however, the usefulness of this technique for recovering tritium from blanket or coolant systems could be impaired if tenacious oxide films impede or block the diffusion of tritium into the sorbent, or if repeated tritide cycling limits the sorbent lifetime. Our experiments indicate that oxide films form quickly on both yttrium and zirconium surfaces and reduce the loading rates to values below the level of detection, and far below any useful rates. Uranium metal, on the other hand, gives rapid uptake, but unfortunately its capacity (at a given pressure) for tritium is significantly less than that of yttrium or even zirconium. Zirconium samples sputter-etched and coated with nickel have also been tested. These samples show much higher sorption rates than the uncoated metals; the rates are probably limited by the permeability of the coating.

Chemical studies of the reactions of the hydrogen isotopes with liquid lithium have included measurements of the equilibrium H_2 and D_2 partial pressures above liquid solutions containing LiH or LiD in lithium over the 800 to 1000°C range. The results have shown that the square root of H_2 or D_2 pressure varies linearly with the LiH or LiD mole fraction in the lithium for mole fractions up to 0.16. Equations for the Sieverts constant as a function of temperature are $\log K_s = 4.360 - 2820/T$ and $\log K_s = 3.980 - 2300/T$ for hydrogen and deuterium respectively. The experimental apparatus has now been assembled for T_2-Li studies. A preliminary mass-spectrographic analysis of the gaseous components above a LiH-Li solution indicated that the vapor above a lithium blanket will contain LiT as well as T_2.

Oxides on steam generator heat transfer surfaces may provide useful impedance to tritium permeation from thermonuclear reactors. Completed studies on three alloys show that, under controlled conditions, oxides can be formed that provide significant impedance to permeation. Similar corrosion films may form on these alloys (Incoloy 800, type 406 stainless steel, and Croloy T9) in a CTR steam generator and serve as barriers to tritium permeation into the environment. Studies are now under way to measure tritium permeation through metals into steam.

Experimental study of molten salts as CTR blanket or coolant fluids has focused on magnetohydrodynamic effects in flowing salt streams; these effects have been simulated by circulating aqueous solutions with electrical conductivities as high as 35/Ω-m through magnetic flux densities to 2.2 T. Observed electromotive forces followed Faraday's law for flow through insulated pipes, and pressure gradients (head losses) resulting from the magnetic field were negligible. A critical compilation of thermophysical properties and heat-transfer performance of Li_2BeF_4 (a proposed blanket fluid) is being prepared.

Publications, Papers, and ORNL Reports

BOOKS AND JOURNAL ARTICLES

I. Alexeff,[1] "Throughput Limit in Mass Spectrograph-Type Isotope Separators," *J. Appl. Phys.* 44, 4592 (1973).

W. B. Ard,[2] R. J. Colchin, E. C. Crume, J. L. Dunlap, G. R. Haste, and J. F. Lyon, "Physics of Target Plasmas in Minimum-B Geometries," p. 401 in *Proceedings of Sixth European Conference on Controlled Fusion and Plasma Physics, Moscow, USSR, July 30 August 3, 1973*, vol. 1, Moscow, 1973.

C. F. Barnett, L. A. Berry, C. E. Bush, J. D. Callen,[3] J. F. Clarke, R. J. Colchin, R. A. Dory, A. C. England, J. T. Hogan, G. G. Kelley, J. R. McNally, Jr., M. Murakami, R. V. Neidigh, M. Roberts, J. A. Rome, and W. R. Wing, "ORMAK and Neutral Injection," p. 67 in *Proceedings of Sixth European Conference on Controlled Fusion and Plasma Physics, Moscow, USSR, July 30 August 3, 1973*, vol. 1, Moscow, 1973.

J. D. Callen,[3] J. F. Clarke, and J. A. Rome, "Theory of Neutral Beam Injection into a Tokamak," p. E14 in *Proceedings, Third International Symposium on Toroidal Plasma Confinement, Garching, March 26 30 1973*, Max-Planck-Institut fur Plasmaphysik, Garching, Munchen, Federal Republic of Germany, 1973.

J. D. Callen[3] and G. E. Guest, "Electromagnetic Effects on Electrostatic Modes in a Magnetized Plasma," *Nucl. Fusion* 13, 87 (1973).

J. D. Callen, J. T. Hogan, and B. V. Waddell,[4] "Quasiclassical Diffusion Processes in Tokamaks," p. B23 in *Proceedings, Third International Symposium on Toroidal Plasma Confinement, Garching, March 26 30, 1973*, Max-Planck-Institut fur Plasmaphysik, Garching, Munchen, Federal Republic of Germany, 1973.

R. A. Dandl, H. O. Eason, A. C. England and J. C. Sprott,[5] "High-Beta Plasma Behavior in a Canted Mirror," *Nucl. Fusion* 13, 693 (1973).

R. A. Dory, J. T. Hogan, and M. M. Widner,[6] "Thermal Stability of a Moderately Large Tokamak Proto-Reactor," p. E13 in *Proceedings, Third International Symposium on Toroidal Plasma Confinement, Garching, March 26 30, 1973*, Max-Planck-Institut fur Plasmaphysik, Garching, Munchen, Federal Republic of Germany, 1973.

A. C. England, "Polarization of Free-Free Bremsstrahlung from Magnetically Confined Plasmas," *Phys. Rev. A* 8, 1475 (1973).

A. C. England and G. R. Haste, "Angular Distribution of Bremsstrahlung from Mirror-Confined Electrons," *Phys. Rev. A* 7, 383 (1973).

A. P. Fraas,[7] "Problems in Coupling a Gas Turbine to a Thermonuclear Reactor," 17th Annual International Gas Turbine Conference, San Francisco, California, March 26 30, 1972, USAEC report CONF-720515-2.

A. P. Fraas,[7] "Materials Problems in the Design of Magnetically Confined Plasma Fusion Reactor," *Trans. Amer. Nucl. Soc.* 17, 133 (1973).

A. P. Fraas,[7] L. Dresner,[7] R. S. Holcomb,[7] and M. E. Lackey,[7] "Analytical and Experimental Investigation of the BLASCON Energy Conversion System for Laser-Fusion Reactors," in Proceedings, American Society of Mechanical Engineers, 72-WA ENER-10, New York, November 12 16, 1972.

H. K. Forsen[8] and J. C. Sprott,[5] "The Use of Synchrotron Radiation to Provide Ionization of Wall Originated Impurities in a Thermonuclear Reactor," *Nucl. Fusion* 12, 1–5 (1972).

G. R. Haste and N. H. Lazar, "Axial Distribution for a Hot Electron Plasma," *Phys. Fluids* 16, 683 (1973).

G. G. Kelley, C. F. Barnett, L. A. Berry, C. E. Bush, J. D. Callen,[3] J. F. Clarke, R. J. Colchin, R. A. Dory, A. C. England, J. T. Hogan, J. R. McNally, Jr., M. Murakami, R. V. Neidigh, M. Roberts, J. A. Rome, and W. R. Wing, "Status of the ORMAK Experiment," p. B3-1 in *Proceedings, Third International Symposium on Toroidal Plasma Confinement, Garching, March 26–30, 1973*, Max-Planck-Institut fur Plasmaphysik, Garching, Munchen, Federal Republic of Germany, 1973.

K. Koyama,[9] "Magnetic Instability in Hard Superconductors," *J. Appl. Phys.* **44**, 5531 (1973).

J. R. McNally, Jr., "Modified Lawson Criterion for d-^{6}Li Fueled Fusion Reactors," *Nucl. Fusion* **13**, 289 (1973).

J. R. McNally, Jr., "Nuclear Fusion Chain Reaction Applications in Physics and Astrophysics," p. 41 in *Proceedings of the Symposium on Applications of Nuclear Data in Science and Technology, Paris, France, March 12–16, 1973*, vol. II, IAEA, Vienna, 1973, CONF IAEA SM-170/49.

J. R. McNally, Jr., and R. V. Neidigh, "Ion Temperatures in ORMAK from Doppler Broadening," *Nucl. Fusion* **13**, 919 (1973).

J. C. Sprott,[5] "The Effect of Magnetic Field Errors on Confinement in Bumpy Tori," *Phys. Fluids* **16**, 115 (1973).

L. D. Stewart, J. D. Callen[3] J. F. Clarke, R. C. Davis, R. A. Dory, J. T. Hogan, T. C. Jernigan, O. B. Morgan, J. A. Rome, and W. L. Stirling, "Neutral Beam Injection Heating of Tokamaks," p. E8 in *Proceedings, Third International Symposium on Toroidal Plasma Confinement, Garching, March 26–30, 1973*, Max-Planck-Institut fur Plasmaphysik, Garching, Munchen, Federal Republic of Germany, 1973.

L. D. Stewart, R. C. Davis, J. T. Hogan, T. C. Jernigan, O. B. Morgan, and W. L. Stirling, "Neutral Beam Injection Heating of ORMAK," p. E12 in *Proceedings, Third International Symposium on Toroidal Plasma Confinement, Garching, March 26–30, 1973*, Max-Planck-Institut fur Plasmaphysik, Garching, Munchen, Federal Republic of Germany, 1973.

P. L. Walstrom and M. S. Lubell, "Calculation of Radial Magnetic Fields for Axisymmetric Solenoids with Rectangular Cross Section," *J. Appl. Phys.* **44**, 4195 (1973).

The following papers were presented at the Fifth Symposium on Engineering Problems of Fusion Research held at Princeton University, November 5–9, 1973. They have been published in *Proceedings of the Fifth Symposium on Engineering Problems of Fusion Research, Princeton University, Nov. 5–9, 1973*, IEEE Nuclear and Plasma Sciences Society, IEEE Pub. No. 73 CHO 843-3-NPS.

J. S. Culver and M. Murakami, "Mechanical and Optical Coupling of a Thomson Scattering Laser T_e Measurement to the ORMAK Machine," p. 398.

R. C. Davis, T. C. Jernigan, O. B. Morgan, L. D. Stewart, and W. L. Stirling, "Engineering Considerations of the DuoPIGatron Ion Source," p. 429.

S. M. DeCamp, Jr., and J. D. Rylander,[10] "Development, Fabrication and Assembly of a Thin Wall, Low Aspect Ratio Liner and the Enclosed Tungsten Limiter for ORMAK," p. 364.

R. W. Derby, "On the Influence of the Between-the-Turns Thermal Insulation on the Duty of a Large, Liquid-Cooled Pulsed Coil," p. 376.

G. R. Dyer and M. Murakami, "A Low-Noise Collection System for the Thomson Scattering Diagnostic Apparatus on ORMAK," p. 403.

J. E. Francis, W. R. Wing, and O. C. Yonts, "ORMAK Data Handling," p. 496.

W. F. Gauster[11] and P. L. Walstrom, "Analysis of the 50 kG Toroidal Field Coil for High Field ORMAK," p. 367.

W. Halchin,[10] S. M. DeCamp, S. O. Lewis,[10] D. C. Lousteau,[10] and J. D. Rylander,[10] "Operation of the ORMAK Fusion Device in a Cryogenic, Vacuum Environment," p. 360.

P. N. Haubenreich,[7] D. D. Cannon,[10] A. P. Fraas,[7] R. S. Lord,[12] and M. Roberts, "Conceptual Design Study for the ORMAK-F/BX Facility," p. 545.

H. M. Long and J. N. Luton, Jr., "Cryogenic Engineering for ORMAK," p. 380.

D. C. Lousteau,[10] S. M. DeCamp, W. Halchin,[10] T. C. Jernigan, S. O. Lewis,[10] O. B. Morgan, J. D. Rylander,[10] and L. D. Stewart, "Mechanical Interfacing of the High Power Neutral Injection Heaters to ORMAK," p. 409.

J. N. Luton, Jr., R. L. Brown, R. W. Derby, and W. C. T. Stoddart,[10] "Development of the 50 kG Toroidal Field Coil for High Field ORMAK," p. 370.

M. Nozawa[9] and D. Steiner, "An Assessment of the Power Balance in Fusion Reactors," p. 96.

M. Roberts, "Engineering and Management Aspects of the ORMAK Program," p. 281.

J. E. Simpkins, "Passivation of the ORMAK Vacuum Liner," p. 385.

L. D. Stewart, R. C. Davis, J. C. Ezell, T. C. Jernigan, O. B. Morgan, W. L. Stirling, and R. E. Wright, "Design of High Power Injection Heaters for the ORMAK System," p. 406.

---

1. Department of Electrical Engineering, University of Tennessee.
2. United Aircraft Research Labs.
3. On leave of absence from Massachusetts Institute of Technology.
4. Massachusetts Institute of Technology.
5. University of Wisconsin.
6. Sandia Laboratories.
7. Reactor Division.
8. Exxon Corporation.
9. Visiting Scientist, Japan Atomic Energy Research Institute.
10. General Engineering Division.
11. Consultant.
12. Physics Division.

PAPERS PRESENTED AT SCIENTIFIC AND TECHNICAL MEETINGS

American Institute of Aeronautics and Astronautics, 11th Aerospace Sciences Meeting and Technical Display, Washington, D.C., January 10 - 12, 1973.

A. P. Fraas,[1] "Engineering Problems in the Design of Controlled Thermonuclear Reactors."

Annual Sherwood Theory Meeting, University of Texas, Austin, Texas, March 12 - 13, 1973.

J. D. Callen,[2] J. F. Clarke, and J. A. Rome, "Theory of Neutral Beam Injection into a Tokamak."

J. T. Hogan and R. A. Dory, "Tokamak Transport Theory at Oak Ridge National Laboratory."

D. B. Nelson and G. O. Spies,[3] "MHD Stability of Toroidal Equilibria."

IAEA Symposium on Applications of Nuclear Data in Science and Technology, Paris, France, March 12 - 16, 1973.

J. R. McNally, Jr., "Nuclear Fusion Chain Reaction Applications in Physics and Astrophysics."

Third International Symposium on Toroidal Plasma Confinement, Max Planck Institute for Plasma Physics, Munich, Germany, March 26 - 30, 1973.

J. D. Callen,[2] J. T. Hogan, and B. V. Waddell,[4] "Quasiclassical Diffusion Processes in Tokamaks."

J. D. Callen,[2] J. F. Clarke, and J. A. Rome, "Theory of Neutral Beam Injection into a Tokamak."

R. A. Dory, J. T. Hogan, and M. M. Widner,[5] "Thermal Stability of a Moderately Large Tokamak Proto-Reactor."

G. G. Kelley, C. F. Barnett, L. A. Berry, C. E. Bush, J. D. Callen,[2] J. F. Clarke, R. J. Colchin, R. A. Dory, A. C. England, J. T. Hogan, J. R. McNally, Jr., M. Murakami, R. V. Neidigh, M. Roberts, J. A. Rome, and W. R. Wing, "Status of the ORMAK Experiment."

L. D Stewart, J. D. Callen,[2] J. F. Clarke, R. C. Davis, R. A. Dory, J. T. Hogan, T. C. Jernigan, O. B. Morgan, J. A. Rome, and W. L. Stirling, "Neutral Beam Injection Heating of Tokamaks."

L. D. Stewart, R. C. Davis, J. T. Hogan, T. C. Jernigan, O. B. Morgan, and W L. Stirling, "Neutral Beam Injection Heating of ORMAK."

International Conference on Waves and Instabilities in Plasmas, Innsbruck, Austria, April 2–7, 1973.

C. O. Beasley, Jr., J. D. Callen,[2] W. M. Farr,[6] H. R. Hicks,[7] J. E. McCune,[4] and A. Sen,[8] "Microinstabilities in Short Mirror Plasmas."

Ninth Annual Symposium of the New Mexico Chapter of the American Vacuum Society, Albuquerque, New Mexico, April 9–11, 1973.

J. E. Simpkins, "Diffusion through Gold Films on Stainless Steel."

American Physical Society, Washington, D.C., April 23–26, 1973 [*Bull. Amer. Phys. Soc.* [II] 18(4) (1973)].

C. F. Barnett, L. A. Berry, and J. A. Ray, "Ion Temperature Measurements in the ORMAK Toroidal Plasma."

L. A. Berry, G. G. Kelley, M. Murakami, and M. Roberts, "Stored Energy Measurements on the ORMAK Plasma."

M. Murakami, W. R. Wing, and J. S. Culver, "Electron Temperature Profiles in the ORMAK Plasma."

R. V. Neidigh, J. F. Clarke, and J. R. McNally, Jr., "An Observation of Toroidal Rotation in a Low Aspect Ratio Tokamak."

J. A. Rome and J. F. Clarke, "Ion Temperature Scaling in ORMAK."

W. R. Wing and J. F. Clarke, "Soft X-Ray Measurements in ORMAK."

VIII International Conference on the Physics of Electronic and Atomic Collisions, Belgrade, Yugoslavia, July 16–20, 1973.

I. Alvarez,[9] C. F. Barnett, and J. A. Ray, "Cross Sections for the Formation of Hydrogen Negative Ions by the Dissociation of H_2^+, H_3^+, and HD_2^+ in Hydrogen Gas."

Sixth European Conference on Controlled Fusion and Plasma Physics, Moscow, USSR, July 30–August 3, 1973.

J. F. Clarke, C. F. Barnett, L. A. Berry, C. E. Bush, J. D. Callen,[2] R. J. Colchin, R. A. Dory, A. C. England, J. T. Hogan, G. G. Kelley, J. R. McNally, Jr., M. Murakami, R. V. Neidigh, M. Roberts, J. A. Rome, and W. R. Wing, "ORMAK and Neutral Injection.

N. H. Lazar, W. B. Ard,[10] R. J. Colchin, E. C. Crume, J. L. Dunlap, G. R. Haste, and J. F. Lyon, "Physics of Target Plasmas in Minimum *B* Geometries."

1973 Cryogenic Engineering Conference, Atlanta, Georgia, August 8–10, 1973.

H. M. Long and J. N. Luton, Jr., "Cryogenic System for a Toroidal Thermonuclear Fusion Experiment."

Second International Conference on Structural Mechanics in Reactor Technology, Federal Institute of Testing, Federal Republic of Germany, September 10–14, 1973.

A. P. Fraas,[1] "Foreseeable Thermal, Mechanical, and Materials Engineering Problems of Fusion Reactor Power Plants."

Conference on Electrical Insulation and Dielectric Phenomena, Research Institute of the Hydro-Quebec Company, Varennes, Quebec, Canada, October 29–31, 1973. (Summary to be published in annual report of the conference.)

W. F. Gauster, R. H. Kernohan,[11] H. M. Long, and S. W. Schwenterly, "Dielectrics for Superconducting Systems."

American Physical Society, Division of Plasma Physics, Philadelphia, Pennsylvania, October 31–November 3, 1973 [*Bull. Amer. Phys. Soc.* [II] 18(10) (1973)].

C. O. Beasley, Jr., R. A. Dory, G. E. Guest, and R. H. Fowler,[7] "Stabilization of Trapped Particle Modes by Deformation of the Plasma Chamber Shape."

L. A. Berry, C. F. Barnett, and J. F. Lyon, "Charge Exchange-Neutral Measurements or the ORMAK Device."

C. E. Bush, "Heavy Ion Beam Probe for the ELMO Bumpy Torus."

J. D. Callen.[2] "Drift-Dissipative Trapped-Electron Instability."

P. Chrisman.[12] J. F. Clarke, G. R. Haste, and A. C. England. "Runaway Escape in Tokamaks."

J. F. Clarke. "Energy Containment and Scaling in Tokamaks."

J. F. Clarke, L. A. Berry, and J. T. Hogan. "Ion Energy Containment in the Oak Ridge Tokamak."

R. J. Colchin, J. D. Callen,[2] S. Matsuda,[13] and J. A. Rome. "Neutral Beam Absorption and Power Deposition in ORMAK."

E. C. Crume. "Relativistic Electron Adiabaticity in the Finite-β Plasmas of ELMO and IMP."

R. A. Dory and R. H. Fowler.[7] "MHD Tokamak Equilibria: Tailoring of Profiles."

J. L. Dunlap, E. C. Crume, G. R. Haste, N. H. Lazar, and J. F. Lyon. "Generation of ECH Plasma in a Shallow Well Mirror Configuration."

R. H. Fowler,[7] E. C. Crume, J. F. Clarke, R. A. Dory, and J. T. Hogan. "Effects of Impurity Diffusion in Tokamaks."

G. E. Guest and R. A. Dory. "Diagnostic Applications of Neutral Injection into Tokamaks: Poloidal Magnetic Field Strength."

J. T. Hogan and R. H. Fowler.[7] "Skin Effect in Tokamaks."

T. C. Jernigan, R. C. Davis, O. B. Morgan, L. D. Stewart, and W. L. Stirling. "The DuoPIGatron Ion Source for Neutral Injection Heating."

N. H. Lazar, W. B. Ard,[10] J. L. Dunlap, G. R. Haste, and J. F. Lyon. "Electron Energy Distributions of ECH Plasmas."

J. F. Lyon and L. A. Berry. "Measurement of the Interaction of the Injected Neutral Beams with the ORMAK Plasma."

S. Matsuda,[13] R. C. Davis, T. C. Jernigan, and O. B. Morgan. "Beam Optics of a DuoPIGatron Ion Source with Multi-Slit Electrodes."

D. G. McAlees[14] and H. K. Forsen,[15] "Thermonuclear Alpha Particle Orbits in a Tokamak."

J. R. McNally, Jr., R. H. Fowler,[7] and J. F. Clarke. "Reactivity of DT and DD Closed Fusion Systems."

M. Murakami and J. T. Hogan. "Electron Scaling in Collisionless Tokamaks."

R. V. Neidigh, J. F. Clarke, J. R. McNally, Jr., and D. J. Sigmar.[4] "The Hot Ion Distribution Function in ORMAK."

M. Roberts, J. F. Clarke, and J. T. Hogan. "Scaling of Impurity Levels in Tokamaks."

J. A. Rome and J. D. Callen.[2] "The Distribution Function of Injected Fast Ions as They Slow Down in a Tokamak Plasma."

D. J. Sigmar[4] and J. F. Clarke. "Enhanced Diffusion and Relaxation of Toroidal Plasma Rotation due to Charge Exchange Reactions."

D. A. Spong[16] and J. F. Clarke. "Runaway Electron Dynamics in Tokamaks."

L. D. Stewart, R. C. Davis, T. C. Jernigan, O. B. Morgan, and W. L. Stirling. "Neutral Injection Heaters for ORMAK."

W. L. Stirling, R. C. Davis, T. C. Jernigan, O. B. Morgan, and L. D. Stewart. "Scaling the DuoPIGatron Multiampere Ion Source."

W. R. Wing. "Soft X-Ray Measurement of 'Z Effective' in the ORMAK Discharge."

Winter Annual Meeting of the American Nuclear Society, San Francisco, California, November 12–16, 1973.

A. P. Fraas,[1] "Materials Problems in the Design of Magnetically Confined Plasma Fusion Reactors" (invited paper).

---

1. Reactor Division.
2. On leave of absence from Massachusetts Institute of Technology.
3. Courant Institute, New York University.
4. Massachusetts Institute of Technology.
5. Sandia Laboratories.
6. University of Arizona.
7. Computer Sciences Division.
8. Physical Research Laboratory, Ahmedabad-9, India.
9. Institute of Physics, UNAM, Mexico, D.F.
10. United Aircraft Research Laboratories.
11. Solid State Division.
12. Summer participant, Massachusetts Institute of Technology.
13. Japan Atomic Energy Research Institute.
14. University of Wisconsin.
15. Exxon Corporation.
16. University of Michigan.

ORNL REPORTS

Author(s)	Title	Number
L. Dresner[1]	Mechanical Stress in the Pressure Vessel of a Lithium-Filled, Exploding Pellet, Thermonuclear Reactor	ORNL-TM-4050
C. L. Hedrick, G. E. Guest, and D. B. Nelson	Some Techniques for Determining Tensor Pressure Equilibria	ORNL-TM-4076
J. F. Etzweiler,[2] J. F. Clarke, and R. H. Fowler	Effect of Fuel Injection on a Cyclic Beta-Limited Radiation Dominated Fusion Reactor	ORNL-TM-4083
A. C. England	Polarization of Free-Free Bremsstrahlung from Magnetically-Confined Plasmas	ORNL-TM-4103
D. B. Nelson, C. L. Hedrick, and G. O. Spies[3]	The Stability of Anisotropic Equilibria in Closed Line Tori	ORNL-TM-4109
I. Alexeff[4]	Bypassing the Instability-Induced Throughput Limit in Calutron Isotope Separators	ORNL-TM-4116
D. A. Spong,[5] J. F. Clarke, and J. A. Rome	Relativistic Electron Production in the ORMAK Device	ORNL-TM-4120
R. A. Dandl, H. O. Eason, A. C. England, and J. C. Sprott[6]	High-Beta Plasma Behavior in a Canted Mirror	ORNL-TM-4153
C. J. McHargue[7]	Fusion Technology Studies, Progress Report for Period Ending December 31, 1972	ORNL-TM-4156
D. Steiner	Analysis of a Bench-Mark Calculation of Tritium Breeding in a Fusion Reactor Blanket: The United States Contribution	ORNL-TM-4177
M. L. Tobias[1] and D. Steiner	Outline of Direct Methods Used in Computing the Cross Section Sensitivity of Neutronic Parameters in a Fusion Reactor	ORNL-TM-4184
Cryoelectrics Section, Engineering Sciences Group	Cryogenic Dielectrics and Superconducting and Cryogenic Materials Technology for Power Transmission – Semi-annual Report – March 1, 1973	ORNL-TM-4187
P. L. Walstrom and M. S. Lubell	Calculation of Radial Magnetic Fields for Axisymmetric Solenoids with Rectangular Cross Section	ORNL-TM-4198

M. Tobias[1] and D. Steiner	Cross-Section Sensitivity of Tritium Breeding in a Fusion Reactor Blanket: Effects of Uncertainties in Cross Sections of ^{6}Li, ^{7}Li, and ^{93}Nb	ORNL-TM-4200
D. E. Bartine,[8] R. G. Alsmiller, Jr.,[8] E. M. Oblow,[8] and F. R. Mynatt[8]	Cross-Section Sensitivity of Breeding Ratio in a Fusion Reactor Blanket	ORNL-TM-4208
A. P. Fraas,[1] D. B. Lloyd,[1] and R. E. MacPherson[1]	Effects of a Strong Magnetic Field on Boiling of Potassium	ORNL-TM-4218
J. T. Kriese[9] and D. Steiner	Magnet Shield Design for Fusion Reactors	ORNL-TM-4256
K. Koyama[10]	Magnetic Instability in Hard Superconductors	ORNL-TM-4265
J. T. Kriese[9]	Coupled Neutron and Gamma-Ray Cross Section Sets for Fusion Reactor Calculations	ORNL-TM-4277
J. N. Luton, Jr.	Safety with High Magnetic Field Systems	ORNL-TM-4313
E. C. Crume, G. R. Haste, and N. H. Lazar	Design Considerations for a Shallow Well Mirror Experiment	ORNL-TM-4319
C. O. Beasley, Jr., H. R. Hicks,[11] and W. M. Farr[12]	Microinstabilities in Inhomogeneous Plasma II: Numerical Results	ORNL-TM-4325
J. A. Rome, J. D. Callen, and J. F. Clarke	Neutral Beam Injection into a Tokamak: I. Fast Ion Spatial Distribution for Tangential Injection	ORNL-TM-4332
W. F. Gauster[13] and P. L. Walstrom	Torus Windings with Asymmetric Magnet Coils	ORNL-TM-4336
Cryoelectrics Section, Engineering Sciences Group	Second Quarterly Technical Progress Report, ORNL Program on Cryogenic Dielectrics and Superconducting and Cryogenic Materials Work	ORNL-TM-4341
M. Roberts	The ORMAK-F/BX Facility - Preliminary Considerations	ORNL-TM-4342
D. Steiner	The Nuclear Performance of Vanadium as a Structural Material in Fusion Reactor Blankets	ORNL-TM-4353
M. Murakami, W. R. Wing, J. S. Culver, and P. H. Edmonds	Thomson Scattering Measurements in ORMAK	ORNL-TM-4354
J. R. McNally, Jr.	Neutral Injection Heating of Tokamaks	ORNL-TM-4363
A. P. Fraas[1] and J. J. Tudor[1]	Mechanical Engineering Design Considerations for a Tokamak Scientific Feasibility Experiment and Plasma Test Reactor	ORNL-TM-4371
K. Koyama[10] and M. S. Lubell	Dynamic Stabilization of Nb_3Sn Tape Superconductors	ORNL-TM-4391
M. Nozawa[14] and D. Steiner	An Assessment of the Power Balance in Fusion Reactors	ORNL-TM-4421
D. Spong[5] and J. F. Clarke	Runaway Electron Dynamics	ORNL-TM-4432
Cryoelectrics Section, Engineering Sciences Group	Cryogenic Power Transmission Technology - Cryogenic Dielectrics, Quarterly Report - July 1 - Sept. 30, 1973	ORNL-TM-4433
D. Steiner	Fusion Reactor Technology Studies at ORNL	ORNL-TM-4439
G. O. Spies[3] and D. B. Nelson	Sufficient Stability Criteria for Plasma Equilibria with Tensor Pressure	ORNL-TM-4452
J. T. Hogan and J. F. Clarke	Fluxes of Charged and Neutral Particles from Tokamaks	ORNL-TM-4474
C. O. Beasley, Jr., and H. R. Hicks[11]	Program IPP6 - Microinstabilities in Inhomogeneous, Mirror-Contained Plasmas	ORNL-TM-4475
Cryoelectrics Section, Engineering Sciences Group	Cryogenic Power Transmission Technology - Cryogenic Dielectrics, Quarterly Report - Oct. 1 - Dec. 31, 1973	ORNL-TM-4476
P. Chrisman,[15] J. Clarke, and J. Rome	Magnetic Island Formation in a Tokamak Plasma from Helical Perturbations of the Plasma Current	ORNL-TM-4501
D. Spong[5] and J. F. Clarke	Hydromagnetic Kink Mode of a Two-Region Runaway Electron Beam	ORNL-TM-4512
J. F. Clarke	Energy Containment and Scaling in Tokamaks (The Phylogeny of a Tokamak Discharge)	ORNL-TM-4585

G. S. McNeilly[11]	Heavy Ion Beam Probe Design Calculations for the ORMAK and ELMO Bumpy Torus Devices	ORNL-TM-4834
Thermonuclear Division Staff	Thermonuclear Division Annual Progress Report for Period Ending December 31, 1972	ORNL-TM-4896

1. Reactor Division.
2. 1972 Summer Participant, University of Wisconsin.
3. Courant Institute, New York University.
4. Department of Electrical Engineering, University of Tennessee.
5. University of Michigan.
6. University of Wisconsin.
7. Metals and Ceramics Division.
8. Neutron Physics Division.
9. Westinghouse Electric Corporation.
10. Electrotechnical Laboratory, Tokyo, Japan.
11. Computer Sciences Division.
12. University of Arizona.
13. Consultant.
14. Visiting Scientist, Japan Atomic Energy Research Institute.
15. 1973 Summer Participant, Massachusetts Institute of Technology.